

Na

7/25/68

THE PHYSICAL ADSORPTION OF ARGON AND NITROGEN
ON SUBLIMATED SODIUM CHLORIDE PARTICLES

A THESIS

Presented to

The Faculty of the Graduate Division

by

Daniel Joseph Jackson Jr.

In Partial Fulfillment
of the Requirements for the Degree
Doctor of Philosophy
in the School of Chemistry

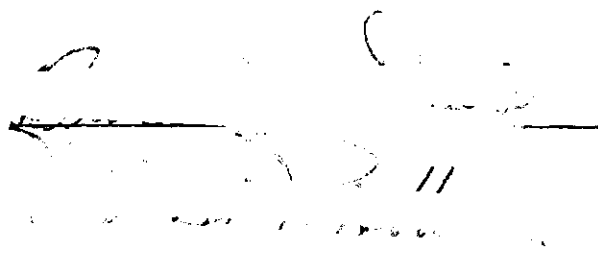
Georgia Institute of Technology

June, 1972

THE PHYSICAL ADSORPTION OF ARGON AND NITROGEN
ON SUBLIMATED SODIUM CHLORIDE PARTICLES

and title page? Imperfect volumes delay return of binding. Thanks.
BOUND BY THE NATIONAL LIBRARY BINDERY CO. OF GA.

Approved:



Date approved by Chairman: 8 June, 1972

ACKNOWLEDGMENTS

The author would like to express his sincere appreciation to those who provided guidance and assistance during the course of this project.

Special thanks are due to Dr. Bruce W. Davis, for his guidance and numerous helpful and encouraging discussions. Dr. Davis was responsible for conceiving the project and obtaining the necessary research funds. Thanks are due also to Mr. Donald Lillie, Mr. Malcolm Rucker and Mr. Gerald O'Brien for their advice and assistance in constructing various parts of the experimental apparatus.

The U. S. Army Research Office at Durham, North Carolina, is also to be thanked for providing the funds for this research project. The U. S. Army, and especially the Chemical Corps and the United States Military Academy, are thanked for their support during the entire course of this study.

TABLE OF CONTENTS

	Page
ACKNOWLEDGMENTS	ii
LIST OF TABLES	v
LIST OF ILLUSTRATIONS	ix
LIST OF SYMBOLS AND ABBREVIATIONS	xi
SUMMARYxviii
CHAPTER	
I. INTRODUCTION	1
Statement of Problem	
Interaction Energy	
Interaction Potential for Ionic Crystal Systems	
Sublimation of Sodium Chloride	
II. EXPERIMENTAL	17
Adsorption Apparatus	
Adsorption System	
The Cryostat	
Thermal Transpiration	
Non-Ideal Gas Behavior	
Sample Preparation	
III. CHARACTERIZATION OF THE SAMPLE	33
Electron Microscopy	
Electron Diffraction	
X-Ray Emission Electron Microprobe Analysis	
Adsorption Experiments	
Discussion	
IV. EXPERIMENTAL RESULTS	48
V. SITE ENERGY DISTRIBUTION ANALYSIS	58
Distribution Functions	
Results	

Chapter	Page
VI. ADSORPTION POTENTIAL	70
Attractive Potential	
Repulsive Potential	
Electrostatic Potential	
Quadrupole Potential	
Total Potential	
VII. ISOSTERIC HEATS	97
Discussion of Results	
Recommendations	
APPENDICES	
A. EXPERIMENTAL DATA AND ISOSTERIC HEATS	117
B. SITE ENERGY DISTRIBUTION ANALYSIS	140
C. FOWLER AND GUGGENHEIM EQUATION	146
D. RESULTS OF THE SITE ENERGY DISTRIBUTION FUNCTION	151
E. THE INVERSE SIXTH POWER SUMMATIONS OF THE MOLECULE-ION DISTANCE	152
F. EXPONENTIAL SUMMATIONS OF DISTANCE	160
G. THE ELECTROSTATIC FIELD	169
H. QUADRUPOLE POTENTIAL SUMMATIONS	172
I. POTENTIAL ENERGY CURVE DATA	175
J. INTEGRATED POTENTIAL	180
BIBLIOGRAPHY	184
VITA	187

LIST OF TABLES

Table	Page
1. Values of the Constants for the Antoine Equation	26
2. Impurities in Fisher Certified ACS Biological Grade Sodium Chloride by % Weight	39
3. Results of Argon and Nitrogen Isotherms on the Treated and Untreated Sample	42
4. Scaling Factors for Argon Isotherms and the Ratio of the Nitrogen Surface Areas	45
5. Isotherm Data Based on $\sigma_{N_2} = 16.2A^{0.2}$	49
6. Parameters for Equation (60)	64
7. Parameters for Equations (62) and (63)	68
8. Modified Buckingham (6 - exp) Parameters	71
9. Polarizabilities and Diamagnetic Susceptibilities	74
10. Potential Parameters	78
11. Parameters for the Argon-Sodium Chloride Potential Curve . .	86
12. Parameters for the Nitrogen-Sodium Chloride Potential Curve	86
13. Weighting Factors	88
14. Results Obtained from the Potential Energy Curve for Argon on the (100) Plane of Sodium Chloride, using the Geometric Mean Combining Rule for the Repulsive Potential Parameter B_{12}	91
15. Results Obtained from the Potential Energy Curve for Argon on the (100) Plane of Sodium Chloride, using the Arithmetic Mean Combining Rule for the Repulsive Potential Parameter B_{12}	93
16. Results Obtained from the Potential Energy Curve for Nitrogen on the (100) Plane of Sodium Chloride	95
17. Total Average Energy and ϕ_{st}^c	96

Table	Page
18. Theoretical and Experimental Isosteric Heats at Zero Coverage	99
19. Values of ψ and ψ'	107
20. Mixed Interaction Parameters from the Potential of Whalley and Schneider	109
21. Potential Minima and Equilibrium Distances	109
22. Data for the Isotherm of Argon on Untreated Sodium Chloride at 77.08°K	118
23. Data for the Isotherm of Nitrogen on Untreated Sodium Chloride at 77.25°K	120
24. Data for the Isotherm of Argon on Sodium Chloride at 77.22°K, after the Initial Heat Treatment	121
25. Data for the Isotherm of Argon on Doubly Heat Treated Sodium Chloride at 72.14°K	122
26. Data for the Isotherm of Argon on Doubly Heat Treated Sodium Chloride at 77.12°K	124
27. Data for the Isotherm of Argon on Doubly Heat Treated Sodium Chloride at 82.88°K	126
28. Data for the Isotherm of Argon on Doubly Heat Treated Sodium Chloride at 89.96°K	128
29. Data for the Isotherm of Nitrogen on Doubly Heat Treated Sodium Chloride at 77.11°K	130
30. Data for the Isotherm of Nitrogen on Doubly Heat Treated Sodium Chloride at 77.11°K	132
31. Data for the Isotherm of Nitrogen on Doubly Heat Treated Sodium Chloride at 82.88°K	134
32. Data for the Isotherm of Nitrogen on Doubly Heat Treated Sodium Chloride at 90.07°K	136
33. Isosteric Heats of Adsorption for Argon on Sodium Chloride .	138
34. Isosteric Heats of Adsorption for Nitrogen on Sodium Chloride	139
35. Results of the Site Energy Distribution Function	151

Table	Page
36. Summations ($\Sigma(\rho)$) of the Inverse Sixth Power of Distance from Equations (157), (159) and (162) for the (100) Plane of the Face Centered Cubic Structure	157
37. Summations ($\Sigma(\rho/2)$) of the Inverse Sixth Power of Distance from Equations (157), (159) and (162) for the (100) Plane of the Face Centered Cubic Structure	158
38. Summations ($\Sigma(\frac{\rho+1}{2})$) of the Inverse Sixth Power of Distance from Equations (157), (159) and (162) for the (100) Plane of the Face Centered Cubic Structure	159
39. Summations of the Exponential of Distance ($\Sigma'(\rho, \beta, a)$) from Equations (171), (172) and (173) for Argon on the (100) Plane of Sodium Chloride	163
40. Summations of the Exponential of Distance ($\Sigma'(\rho/2, \beta, 2a)$) from Equations (171), (172) and (173) for Argon on the (100) Plane of Sodium Chloride	164
41. Summations of the Exponential of Distance ($\Sigma'(\frac{\rho+1}{2}, \beta, 2a)$) from Equations (171), (172) and (173) for Argon on the (100) Plane of Sodium Chloride	165
42. Summations of the Exponential of Distance ($\Sigma'(\rho, \beta, a)$) from Equations (171), (172) and (173) for Nitrogen on the (100) Plane of Sodium Chloride	166
43. Summations of the Exponential of Distance ($\Sigma'(\rho/2, \beta, 2a)$) from Equations (171), (172) and (173) for Nitrogen on the (100) Plane of Sodium Chloride	167
44. Summations of the Exponential of Distance ($\Sigma'(\frac{\rho+1}{2}, \beta, 2a)$) from Equations (171), (172) and (173) for Nitrogen on the (100) Plane of Sodium Chloride	168
45. The F_z Component of the Electrostatic Field over the Ions of the (100) Plane of Sodium Chloride, from Equation (92) . . .	171
46. Values of σ from Equations (183), (184), (185) and (186) for the (100) Plane of Sodium Chloride	174
47. Total Potential for Argon above the (100) Plane of Sodium Chloride using the Harmonic Mean Combining Rule, for the Repulsive Potential Parameter B_{12}	176
48. Total Potential for Argon above the (100) Plane of Sodium Chloride using the Arithmetic Mean Combining Rule, for the Repulsive Potential Parameter B_{12}	177

Table	Page
49. Total Potential for Argon above the (100) Plane of Sodium Chloride using the Geometric Mean Combining Rule, for the Repulsive Potential Parameter B_{12}	178
50. Total Potential for Nitrogen above the (100) Plane of Sodium Chloride using the Geometric Mean Combining Rule, for the Repulsive Potential Parameter B_{12}	179
51. Total Potential for Argon on Sodium Chloride from Equation (196)	183

LIST OF ILLUSTRATIONS

Figure	Page
1. Typical Isothermic Heat Curve	8
2. Schematic Diagram of Adsorption System	18
3. Schematic Diagram of Cryostat	23
4. Schematic Diagram of Sublimation Apparatus	31
5a. Untreated NaCl	36
5b. Doubly Heat Treated NaCl	36
5c. Stereo Scanning Electron Micrograph of Doubly Heat Treated NaCl	36
6a. Diffraction Pattern of the Untreated Sample	38
6b. Diffraction Pattern of the Doubly Heat Treated Sample	38
7. Isotherms of Argon on NaCl at 77°K	43
8. Isotherms of Nitrogen on NaCl at 77°K	44
9. Argon Isotherm on NaCl at 72.14°K	50
10. Argon Isotherm on NaCl at 77.12°K	51
11. Argon Isotherm on NaCl at 82.88°K	52
12. Argon Isotherm on NaCl at 89.96°K	53
13. Nitrogen Isotherm on NaCl at 72.12°K	54
14. Nitrogen Isotherm on NaCl at 77.11°K	55
15. Nitrogen Isotherm on NaCl at 82.88°K	56
16. Nitrogen Isotherm on NaCl at 90.07°K	57
17. Interaction Energy Distributions for N ₂ on BN using Various Local Isotherms: (a) Langmuir; (b) Fowler and Guggenheim Equation; (c) Van der Waals	62

Figure	Page
18. Interaction Energy Distribution for Nitrogen on Sodium Chloride	66
19. Interaction Energy Distribution for Argon on Sodium Chloride	67
20. Potential Curves for Argon on the (100) Plane of NaCl using the Geometric Mean Combining Rule for the Repulsive Potential Parameter B_{12}	90
21. Potential Curves for Argon on the (100) Plane of NaCl using the Arithmetic Mean Combining Rule for the Repulsive Potential Parameter B_{12}	92
22. Potential Curves for Nitrogen on the (100) Plane of NaCl	94
23. Isothermic Heat of Adsorption of Nitrogen on NaCl	100
24. Isothermic Heat of Adsorption of Argon on NaCl	101
25. Calculated versus Theoretical Repulsive Potential for Ar-Kr System	104
26. Partially Integrated Potential Curves for Argon over the Center of a Cell on the (100) Plane of NaCl	110
27. Partially Integrated and Summed Potential Curves for Argon over the Center of a Cell on the (100) Plane of NaCl	111
28. Typical Plot of the Fowler and Guggenheim Equation (60)	143
29a. Typical Plot of Θ_{obs} versus X/P	144
29b. Typical Plot of Θ versus F at Pressure P_i	144

LIST OF SYMBOLS AND ABBREVIATIONS

a	= ion-ion distance (one half the crystal lattice parameter)
a_o	= crystal lattice parameter
\AA	= Angstrom
A_s	= area of adsorbent
B	= pre-exponential repulsive potential parameter
B_{11}	= self-interaction pre-exponential repulsive potential parameter
B_{12}, B_{13}	= mixed-interaction pre-exponential repulsive potential parameters
b	= 1. constant 2. factor in the Fowler and Guggenheim equation
b_o	= constant in the Fowler and Guggenheim equation
BS	= break seal
$B(T)$	= second virial coefficient for volume expansion
$B'(T)$	= second virial coefficient for pressure expansion
c	= 1. constant 2. velocity of light
C	= dispersion forces constant
C_{11}	= self-interaction dispersion force constant
C_{12}, C_{13}	= mixed-interaction dispersion force constants
C_{SG}	= Starkschall and Gordon dispersion force constant
C_{KM}	= Kirkwood-Müller dispersion force constant
$^{\circ}\text{C}$	= degrees Centigrade
CC	= center of cell
CE	= center of edge

CF	= coarse frit
CT	= 1. cold trap 2. copper tube
cm	= centimeter
D	= dewar
E_{av}	= average energy
E_{av}^T	= total average energy
E_g	= energy of adsorbate in gas phase
E_m	= potential well minimum
E_o	= zero point energy
E_s	= energy of adsorbate in adsorbed phase
E_{vib}	= vibrational energy
F	= 1. integral distribution function 2. electrostatic field
F_z	= electrostatic field perpendicular to the surface
FM	= flowmeter
$f(Q)$	= differential distribution function
gm	= gram
h	= Planck's constant
HM	= heating mantle
$\Delta \bar{H}_s$	= heat of sublimation
$\Delta \bar{H}_v$	= heat of vaporization
I.D.	= inside diameter
int	= internal
J	= characteristic energy
k	= Boltzmann constant
k_z	= force constant

$^{\circ}\text{K}$	= degrees Kelvin
z	= reduced distance, z/a
m	= 1. mass of electron 2. mass 3. reduced distance, y/a
MC	= McLeod gauge
MF	= medium frit
x	= reduced distance, x/a
N°	= Avogadro's number
N_{ads}	= amount adsorbed
N_{ads}/W	= micromoles adsorbed per gram
N_i	= i th dose of adsorbate
N_j	= amount of adsorbate in V_m and the dead space
N_m	= monolayer capacity
n_g	= moles of adsorbate in gas phase
n_s	= moles of adsorbate in adsorbed phase
O.D.	= outside diameter
P	= 1. pressure 2. potential field
P'	= pressure corrected for thermal transpiration
P°	= vapor pressure of the pure adsorbate
P_o	= potential field at center of adsorbate molecule
P.F.	= canonical partition function
PT	= platinum boat
q	= differential heat of adsorption
Q	= 1. integral heat of adsorption 2. interaction energy of a patch of surface 3. quadrupole moment

q_{V_g, V_s, A_s}	= differential heat of adsorption q_d
$q_{P, A_s, T}$	= differential heat of adsorption q_{st}
q_{st}	= isosteric heat of adsorption
q_{vib}	= molecular vibrational partition function
q_{rot}	= molecular rotational partition function
q_g	= molecular partition function for the gas phase
q_s	= molecular partition function for the adsorbed phase
R	= gas constant
R_o	= lower limit of integration
RS	= relay switch
r	= intermolecular distance
r_m	= equilibrium separation
S	= surface area
S_g	= entropy of adsorbate in gas phase
S_s	= entropy of adsorbate in adsorbed phase
SB	= sample bulb
SC	= stopcock
$S_+(\phi)$	= Summation of inverse sixth power of distance to positive ions
$S_-(\phi)$	= Summation of inverse sixth power of distance to negative ions
$S_+(\phi, \beta, a)$	= Summation of exponential of distance to positive ions
$S_-(\phi, \beta, a)$	= Summation of exponential of distance to negative ions
t	= axis of symmetry of quadrupole
T	= temperature
T_a	= room temperature (ambient)
T_2	= temperature of cryostat
TC	= teflon cover

trans	= translational
$u(r_i)$	= potential between an atom A and an ion
$u(r_i)$	= potential between an atom A and all the ions
$u_{i,dis}$	= potential between an atom A and an ion due to dispersion forces
$u_{i,rep}$	= potential between an atom A and an ion due to repulsive forces
$u_{i,ind}$	= potential between an atom A and an ion due to inductive forces
V_g	= volume of adsorbate in gas phase
V_s	= volume of adsorbate in adsorbed phase
V^{id}	= ideal gas volume
V_D	= dead space
V_{DH}	= warm dead space
V_{DC}	= cold dead space
V_{Deff}	= effective dead space
V_{m_l}	= manifold volume on low pressure side
V_{m_h}	= manifold volume on high pressure side
VPT	= vapor pressure thermometer
VS	= vacuum system
x	= P/P^0
z	= number of nearest neighbors

Greek symbols

α	= polarizability
β	= exponential parameter of repulsive potential
γ	= parameter of the (6 - exp) potential
ϵ_0	= potential well minimum

θ	= 1. fraction of surface covered 2. local isotherm function
Θ	= fraction of total surface covered
Θ_{obs}	= observed surface coverage
μ_g	= chemical potential of adsorbate in gas phase
μ_s	= chemical potential of adsorbate in adsorbed phase
$\mu moles$	= micromoles
ν	= characteristic vibrational frequency perpendicular to the surface
ρ	= reduced perpendicular distance, z/a
ρ_e	= electron density of adsorbate atom
σ	= cross sectional area of adsorbate
$\sigma_{A,B,C,D}$	= summations to all the ions
Σ_1	= summation of inverse sixth power of distances from a point above the center of a cell to all the ions
Σ_2	= summation of inverse sixth power of distance from a point above the mid point of a cell edge to all the ions
Σ_3	= summation of inverse sixth power of distance from a point above an ion to all the ions
Σ'_1	= summation of exponential of distances from a point above the center of a cell to all the ions
Σ'_2	= summation of exponential of distances from a point above the mid point of a cell edge to all the ions
Σ'_3	= summation of exponential of distances from a point above an ion to all the ions
$d\tau$	= volume element
ϕ_T	= total potential
ϕ_D	= dispersion potential
ϕ_R	= repulsive potential
ϕ_E	= electrostatic potential

ϕ_Q	= quadrupole potential
χ	= diamagnetic susceptibility
ψ, ψ'	= constants
ω	= adsorbate-adsorbate interaction energy

SUMMARY

A sample of sodium chloride was prepared by sublimation. Electron microscopy and diffraction studies indicated the particles were amorphous and predominantly spherical in shape. The sublimated sample was then thermally treated at $300 \pm 10^\circ\text{K}$ under a pressure of 550 torr of dry nitrogen, for a period of 144 hours. Subsequent electron microscopy and diffraction studies showed that the particles remained essentially spherical in shape, but now had become crystalline. Some sintering of the particles was also observed.

The interaction of argon and nitrogen with the surface of the thermally treated sample was investigated using physical gas adsorption techniques. Isotherm measurements were made for argon and nitrogen at four different temperatures: 72.1°K , 77.1°K , 82.1°K and 90.1°K , using a standard volumetric gas adsorption apparatus. Pressures in the range of 10^{-4} torr to 28 torr were measured on a McLeod gauge with a confidence limit of $\pm 2\%$. A U-tube mercury manometer was used to measure pressures in the range of 28 torr to 760 torr with a confidence limit of $\pm 1.8\%$. A cryostat based on the principle of cooling by injection of helium gas into a cryogenic liquid is described. The temperature of the sample was controlled to $\pm 0.01^\circ\text{K}$ over the range from 72 to 90°K . Liquid nitrogen and oxygen were employed as the cryogenic liquids.

A site energy distribution analysis was determined from the isotherm data using the method outlined by Adamson.^a The results of this analysis for the primary surface were fitted to an analytical function

of the form

$$f(Q) = A \exp (-c |Q - Q_0|^n)$$

where $f(Q)$ is the distribution function, Q is the energy corresponding to a particular value of the distribution function and Q_0 is the mean value of Q . The parameters A , c and n were varied until the best fit with the experimental data could be obtained. For nitrogen on sodium chloride the 95% confidence limit was found to be ± 0.125 kcal/mole, and for argon on sodium chloride, ± 0.014 kcal/mole. These results indicated that predominantly one plane, with a narrow distribution of energy, was exhibited on the surface of the sodium chloride particles. The isotherms show a small step in the low pressure region, which is attributed to a secondary surface of higher interaction energy. Using the point B method, the area of these high energy sites was estimated as about 2% of the total surface. These high energy sites were not observed using the present method of determining the site energy distribution.

The experimental isosteric heats of adsorption were determined from the slope of the isosteres of each adsorbate, using the Clausius-Clapeyron equation. Zero coverage isosteric heats of adsorption were determined from the isosteric heat curves and compared to theoretical values calculated from the summation procedures outlined by Orr,^b for the (100) plane of sodium Chloride. The parameters of the modified Buckingham (6 - exp) potential for the adsorbate-adsorbate self-interaction potential were used in the calculation. The results are

shown in the table below.

Gas	$q_{st}(\text{kcal/mole})$	
	Experimental	Theoretical
Ar	$1.630 \pm .076$	1.044
N ₂	$3.040 \pm .127$	2.596

Besides the (100) plane of sodium chloride, a common equilibrium crystal face is the (111) plane found on octahedral sodium chloride. Two types of (111) planes are possible, one made up of all sodium ions and one made up of all chloride ions. Young has calculated the energy of interaction for argon on the (111) planes of octahedral potassium chloride. He found the difference in the energy of interaction between the two (111) planes amounted to over 500 cal/mole. Since the polarizability of the potassium ion (1.228 \AA^3) is much greater than that of the sodium ion (0.303 \AA^3), it is expected that the difference in the (111) planes of sodium chloride would be even greater. Since the site energy distribution analysis indicates a very narrow energy distribution for the primary surface, the (111) planes are not considered as likely for the sample of this study as the (100) planes. This study, however, does not rule out the possibility of having only one of the (111) planes exhibited by the primary surface of the particles.

- a. A. Adamson, "Physical Chemistry of Surfaces," Interscience, New York, 1967.
- b. W. Orr, Trans. Faraday Soc., 35, 1247 (1939).
- c. D. M. Young, Trans. Faraday Soc., 48, 548 (1958).

CHAPTER I

INTRODUCTION

Statement of Problem

The purpose of this study was to develop a sample of sodium chloride exhibiting predominantly one surface crystal face and to investigate the interaction of non-polar gases with this homogeneous surface. A surface exhibiting predominantly one crystal face with a minimum of impurities and crystal face defects is defined as a homogeneous surface. Sublimation was selected as the method for preparing the sodium chloride sample in this study, since this method of preparing ionic crystals has been shown¹ to form homogeneous surfaces.

The interaction of non-polar gases with the sodium chloride sample was investigated using physical gas adsorption measurements. Argon and nitrogen gases were employed as the adsorbates. Although these gases are similar with respect to their polarizabilities, they differ in that nitrogen is a homonuclear diatomic molecule possessing a quadrupole moment. Their energies of interaction with the sodium chloride sample are thus expected to be significantly different.

Interaction Energy

The energy of interaction of an atom A with an ion in a crystal can be separated into three separate contributions²

$$u(r_i) = u_{i,dis} + u_{i,rep} + u_{i,ind} \quad (1)$$

where r_i is the distance between the i th ion of the crystal and the atom A. This separation is based on the assumption that the contributions are additive. The term $u_{i,dis}$ is the attractive part of the potential due to the dispersion forces and has the form of a multipolar expansion

$$u_{dis}(r) = \sum_{i \geq 0} C^{(i)} / r^{(6 + 2i)} \quad (2)$$

in the limit of large distances.

The constants C^i are determined by the properties of the atom A and the ion of the crystal. The energy due to the fluctuating dipole-dipole interaction is given by C^0/r^6 , the energy due to the fluctuating dipole-quadrupole interaction is given by C^1/r^8 , etc. These fluctuating dipole and higher order multipolar interactions constitute the dispersion forces. Evaluation of the C^i 's has been carried out by several workers and some of these will be discussed in the next section. The multipolar expansion is not valid at short distances. The value of the C^i 's will be dependent on the repulsive part of the potential at close intermolecular distances.

The repulsive part of the potential between the atom A and the ion of the crystal is given by $u_{i,rep}$. Several forms for the repulsive potential have been proposed and are discussed by Pierotti and Thomas² and by Young and Crowell³.

The collection of ions in an ionic crystal produces an electrostatic field above the crystal surface. A neutral polarizable atom or molecule in the presence of this field, experiences a force due to the induction of a dipole in the atom or molecule. In addition, if the molecule possesses a permanent dipole or quadrupole moment, it will experience an electrostatic force. These inductive interactions are represented by the term $u_{i,ind}$ in equation (1).

The energy of interaction of an atom A with the entire crystal may then be approximated by

$$u(\tilde{r}) = \sum_i u(r_i) = \sum_i (u_{i,dis} + u_{i,rep} + u_{i,ind}) \quad (3)$$

where atom A is at a position \tilde{r} relative to a reference point in the crystal and the summation is over all of the ions in the crystal.

Equation (3) is based on the assumption of pairwise additivity.

Margenau⁴ has shown this to be a reasonable approximation for the portion of the potential due to dispersion forces.

The energy of interaction as obtained by equation (3) may be related to the experimental data of physical adsorption in the following manner.³ Consider an isothermal process, wherein the adsorption of dn_g moles of adsorbate is accompanied by a transfer of heat, dQ , to the surroundings. In general the various differential heats of adsorption are defined as

$$q = dQ/dn_g \quad (4)$$

and an integral heat of adsorption is defined as

$$Q = \int_0^{n_s} q \, dn_s \quad (5)$$

From the First Law of Thermodynamics

$$dE = \delta q' - \delta w \quad (6)$$

or

$$\delta q' = dE + \delta w \quad (7)$$

where the prime mark on q' distinguishes this quantity from the differential heat of adsorption q . If only pressure-volume work is done, then $\delta w = p \, dV$ and equation (7) becomes

$$\delta q' = dE + p \, dV \quad (8)$$

In the case of adsorption, if the heat of adsorption Q is considered as a positive quantity, that is, the heat is lost by the system, then equation (8) becomes

$$\delta Q = -dE - p \, dV \quad (9)$$

If the adsorbent is considered as inert, such that the energy E_s , entropy S_s , volume V_s and related functions are properties of the adsorbed layer only, then $E = E_g + E_s$ and $V = V_g + V_s$, where E_g and V_g are the energy and volume of the adsorbate in the gas phase. Consider a process whereby V_s , V_g and A_s , the area of the adsorbent, remain

constant, then

$$\delta Q_{V_s, V_g, A_s} = -dE_g - dE_s \quad (10)$$

Defining $E_g = n_g \bar{E}_g$, $E_s = n_s \bar{E}_s$ and $dn_g = -dn_s$, where n_g and n_s are the moles of adsorbate in the gas phase and the adsorbed phase respectively, then

$$\delta Q / \delta n_s = q_{V_g, V_s, A_s} = \bar{E}_g - \bar{E}_s \quad (11)$$

The quantity q_{V_g, V_s, A_s} is defined as the differential heat of adsorption q_d , and thus is equal to the change in partial molar energy of the adsorbate upon adsorption, which is the same as the interaction energy determined by equation (3).

Now consider a process where A_s is constant and the adsorption chamber contains a piston, so that the isothermal process is also isobaric, then equation (9) becomes

$$\delta Q_{P, A_s, T} = -dE_g - dE_s - p dV_g - p dV_s \quad (12)$$

Again assuming the adsorbent is inert, the quantity dE_s has been defined as³

$$dE_s = T dS_s - p dV_s - \phi dA_s + \mu_s dn_s \quad (13)$$

where $\phi = -(\partial E / \partial A)_{S_s, V_s, n_s}$ and μ_s is the chemical potential of the adsorbed phase. Equation (12) then becomes

$$\delta Q_{P,A_s,T} = -d(E_g + p V_g) - T dS_s - \mu_s dn_s \quad (14)$$

since $dA = 0$.

Now,

$$-d(E_g + p V_g) = -d(H_g) = -\bar{H}_g dn_g = \bar{H}_g dn_s \quad (15)$$

and

$$dS_s = \bar{S}_s dn_s \quad (16)$$

Substituting equations (15) and (16) into equation (14)

$$\delta Q_{P,A_s,T} = \bar{H}_g dn_s - T \bar{S}_s dn_s - \mu_s dn_s \quad (17)$$

At equilibrium,

$$\mu_s = \mu_g = \bar{H}_g - T \bar{S}_g \quad (18)$$

therefore,

$$\delta Q_{P,A_s,T} = -T \bar{S}_s dn_s + T \bar{S}_g dn_s \quad (19)$$

or

$$q_{P,A_s,T} = (\delta Q / \delta n_s)_{P,A_s,T} = T(\bar{S}_g - \bar{S}_s) \quad (20)$$

The quantity $(\bar{S}_g - \bar{S}_s)$ can be shown to be equal to

$$(\bar{S}_g - \bar{S}_s) = RT(\partial \ln p / \partial T)_{n_s, A_s} \quad (21)$$

The heat $q_{P, A_s, T}$ is defined as the isosteric heat of adsorption q_{st} and may be determined from the data of physical adsorption experiments at several different temperatures using the equation

$$q_{st} = RT^2(\partial \ln p / \partial T)_{n_s, A_s} \quad (22)$$

A typical plot of the isosteric heat of adsorption versus the fraction of the surface covered θ , on a **nearly homogeneous surface** is represented in Figure 1. The initial fall in the isosteric heats at **low coverage** is attributed to adsorption on heterogeneous⁵ patches of high interaction energy. If the interaction of the gas molecules with the surface is the only contribution to the isosteric heats, then the curve would be expected to drop as the high energy sites were filled and then level off as adsorption occurred on the predominate surface. As the number of adsorbed molecules increases however, there will be an increase in the isosteric heats due to adsorbate-adsorbate interactions. The counterbalancing of the adsorbate-adsorbate interactions by the adsorbate-adsorbent interactions results in a minimum in the isosteric heats at low coverages. The adsorbate-adsorbate interactions result in a maximum in the isosteric heat just before completion of the first layer. As the surface becomes covered with a layer of adsorbate, a second layer forms and the isosteric heats will then decrease below and finally

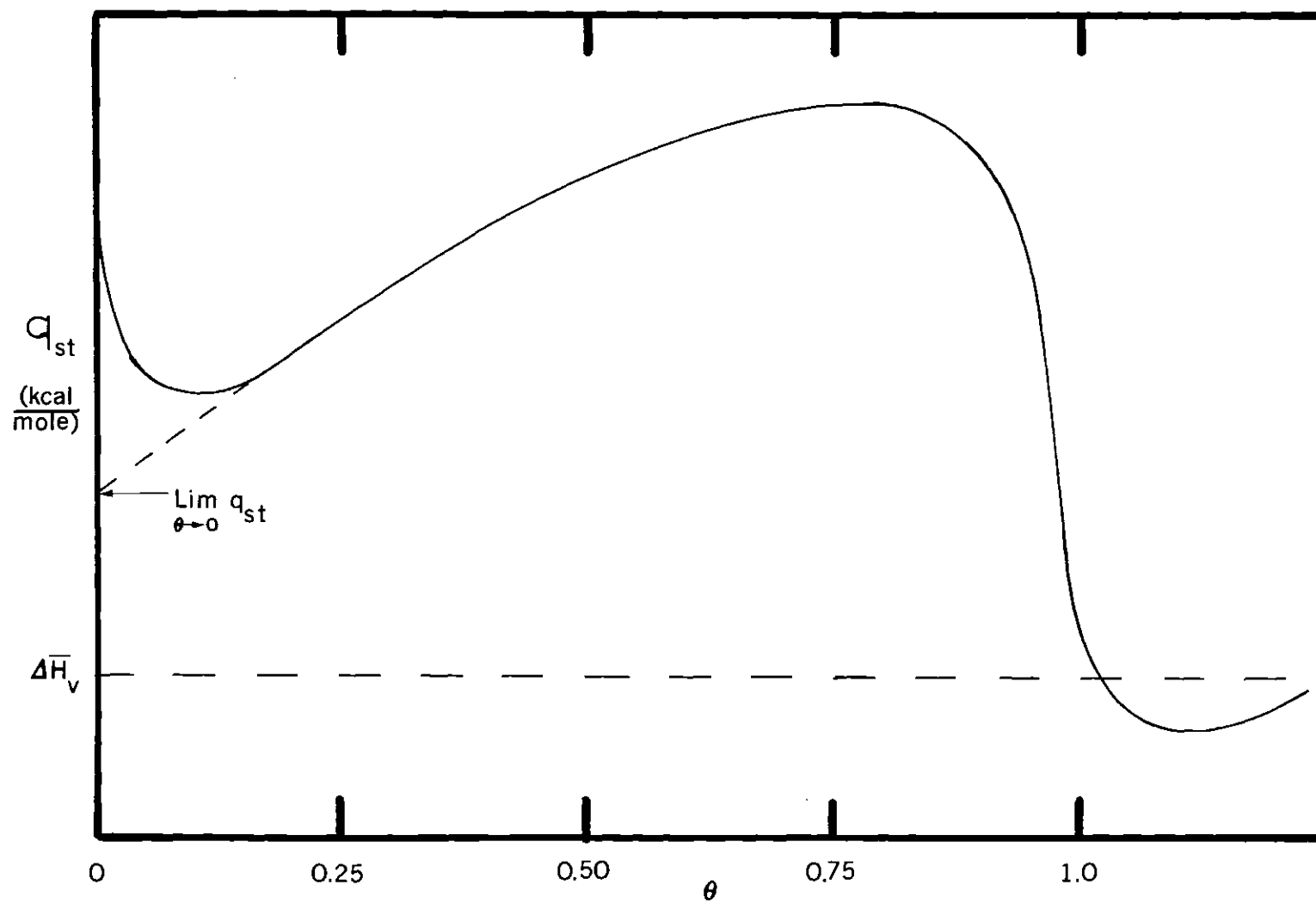


Figure 1. Typical Isosteric Heat Curve.

increase to the heat of vaporization of the adsorbate ΔH_v . For a system where the subsequent layers form stepped isotherms, the tail of the isosteric heat curve beyond $\theta = 1$ will form small maxima and minima about the heat of vaporization.

To relate the isosteric heats to the adsorption potential of equation (3) it is necessary to find the isosteric heats where the adsorbate-adsorbate interactions approach zero. This may be obtained by extrapolating the isosteric heat curve to $\theta = \text{zero}$, as shown by the dashed line in Figure 1. The basis for this linear extrapolation is given by Aston and coworkers⁶. This extrapolation assumes that the rising portion of the heat curve corresponds to adsorption on the predominant surface of the adsorbent, and that the rise is due to adsorbate-adsorbate interactions. From Figure 1, it can be seen that as the heterogeneity of the surface is decreased, a smaller extrapolation will be required and a more reliable result will be obtained.

By comparing equations (11) and (20), Young and Crowell³ have shown,

$$q_d = q_{st} - p \bar{V}_g + T(\partial p / \partial T)_{n_s, A_s, V_s} (\partial V_s / \partial n_s)_{A_s, T, P} \quad (23)$$

Assuming that the gas phase behaves ideally, so that $p \bar{V}_g = RT$ and that $(\partial V_s / \partial n_s)_{A_s, T, P} \approx 0$, then

$$q_d = q_{st} - RT \quad (24)$$

Therefore as θ approaches zero, the value of the isosteric heat of adsorption is related very nearly to the interaction energy of equation (3) by

$$q_{st \lim \theta \rightarrow 0} = E_{av.}^T + RT \quad (25)$$

The average energy of interaction $E_{av.}^T$, may be estimated from the potential of equation (3) and is discussed in Chapter VI.

Interaction Potential for Ionic Crystal Systems

One of the first investigations of the interaction of gases with ionic crystals was carried out by Lenel.⁷ The theoretical interaction energy for argon and krypton on potassium chloride was calculated from a potential of the form

$$u(\tilde{r}) = u_{dis} + u_{ind} \quad (26)$$

where u_{dis} was given by the London⁸ equation

$$u_{dis} = 3/2 \left[\frac{\alpha_E \alpha_J J_E J_J}{J_E + J_J} \right] r^{-6} \quad (27)$$

The terms α_E and α_J and J_E and J_J are the polarizabilities and characteristic energies of the adsorbed atoms and the ions of the crystal

respectively. The characteristic energies were taken to be the ionization potentials of the respective species. All of the polarizabilities and ionization potentials were taken from a compilation by Mayer⁹. The equilibrium distance r was simply estimated as one half the sum of the radius of the respective ion and one half the internuclear separation of the adsorbate atoms in crystalline adsorbate, since no repulsive potential was introduced explicitly. The radius of the ions was taken from Goldschmidt¹⁰, and the internuclear separation of the adsorbate atoms was determined from X-ray diffraction data.¹⁰ The maximum interaction energy due to the dispersion forces was obtained when the adsorbate atom was over the center of a lattice cell.

The inductive force was obtained from

$$u_{\text{ind}} = \int \frac{(P - P_0)^2 \rho_e}{J_E} d\tau \quad (28)$$

where P_0 is the potential field at the center of the adsorbate atom, P is the potential at a particular point, ρ_e is the electron density of the adsorbate, $d\tau$ is a volume element experiencing the potential P and the integration is over the entire adsorbate atom. The maximum interaction energy due to the induction force was found to be over the positive ion. Over the center of a lattice cell the inductive force was estimated to be 10-20% less than its maximum value. It is not clear from Lenel's paper how this estimate was obtained. Lenel assumed that the repulsive part of the potential was cancelled by the dipole-quadrupole interactions in the tail of the potential curve and thus

they were omitted in the calculations. Although close agreement with his experimental values was claimed, experimental isosteric heat curves were not reported and thus it is not possible to determine how the zero coverage isosteric heats of adsorption were determined. In those days, however, homogeneous surfaces were generally not available and his samples probably contained a large degree of heterogeneity.

A more detailed investigation of the interaction of argon, nitrogen and oxygen on potassium chloride was carried out later by Orr¹¹. A potential of the form of equation (3) was employed. The value of C^0 was determined from the Kirkwood-Müller¹² expression for the dispersion energy

$$\phi_A = \sum_i u_{i,\text{dis}} = - \left(\frac{\alpha_1 \alpha_2}{\alpha_1/\chi_1 + \alpha_2/\chi_2} \right) 6mc^2 \left(\sum_i r_i^{-6} \right) \quad (29)$$

where m is the mass of an electron, c is the velocity of light, r the interatomic distance and α and χ the polarizability and diamagnetic susceptibilities of the two species.

An exponential form was used for the repulsive part of the potential

$$\phi_R = \sum_i u_{i,\text{rep}} = B \sum_i \exp(-\beta r_i) \quad (30)$$

The constants B and β were determined from the data of Huggins and Mayer¹³ for the ions and Herzfeld¹⁴ for the adsorbates. The inductive

force was calculated from an expression, derived by Lennard-Jones¹⁵, for the electrostatic field over the sodium chloride surface

$$\phi_E = u_{i,ind} = -1/2(\alpha F_z^2) \quad (31)$$

where α is the polarizability of the adsorbate and F_z is the component of the electrostatic field perpendicular to the crystal surface. Equation (31) is based on the assumption that the adsorbate molecule can be considered as a polarizable point.

The total interaction was then given by

$$\phi_T = \phi_A + \phi_R + \phi_E \quad (32)$$

Summations were carried out over the 250 nearest ions and the remaining contributions were found by integration. Calculations were made for four possible adsorption sites; over a positive ion, over a negative ion, over the center of a lattice cell and over the mid-point of a lattice cell edge. The greatest interaction occurred in the case of adsorption over the center of a lattice cell. Orr compared this value of ϕ_T for adsorption over the center of a lattice cell, after correcting for the zero point energy, to his experimental values and found close agreement. Since Orr did not report his isosteric heat curves, it is not possible to determine how he obtained his zero coverage isosteric heats. As with Lenel's work, Orr's sample of adsorbent may have contained a large degree of heterogeneity.

The most detailed investigations to date on the adsorption of gases on ionic surfaces have been carried out by Hayakawa¹⁶⁻²⁰ in a series of papers. The interaction of argon, nitrogen, oxygen and carbon dioxide with the (100) face of cubic sodium chloride were investigated. The interaction energies were determined from equation (3), using equation (28) for the dispersion potential, equation (29) for the repulsive portion of the potential and equation (30) for the electrostatic potential. The constants of Mason and Rice²¹ for argon and nitrogen and the constants of Huggins and Mayer¹³ for the ions were used to calculate the values of B and β for the repulsive portion of the potential. In addition, Hayakawa determined the contributions to the total potential from the interaction of quadrupole moments of nitrogen and oxygen with the electrostatic field following the method of Drain²². Following Orr, summations were carried out over the 280 nearest ions and the remaining contributions were estimated by integration.

The total potential was given by

$$\phi_T = \phi_A + \phi_R + \phi_E + \phi_Q \quad (33)$$

where ϕ_Q is the quadrupole interaction contribution to the total potential. The same four adsorption sites considered by Orr were considered by Hayakawa. For sodium chloride, the greatest interaction was found to occur over the sodium ions. After correcting for the zero point energy, Hayakawa compared the potential obtained over the sodium ion to his experimental results and found close agreement. The experimental zero coverage isosteric heats were obtained by extrapolating to zero coverage

that portion of the isosteric heat curves attributed to heterogeneities. Extrapolation of the isosteric heat curves as discussed earlier predicts adsorption energies near zero. A value of zero for the adsorption energy would indicate that little if any adsorption actually occurred, and thus this extrapolation is probably meaningless. This may be attributed to the large degree of heterogeneity in the sodium chloride samples used by Hayakawa. The sodium chloride samples were prepared by precipitation from aqueous solutions and probably contained a large amount of adsorbed water.

Other investigations of this type have been carried out (see, for example, references 23 through 28), but the three just discussed illustrate the state of development of solutions to this problem.

Sublimation of Sodium Chloride

In most of the studies conducted on ionic crystals, the adsorbent was prepared by precipitation from an aqueous solution as was pointed out in the discussion of Hayakawa's work. Since sodium chloride readily retains water, this method of preparation probably results in imperfect surfaces contaminated with water. Removal of this adsorbed water requires heating at high temperatures, above 300°K, and this results in excessive sintering of the particles. Several authors²⁹⁻³² have reported the preparation of sodium chloride samples of large surface areas through a sublimation technique. McIntosh and co-workers^{29,30} were able to produce sodium chloride particles possessing a surface area of up to 80 m.²/gm. via sublimation. Electron microscopy investigations showed the particles to be primarily spherical but upon exposure to water vapor,

the particles readily changed to cubic. This was attributed to the hydration of the ions, thereby increasing their mobility, and allowing recrystallization of the sodium chloride particles.

Ross³³⁻³⁵ in a series of papers studied the adsorption of xenon methane, ethane and diborane on sodium chloride prepared and maintained under anhydrous conditions. In all cases two dimensional condensation was observed. This phenomenon is normally observed only on adsorbents possessing a highly homogeneous surface.

Other halides have been prepared by this method and have been found to be homogeneous. Larher¹ investigated the adsorption of argon, krypton and xenon on samples of NiCl_2 , CoCl_2 , FeCl_2 , CdCl_2 , CdBr_2 , CdI_2 and PbI_2 prepared by sublimation. The two dimensional condensation phenomenon was observed in all cases as well as distinct second and third layer steps in the adsorption isotherms. Although these are probably layered halides in the form of platelets, this was not confirmed since electron microscopy studies were not conducted. Thus it appears on the basis of these investigations that the sublimation method of preparing sodium chloride can produce a fairly homogeneous surface possessing a specific surface area sufficient for volumetric gas adsorption measurements.

CHAPTER II

EXPERIMENTAL

Adsorption Apparatus

The adsorption apparatus used in this study was a modified version of an existing standard volumetric gas adsorption apparatus.³⁶ Basically the apparatus is composed of two systems; the gas adsorption system and the temperature measurement and control system. The amount of gas admitted to and consequently adsorbed by the sample was measured in the gas adsorption system. The temperature of the sample was measured on a vapor pressure thermometer (VPT) and controlled by a cryostat. Thus a detailed description of the adsorption apparatus may be conveniently given in terms of these systems and is presented in the following sections.

Adsorption System

The gas adsorption system, shown in Figure 2, consists of three major parts; the vacuum system (VS), the pressure measuring system and the gas measuring and handling system.

A Model 1405 Welch vacuum pump coupled to a mercury diffusion pump constituted the means of evacuating the system. Both pumps were separated from the adsorption system by a cold trap surrounded by a dry ice-acetone bath. This system was capable of lowering the pressure to about 10^{-6} torr. In addition to this main pumping system, a secondary

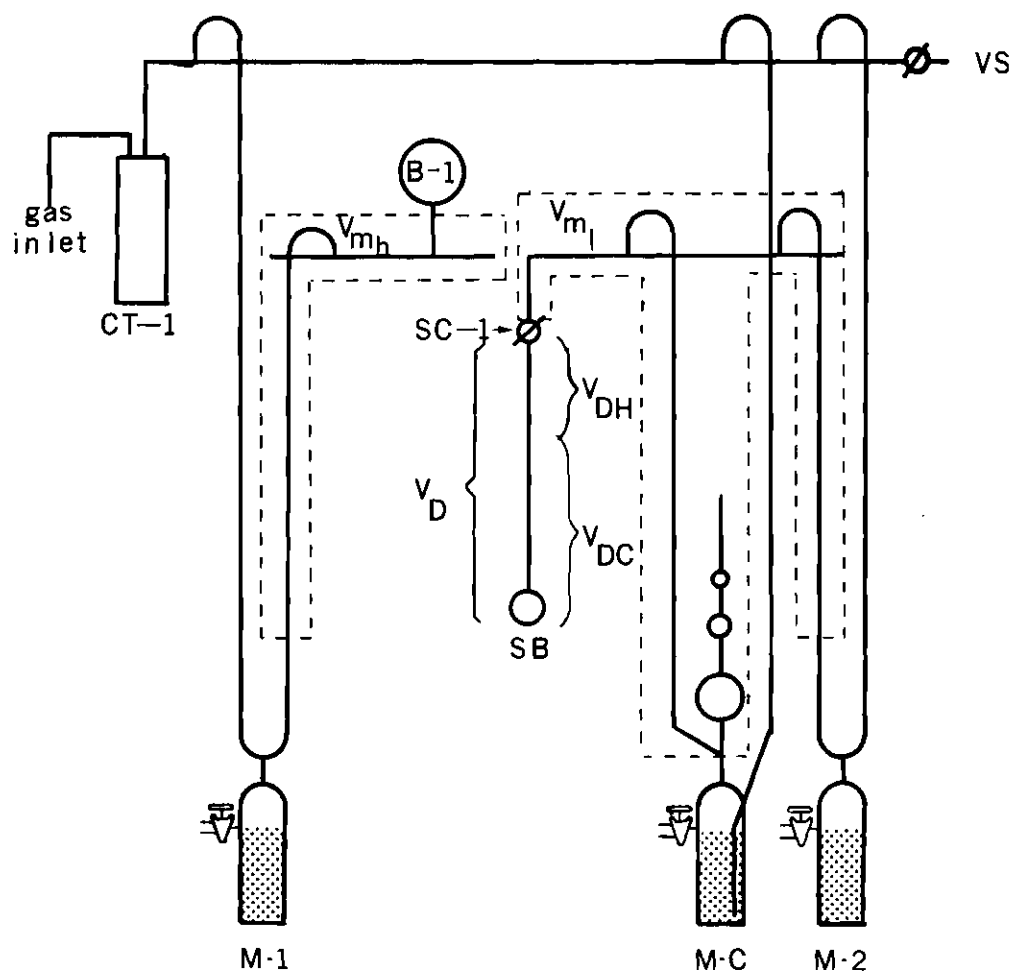


Figure 2. Schematic Diagram of Adsorption System.

pumping system was employed to adjust the mercury levels in the McLeod gauge and the various manometers.

The pressures in the system were measured in two ranges, zero to 28 torr and 28 to 760 torr. The range from zero to 28 torr was measured on a three stage McLeod gauge MC (Figure 2). This McLeod gauge was built and calibrated with mercury by Dr. B. W. Davis. The ranges of the respective stages are 10^{-4} to 0.2 torr for the first stage, 0.2 torr to 5 torr for the second stage and 5 to 28 torr for the third stage. The first two stages have a confidence limit of approximately ± 2.0 per cent and the third stage has a confidence limit of approximately ± 1.0 per cent.

Pressures in the range from 28 to 760 torr were measured on a U-tube mercury manometer M1 (Figure 2) with a confidence limit of approximately ± 1.8 per cent.

The gas handling system is composed of two parts, the low pressure side from 10^{-4} to 28 torr and the high pressure side from 28 to 760 torr. Adsorption measurements were first made on the low pressure side of the adsorption system and then the sample bulb SB (Figure 2) was transferred to the high pressure side.

Prior to making adsorption measurements, the volume of the adsorption system and the dead space of the sample bulb were determined by expansion experiments using helium gas (Matheson, high purity, 99.995% min.). Assuming ideal gas behavior, the manifold volume V_{m_1} (Figure 2) on the low pressure side was found by expanding the helium from the McLeod gauge of known volume into V_{m_1} . On the high pressure

side the manifold volume V_{m_h} (Figure 2) was obtained by expanding from the storage bulb B1 (Figure 2), of known volume, into V_{m_h} . The volume V_{m_l} included the McLeod gauge volume. The volume V_{m_h} did not include the storage bulb B1 volume, as it would result in too large a volume for the present purposes.

The dead space V_D (Figure 2) was calibrated at three temperatures, room temperature, hereafter denoted by T_a (the ambient temperature), liquid nitrogen (77°K) and dry ice temperatures (195°K). The dead space volume consists of two parts, the warm dead space V_{DH} and the cold dead space V_{DC} . These are related by

$$V_D = V_{DC} + V_{DH} \quad (34)$$

The dead space volume V_D was determined at room temperature by expansion of helium gas from V_{m_l} into $V_{m_l} + V_D$.

From the calibrations at liquid nitrogen and dry ice temperatures, the warm and cold dead space volumes were found by solving the simultaneous equations (which assumes a two temperature approximation)

$$V_{Deff} = V_{DH} + V_{DC}(T_a/T_{N_2}) \quad (35)$$

and

$$V_{Deff} = V_{DH} + V_{DC}(T_a/T_{CO_2}) \quad (36)$$

where, V_{Deff} is the effective dead space volume, T_{N_2} is the temperature

of liquid nitrogen and T_{CO_2} is the temperature of dry ice. The dead space volumes obtained in this manner had a standard deviation from the mean of ± 1.3 per cent.

Adsorption experiments were conducted in a similar manner on both the high and low pressure sides of the adsorption system. On the low pressure side, a dose of adsorbate, N_i , was admitted into V_{m_1} and its pressure was measured on the McLeod gauge. The stopcock SC-1 was then opened and the dose was admitted to the sample bulb. The adsorbate already in the sample bulb, N_{i-1} , both in the dead space and adsorbed on the adsorbent, was added to N_i . When equilibrium was obtained, the pressure was measured on the McLeod gauge and the amount of gas N_j , excluding the amount adsorbed, in the volumes V_{m_1} , V_{DC} and V_{DH} was determined by

$$N_j = (P/RT_a)(V_{m_1} + V_{DH}) + (P/RT_2)(V_{DC}) \quad (37)$$

where T_2 is the temperature of the sample bulb. The amount of gas adsorbed N_{ads} was then obtained from

$$N_{ads} = N_i + N_{i-1} - N_j \quad (38)$$

The stopcock SC-1 was then closed and the procedure repeated.

On the high pressure side, the same procedure was employed, except V_{m_1} was replaced by V_{m_h} and pressure measurements were made on a U-tube mercury manometer. There are two factors which have not been

discussed, thermal transpiration and non-ideal gas behavior. These will be discussed later in the Chapter.

The adsorbates, argon and nitrogen, were supplied by the Matheson Company in lecture bottles with the following minimum purities: argon, prepurified grade (99.998%) and nitrogen, prepurified grade (99.997%). To further insure the dryness of these gases as well as that of the helium gas used for calibration, they were passed through a cold trap CT-1 (Figure 2), prior to admitting them to the gas adsorption apparatus.

The Cryostat

Measurements of the adsorption of a gas by a solid in a gas volumetric assembly requires a constant controlled temperature about the adsorption sample bulb. In the range of liquid air temperatures, a constant temperature at the boiling point of nitrogen and oxygen is readily obtained by use of a bath of either liquid nitrogen or liquid oxygen respectively. For temperatures below the boiling points of these liquids, a cryostat (Figure 3) based on the principle of cooling by injection of helium gas³⁷ was constructed. Basically the temperature of the cryostat bath was obtained by adding a cryogenic liquid, either liquid nitrogen or liquid oxygen or a mixture of both to the dewar (D). Helium was then bubbled into the bath, causing the cryogenic liquid to boil quickly and thus lowering the temperature. When the desired temperature was obtained, as measured by the vapor pressure thermometer (VPT-B), the flow of helium was stopped. When the temperature began to rise, the flow of helium was again started.

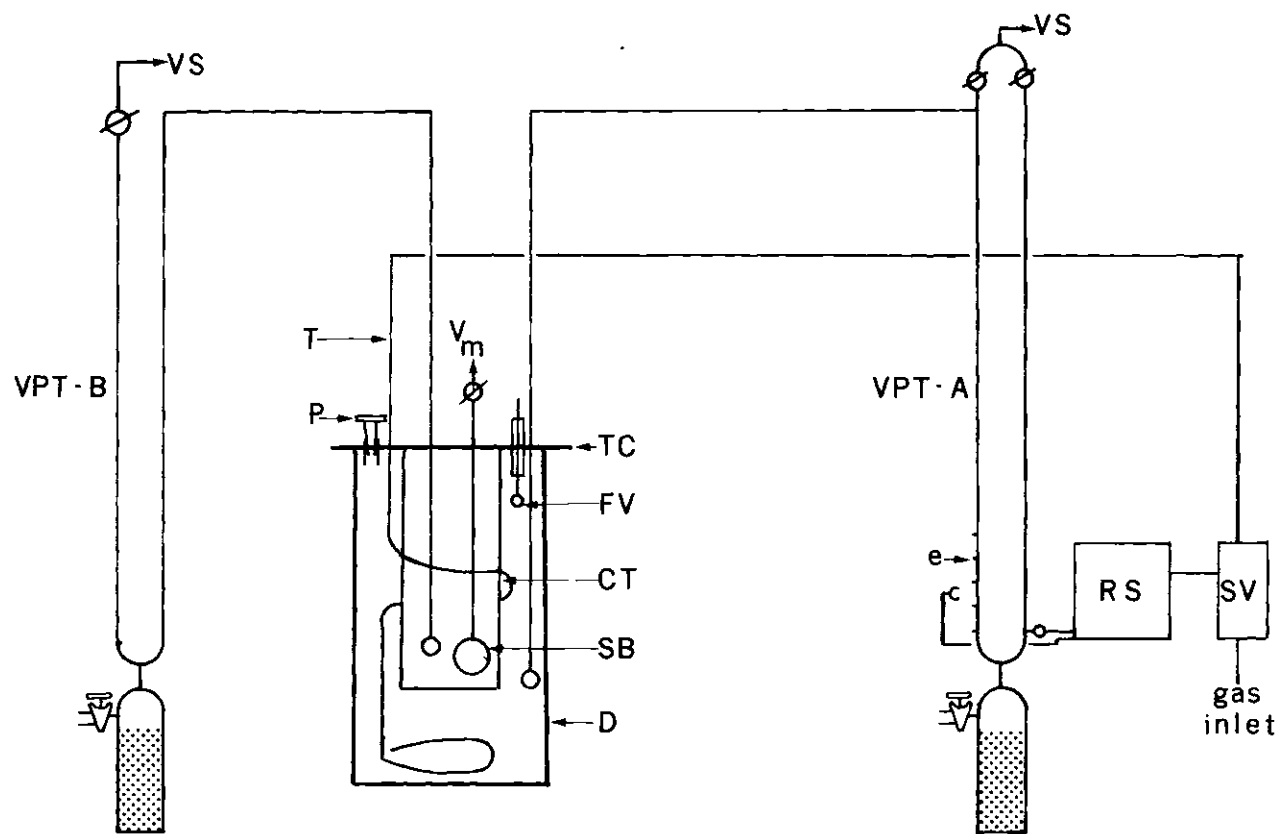


Figure 3. Schematic Diagram of Cryostat.

Automatic control of the temperature was achieved by use of a second vapor pressure thermometer (VPT-A), in conjunction with a relay switch (RS) and solenoid valve (SV). The thermometer VPT-A was constructed with an electrode mounted in the right hand side of the manometer which remained in constant contact with the mercury. On the left hand side, a series of five electrodes (e) were spaced five cm. apart to allow temperature control at several different temperatures by merely selecting a different probe and adjusting the overall mercury height.

The cryogenic bath consisted of a large dewar fitted with a 1/4 inch thick sheet of teflon as a cover (TC). Holes were drilled in the teflon cover, large enough to permit the adsorption sample bulb (SB), the VPT-A and VPT-B probes, the float valve (FV) and the helium supply line (T) to enter the bath. The excess space between the tubing of these probes and the teflon cover was packed with paper asbestos to maintain insulation of the bath. A teflon plug (P) was designed to seal off the entrance port after the cryogenic liquid was admitted to the bath.

A nine inch length of copper tubing (CT) with a wall thickness of 1/16 inch and an inside diameter of two inches was mounted around the adsorption sample bulb and the VPT-B probe. The void space in the copper tube was packed with glass wool and the bottom of the tube was covered with a copper mesh screen. This served to prevent the helium bubbles from coming in direct contact with the adsorption sample bulb and the VPT-B probe, thus preventing momentary supercooling and temperature fluctuations. The temperature of the system was measured on VPT-B. For liquid oxygen temperatures, the vapor pressure thermometers were

filled with oxygen, at liquid nitrogen temperatures and below, nitrogen was used, while at temperatures in between these two extremes, argon was employed.

Helium used in the cryostat was of high purity grade (99.995%) obtained from the Air Products and Chemicals Company. It was admitted to the bath through 1/4 inch O.D. copper tubing. The tubing made two complete loops in the bath thus allowing precooling of the helium before it was bubbled into the bath. The exhaust gases from the bath were forced through a 1/2 inch tygon tube which surrounded the helium delivery tube, thus allowing additional precooling of the helium. The end of the copper tube was sealed off thus forcing the bubbles out of 1/16 inch diameter holes drilled one cm. apart on the final loop of the copper tubing which rested near the bottom of the dewar.

For temperatures of 77.1°K and 90.1°K , liquid nitrogen and liquid oxygen baths respectively, were used alone, without helium injection. For temperatures below 77.1°K , liquid nitrogen was used and for the range between 77.1°K and 90.1°K , approximately equal volumes of liquid nitrogen and liquid oxygen were used with helium injection. After a cooling period of two hours, the bath was topped off with the cryogenic liquid. This caused a temporary rise in temperature which settled back to the desired temperature in about five minutes. The level of the bath was monitored by a float valve and it was found that the liquid level dropped by only one cm. after one half hour of operation. This cryostat enabled the control of temperatures between 70°K and 90°K with a precision of $\pm 0.01^{\circ}\text{K}$.

The temperature was determined from VPT-B by use of the Antoine

Equation

$$\log_{10} P = A - \frac{B}{C + t} \quad (39)$$

where, P is expressed in millimeters and t is in degrees Centigrade. The constants A, B and C were obtained from the TRC³⁸ tables and are tabulated in Table 1.

Table 1. Values of the Constants for the Antoine Equation

Gas	State	A	B	C
O ₂	liquid	6.69144	319.013	266.697
N ₂	liquid	6.49457	255.680	266.550
	solid	7.34542	322.222	269.980
Ar	liquid	6.61651	304.227	267.320
	solid	7.50581	399.085	272.630

Thermal Transpiration

The adsorption bulb is connected to the adsorption system via a glass tube which exists in two temperature extremes, room temperature and T₂, the temperature of the cryostat. This change in temperature creates a pressure gradient in the tubing. If the bore of the tubing is very much smaller than the mean free path of the adsorbate then the

pressure P_2 in the cryostated portion of the tube is given by³

$$P_2 = P_1 (T_2/T_1)^{\frac{1}{2}} \quad (40)$$

where P_1 is the pressure in the portion of the tube at room temperature.

On the other hand if the bore of the tubing is larger than the mean free path of the adsorbate, then P_2 is given by Maxwell's equation⁵

$$P_2^2 - P_1^2 = (C/d^2) (T_2^2 - T_1^2) \quad (41)$$

where d is the diameter of the tubing and C is a characteristic constant for each gas.

For the case where the bore of the tubing is of the same order of magnitude as the mean free path, an exact solution is not available. This is the situation normally encountered in physical gas adsorption experiments. Assuming that the gas molecules are hard spheres, whose size is temperature dependent and that they undergo no specular reflection off the walls of the tube, Weber³⁹ developed an equation for the thermal transpiration of a gas along a closed cylindrical tube

$$dP/dT = P/2T(\alpha y^2 + \beta y + u)^{-1} \quad (42)$$

where

$$y = d/\lambda \quad (43)$$

and P is the pressure, T the temperature, d the tubing diameter and λ the mean free path of the gas molecules. The coefficients are given by the relations

$$\alpha \approx \pi/128$$

$$\beta \approx \pi/12$$

$$u = (1 + gy)/(1 + hy)$$

$$g - h + \beta = 1 \text{ or } 3/4$$

$$g/h \approx 1.25$$

A useful approximate solution to Weber's equation has been developed by Miller⁴⁰

$$P_2 = P_1 \left[1 - \pi \{1 - (T_2/T_1)^{\frac{1}{2}}\} \right] \quad (44)$$

where

$$\pi = (0.0300y^2 + 0.245y + \frac{1 + 2.5y}{1 + 2y})^{-1} \quad (45)$$

and

$$y = d/\lambda = P_2 d \sigma^2 / 2.33T \quad (46)$$

where P_2 is in mm., σ is in \AA^0 , and $T = (T_1 + T_2)/2$. Values of σ as a function of T have been tabulated by Landolt and Bornstein.¹⁰

The equilibrium pressure of the adsorbate is then corrected for thermal transpiration and is denoted as P' . Equation (37) then becomes

$$N_j = (P/RT_a)(V_{m_1} + V_{DH}) + (P'/RT_2)(V_{DC}) \quad (47)$$

Non-Ideal Gas Behavior

At pressures below 760 torr, the ideal gas approximation is reasonable for the gases, argon and nitrogen, at room temperature. However, at low temperatures, such as those near the boiling point of liquid nitrogen, this approximation is not valid. Therefore a correction must be made for the non-ideal gas behavior in the cold dead space volume V_{DC} . This correction is made by use of the pressure virial equation of state, truncated after the second term

$$V = (NRT/P)(1 + P B'(T)) = V^{id}(1 + P B'(T)) \quad (48)$$

where $B'(T)$ is the second pressure virial coefficient and V^{id} is the ideal gas volume.

The term $B'(T)$ is related to the volume virial equation of state's second coefficient by

$$B'(T) = \frac{B(T)}{RT} \quad (49)$$

Therefore equation (47) becomes

$$V = V^{id} (1 + P B(T)/RT) \quad (50)$$

Values of $B(T)$ were determined from the tables of Hirschfelder, Curtiss and Bird⁴¹. Applying this correction to equation (47) yields

$$N_j = (P/RT_a)(V_{m_1} + V_{DH}) + (P'/RT_2)(V_{DC}^{id}(1 + P'B(T)/RT_2)) \quad (51)$$

Sample Preparation

The sodium chloride sample was prepared in the apparatus shown in Figure 4. The 14 inch long tube (QT) containing the sublimation boat was made of Quartz tubing with an O.D. of 1-1/6 inches and an I.D. of 7/8 inches.

Dry nitrogen, further dried by passage through a dry ice-acetone bath (CT) was used as the carrier gas. The flow rate of the nitrogen was measured on a Matheson Mounted, single tube Flowmeter (FM), series 620.

The collection bulb was designed with a coarse frit (CF) on top to allow passage of the carrier gas out of the system. The sublimated salt collected at both the top and bottom frits. The sample bulb had a medium size frit (MF) to enable the adsorbate gases to be admitted to the sample, after the sample bulb was connected to the adsorption system. In the tubing directly beneath the medium frit a break seal (BS) was employed to prevent the sample from coming into contact with the atmosphere. The salt collected at the top frit was gently loosened by

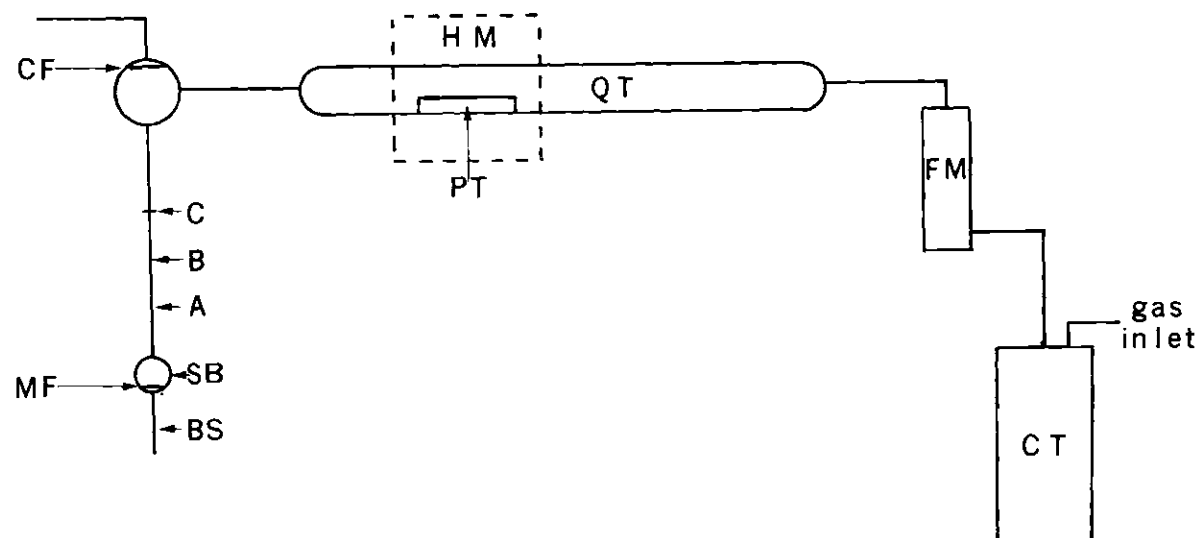


Figure 4. Schematic Diagram of Sublimation Apparatus.

vibration and collected in the sample bulb (SB). When the sample bulb was filled, it was sealed off with a torch at point A and transferred to the gas adsorption system. When secured to the gas adsorption system, the break seal was broken by a glass encased magnet. After removing the sample bulb, a small sample of salt was collected in the tube from point A to point B for electron microscopy studies.

An O-ring seal was employed at point C to enable the collected sodium chloride to be weighed. The entire adsorption bulb was then weighed both before and after the sample was collected.

The fused salt was placed into a platinum boat (PT) for sublimation. Other materials such as quartz, porcelain or stainless steel were unsatisfactory for the boats due to the corrosive nature of molten sodium chloride. The sublimation temperature was obtained by use of a heating mantle (HM) and was monitored on a Rustrak Model 122 Recording Pyrometer, serial number 10060, with an accuracy of $\pm 16^{\circ}\text{C}$.

Approximately five grams of sodium chloride, Fisher Certified ACS Biological Grade, was placed in the platinum boat and fused at 900°K in an air atmosphere. The platinum boat containing the fused sodium chloride was then loaded into the quartz tube. After assembly of the apparatus, the sodium chloride was outgassed at $300 \pm 10^{\circ}\text{C}$ for 24 hours in vacuo.

The sample temperature was then raised to $916 \pm 16^{\circ}\text{C}$ and the carrier gas was passed over the boat at a rate of 1-1/2 liters per minute. A total of 2.4213 grams of sodium chloride was collected after 72 hours of operation.

CHAPTER III

CHARACTERIZATION OF THE SAMPLE

The sodium chloride particles obtained from sublimation were characterized by several experimental techniques. Initially the sample was examined by electron microscopy, electron diffraction and gas adsorption studies. In order to conduct successive gas adsorption experiments it is necessary to properly outgas the sample before each isotherm. This involves heating and pumping, which may cause some sintering of the particles. To bring the sample to a constant surface area, the sample was placed under 550 torr of nitrogen and heated at $300 \pm 10^{\circ}\text{C}$ for 120 hours. A nitrogen atmosphere was employed, since Grinberg⁴² has shown that sodium chloride sinters to a lesser extent when it is in the presence of nitrogen gas. An argon isotherm was then determined on the heat treated sample. The isotherm showed a reduction in surface area for the sample and a small reduction of the concave portion of the low pressure region. Dividing the change in surface area, resulting from the heating process, by the total time of heating indicated a rate of reduction in surface area of $7.5 \times 10^{-3} \text{ m}^2/\text{gm per hour}$. To determine whether additional heating would have an effect on the sodium chloride sample, it was again placed under 550 torr of nitrogen and heated at $300 \pm 10^{\circ}\text{C}$ for 24 hours. A subsequent argon isotherm showed a reduction in surface area, but no shape change in the isotherm. The rate of reduction in surface area resulting from this second heat

treatment was $8.3 \times 10^{-3} \text{ m}^2/\text{gm}$. Thus it appears that the rate of reduction of surface areas is comparable for the first and second heat treatments. Nitrogen adsorption measurements were carried out on the untreated sample and on the doubly heat treated sample to determine the surface areas. Electron microscopy and electron diffraction studies were then conducted on the doubly heat treated sample. This doubly heat treated sample was used for all the adsorption experiments in the present study. The results of these investigations will now be discussed in subsequent sections.

Electron Microscopy

Transmission electron micrographs on both the untreated and the doubly heat treated samples were made on a Phillips EM-200 electron microscope. Special procedures were employed in handling and loading the samples into the microscope to prevent contamination by water vapor. The electron microscope grids were prepared in a dry box under a positive pressure of dry nitrogen. A glove bag was used to load the grid into the electron microscope. The untreated sample was found to consist of primarily spherical particles (Figure 5a). It was not possible to make micrographs of the smaller particles, as they readily evaporated when exposed to the electron beam. It was also found, as reported by other authors²⁹⁻³², that the particles converted to cubes upon exposure to water vapor. The smaller particles were converted in a few minutes whereas the larger particles required several hours exposure.

In an attempt to estimate the surface area of the untreated sample, the particles were assumed to be spherical and the diameters (d_1) of 75

particles were measured. The surface area S was then determined from

$$S = (6/\rho) \sum_i d_i^3 / \sum_i d_i^2 \quad (52)$$

where ρ is the density of sodium chloride, assumed to be 2.165 gm./cm.³ and the summation is over all the particles. This procedure gave a surface area of 5.0 m²/gm. As will be discussed later this specific surface area is somewhat lower than that obtained from adsorption experiments. This is probably due to the fact that the smaller particles evaporate in the electron beam and thus they were not observed on the micrographs. Because of the unreliability of the microscopy results for sodium chloride, it was not deemed worthwhile to carry out a surface area determination of the doubly heat treated sample.

Electron micrographs of the doubly heat treated sample showed the particles to be somewhat spherical with some flattened sides (Figure 5b). In order to obtain a perspective view of the particles, micrographs were taken on a Cambridge Steroscan Mark II scanning electron microscope. Although the resolution of this microscope is only of the order of 200Å⁰, the micrographs (Figure 5c) confirm that the particles are roughly spherical. Some linking of the particles is also observed. The photos in Figure 5c form a stereo picture. This stereo picture may be seen by looking at the mid point between the photos and adjusting the distance between the eye and this point, until the images can be allowed to drift together.

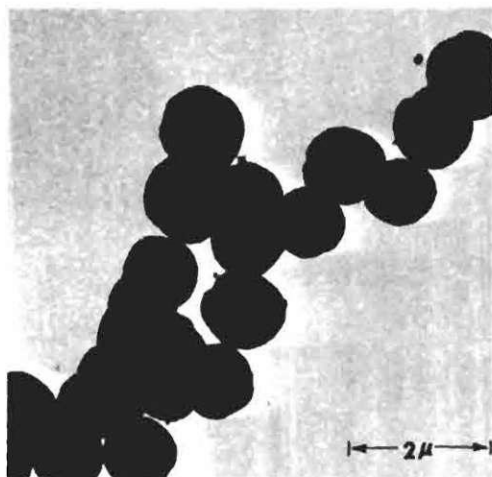


Figure 5a. Untreated NaCl

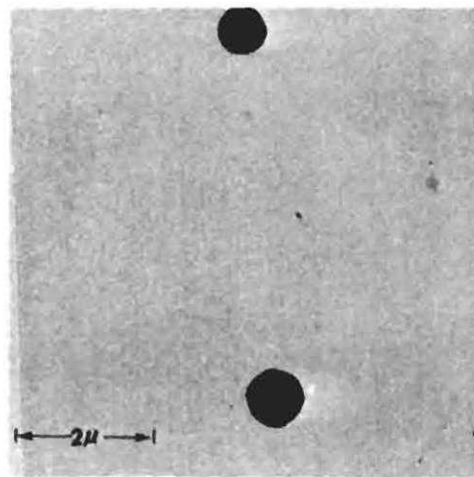


Figure 5b. Doubly Heat Treated NaCl

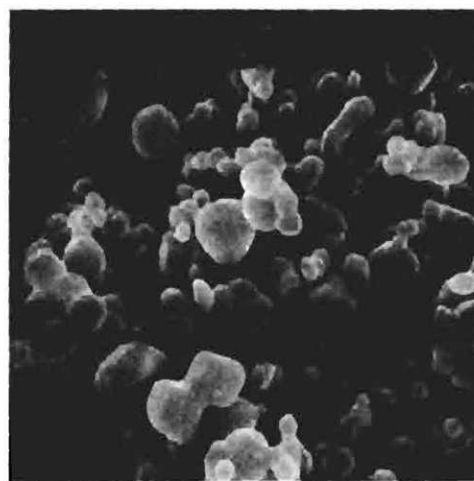
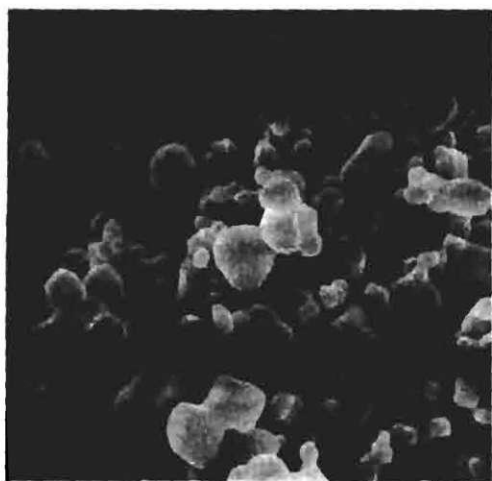


Figure 5c. Stereo Scanning Electron Micrograph of Doubly Heat Treated Sodium Chloride.

Electron Diffraction

Electron diffraction patterns of the freshly prepared untreated samples revealed no distinctive rings or spots (Figure 6a). This is normally indicative of an amorphous material.

Diffraction patterns on the doubly heat treated sample, however, showed the characteristic rings of crystalline sodium chloride (Figure 6b). The eight rings of the pattern, from the center of the pattern outward, have been identified with the following sodium chloride reflections: (111), (200), (220), (311), (222), (400), (420) and (422). The lattice cell constant was calculated to be $5.63 \pm 0.02 \text{ \AA}$ which is in close agreement with the reported value of 5.6402 \AA .⁴³ The electron diffraction pattern of the doubly heat treated sample was calibrated with the electron diffraction pattern of MgO. For MgO there was an increase of only 0.003% in the camera constant in going from the center ring to the outer ring of the pattern. In the interpretation of the sodium chloride rings, the camera constant was taken as that calculated for the MgO ring nearest to the sodium chloride ring of interest.

X-Ray Emission Electron Microprobe Analysis

The sodium chloride used in the sublimation process was Fisher Certified ACS Biological Grade. The impurities present in the sodium chloride, as listed by the supplier are shown in Table 2.



Figure 6a. Diffraction Pattern of the Untreated Sample



Figure 6b. Diffraction Pattern of the Doubly Heat Treated Sample.

Table 2. Impurities in Fisher Certified ACS Biological Grade Sodium Chloride by % Weight.

Insoluble Materials	HCl	Br	I	Ba	Fe	K	NO ₃
.004	.002	.005	.001	.001	.0001	.002	.003

An electron microprobe analysis was performed of the doubly heat treated sodium chloride with an Electron Probe X-Ray Microanalyzer (Acton Laboratories, Model MS 64). The entire range of the periodic table from boron on up was scanned. With the exception of sodium and chlorine, only oxygen was detectable within the limits of detection. These limits are 0.01 per cent for elements lighter than sodium and between 0.001 and 0.0001 per cent for elements heavier than sodium. Since standard samples of sodium chloride with known amounts of oxygen present were not available, it was not possible to calculate the exact amount of oxygen present in this sample. However, the amount of oxygen was estimated to be less than one per cent.

The source of oxygen was probably due to water vapor. Although special techniques could be employed in handling the sample for electron microscopy and diffraction work, it was necessary for electron probe analysis to expose the sample to the atmosphere for a period of several hours.

A standard sodium chloride crystal prepared by the Physical Sciences Division of the Engineering Experiment Station at the Georgia

Institute of Technology was compared to the doubly heat treated sample to confirm the sodium and chlorine stoichiometry. Taking the sodium to chlorine ratio of the standard as unity, the sodium to chlorine ratio of the doubly heat treated sample was found to be 1.000 ± 0.001 . Thus it may be concluded that the sample has the same stoichiometry as the standard crystal.

Adsorption Experiments

The bulk of the physical gas adsorption experiments will be discussed in Chapter IV, but some of the results are discussed here as they provide some insight as to the nature of the sublimated sodium chloride particles.

An argon and a nitrogen isotherm at liquid nitrogen temperatures were determined on the untreated sodium chloride sample. The monolayer capacities N_m and the surface areas S , calculated from the N_m are shown in Table 3.

The monolayer capacity of the nitrogen isotherm was estimated from the BET equation in the form

$$\frac{x}{N_{ads}(1-x)} = \frac{1}{CN_m} + \frac{1}{N_m} \quad (53)$$

$$x = P/P^0$$

where P is the pressure, P^0 the vapor pressure of the adsorbate at the temperature of the isotherm, N_{ads} the number of micromoles of adsorbate adsorbed at pressure P and N_m the monolayer capacity. For nitrogen the

plot of equation (53) was found to be linear in the region from $x = 0.01$ to $x = 0.12$. The surface area S was found from

$$S = (N_m)(\sigma)(N^0) \quad (54)$$

where σ is the cross sectional area of nitrogen, assumed to be 16.2 \AA^2 and N^0 is Avogadro's number.

The argon isotherm, however, did not fit the BET equation. The monolayer capacity, therefore, was determined by the point B method. This was accomplished by visually locating the point where the linear portion of the isotherm deviated from linearity just above the "knee" of the isotherm. Using the value of S obtained from the nitrogen isotherm, the value of σ was then calculated for the argon molecules. The results are shown in Table 3. Using the point B method for the nitrogen isotherms gave surface areas which differed by only $\pm 0.02 \text{ m}^2/\text{gm}$ from the BET surface areas. Since these are approximately the same, only the BET nitrogen surface areas will be considered further.

A second argon isotherm was determined on the sample after the first heat treatment. Assuming the value of σ for argon as determined by the first argon isotherm, the surface area was determined by the first argon isotherm, the surface area was determined and is shown in Table 3.

After the final heat treatment, a third argon and a second nitrogen isotherm were determined. The monolayer capacities and surface areas determined are listed in Table 3. The argon isotherms were then visually scaled so as to superimpose the low pressure portion of the isotherms

(Figure 7). The scaling factors (Table 4) are favorably comparable to the ratio of the BET nitrogen surface areas for both the untreated and the doubly heat treated sample (Figure 8). The decrease in surface area due to heat treatment amounted to approximately 16 per cent.

This reduction in surface area is considerably smaller than that observed by McIntosh.³⁰ In his studies on sublimated sodium chloride particles, McIntosh found the surface area to decrease by 42%, when the sample was heated at 55°C in the presence of 2.8 torr of water vapor for 128 hours. He found that further heating under these conditions for up to 272 hours resulted in no further change in the surface area. However, increasing the water vapor pressure to 5.9 torr, resulted in an additional decrease in surface area to 48% of the original area. Thus it appears that the presence of water vapor plays an important role in the sintering of sodium chloride. Since the sample in the present study was excluded from water vapor, its relatively smaller reduction in surface area upon heating is consistent with the results of McIntosh.

Table 3. Results of Argon and Nitrogen Isotherms on the Treated and Untreated Sample.

Gas	Sample	T (°K)	N _m (μ mole/gm)	(A° ²)	S (M ² /gm)	
					Equation (54)	Equation (52)
Ar	untreated	77.1	71.8	15.7	6.8	5.0
	1st treatment	77.2	62.9	15.7	5.9	
	2nd treatment	77.1	60.3	15.7	5.7	
N ₂	untreated	77.3	69.6	16.2	6.8	5.0
	2nd treatment	77.1	58.6	16.2	5.7	

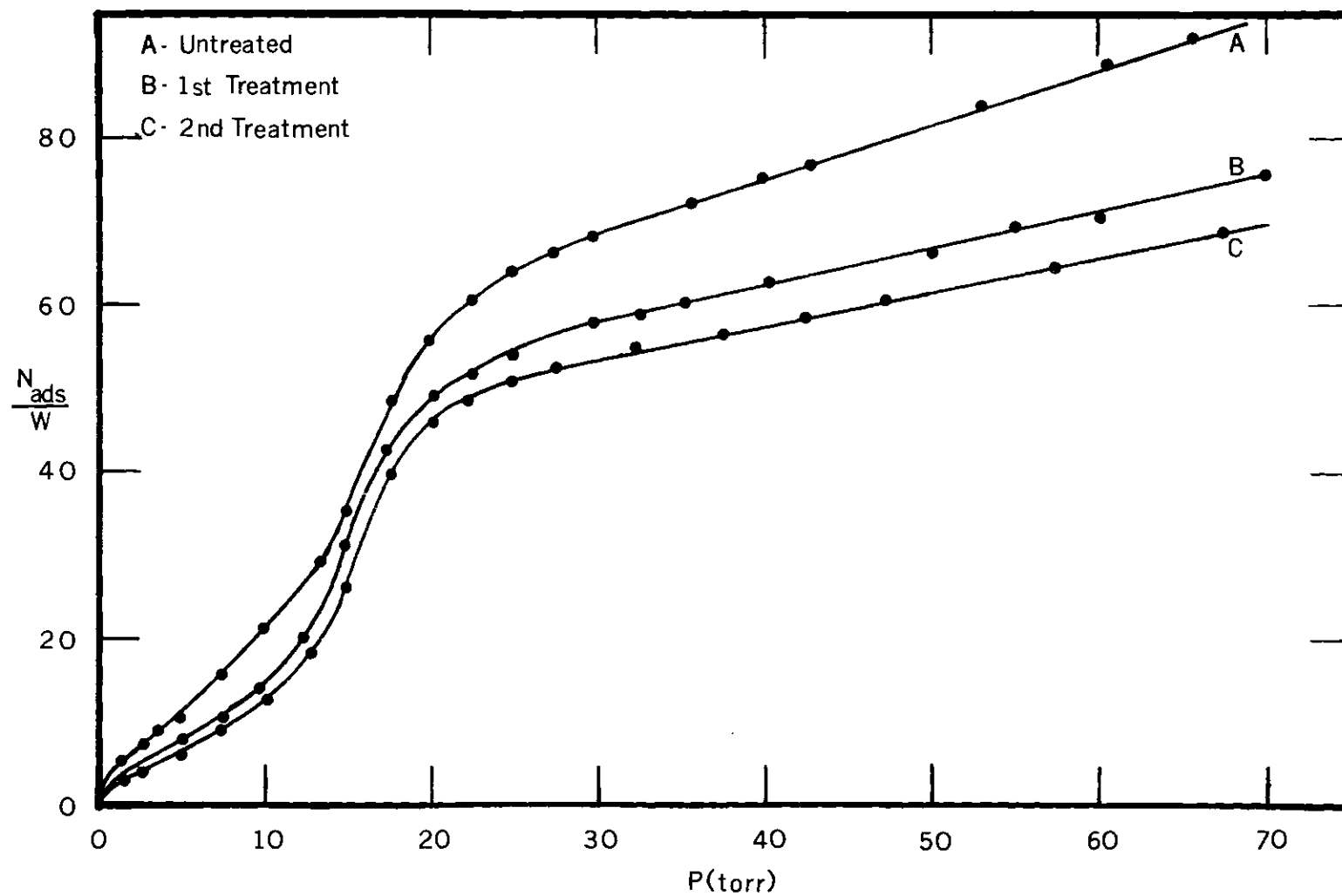


Figure 7. Isotherms of Argon on NaCl at 77°K.

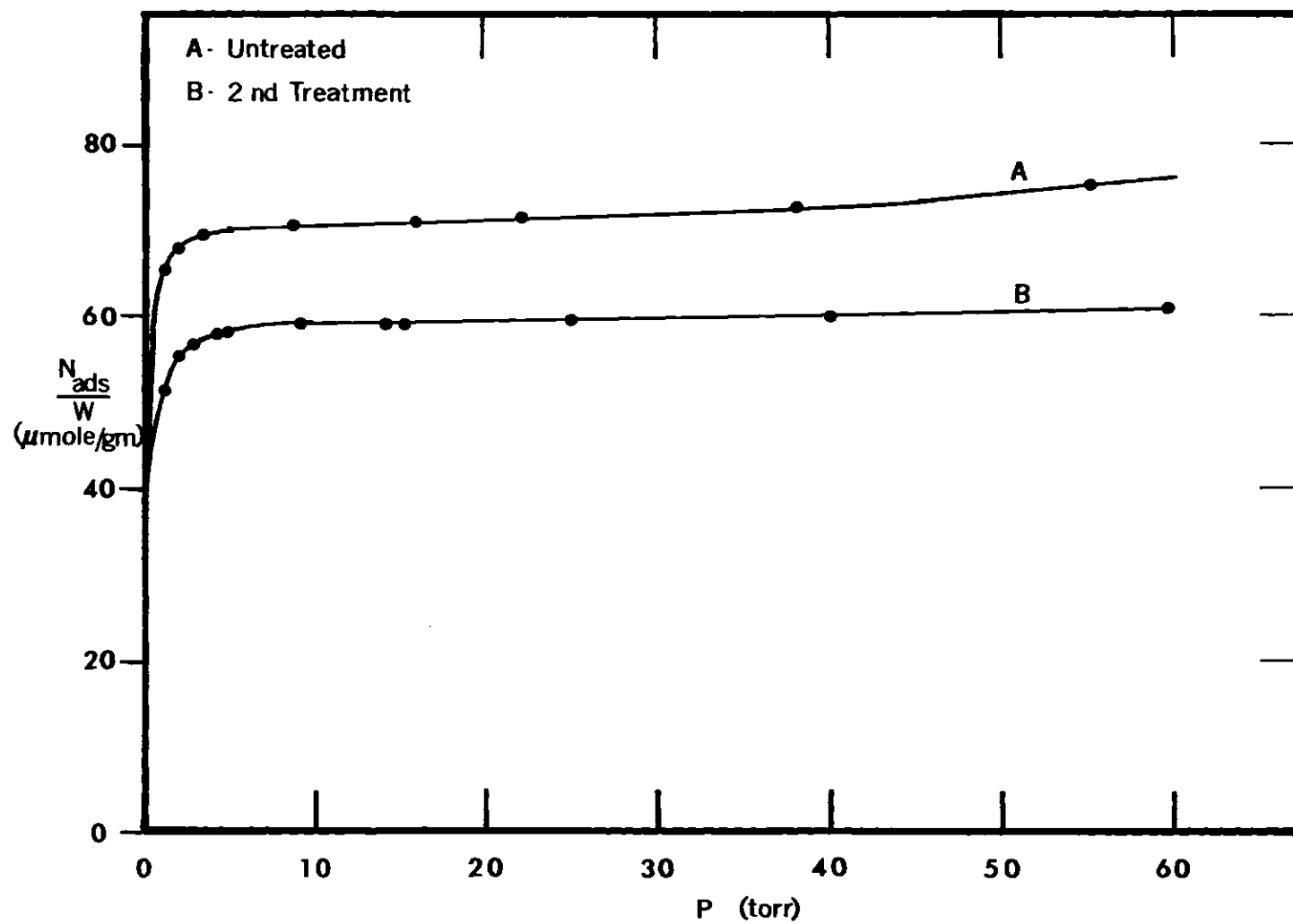


Figure 8. Isotherms of Nitrogen on NaCl at 77°K.

Table 4. Scaling Factors for Argon Isotherms and the Ratio of the Nitrogen Surface Areas.

Argon Isotherms	Scaling Factor	Ratio of Nitrogen Surface Areas
1st - 2nd	1.141	1.189
1st - 3rd	1.191	
2nd - 3rd	1.084	

If localized adsorption occurred for the nitrogen molecules on the (100) plane of the sodium chloride particles, then two nitrogen molecules could occupy one lattice cell having a lattice cell edge length of 5.64 \AA . The area of a lattice cell is 31.8 \AA^2 , therefore, the nitrogen molecules would each occupy 15.9 \AA^2 . Using this area for the value of σ for nitrogen would decrease the areas reported in Table 3 by 1.8 per cent. Since this reduction is insignificant, it will not be considered further.

Discussion

From the results of the electron microscopy and diffraction studies on the untreated sample, it appears that the nearly spherical particles are amorphous. This is in agreement with the results of Kerker³², who found the spherical particles obtained from sublimation gave no diffraction patterns; however after exposure to water vapor, he observed a sharp diffraction pattern characteristic of crystalline sodium chloride.

After the final heat treatment, the particles remained somewhat

spherical; however, some flattened faces were observed. The diffraction patterns clearly showed the sharp distinctive rings of crystalline sodium chloride. It is possible that these particles are composed of micro-crystals of sodium chloride. If this were the case, then it would be difficult at best to determine which crystalline plane or planes compose the surface of the particles. A site energy distribution analysis was made on the doubly heat treated sample, and the results indicate that the surface is nearly homogeneous. Thus it may be concluded that predominately one crystal plane is exhibited on the surface of the particles although this is not apparent from the micrographs. Details of the site energy distribution analysis are given in Chapter V.

The close agreement between the scaling factors for the argon isotherms and the ratio of the surface areas as determined from the nitrogen isotherms, lends support to the conclusion that the surface area is reduced by 16% upon heat treatment.

An interesting feature of both the argon (Figure 7) and nitrogen (Figure 8) isotherms is the lack of multilayer structure. This is in agreement with the work of others on the alkali halides.^{25-27, 33-35} The discrepancy between the surface areas obtained from the nitrogen isotherms and from the electron micrographs is attributed to the evaporation of the smaller particles when subjected to the electron beam.

The small change in the shape of the argon isotherms upon going from the untreated to the doubly heat treated sample, in the low pressure regions is attributed to a decrease in high energy sites upon heating. These sites may be either face defects or different crystal faces or a combination of both. Since all the isotherms discussed in this Chapter

were conducted on the high pressure side of the adsorption system, the structure of the low pressure regions of the isotherms cannot be given too much weight because of a lack of precision in the pressure measurements. On the high pressure side of the adsorption system, a pressure of 10 torr has a precision of $\pm 2\%$, while a pressure measurement of one torr has a precision of $\pm 20\%$.

CHAPTER IV

EXPERIMENTAL RESULTS

Adsorption isotherms for the argon-sodium chloride and the nitrogen-sodium chloride systems were conducted at four temperatures on the doubly heat treated sample. Additional isotherms at liquid nitrogen temperature, which followed the change in the surface of the sodium chloride during heat treatment were discussed in Chapter III. The experimental data for all isotherms is presented in Appendix A. Plots of the four argon and four nitrogen isotherms on the doubly heat treated sample are presented in Figures 9 through 16. The data is plotted as micromoles per gram (N_{ads}/gm) versus pressure P (torr).

The monolayer capacity of the nitrogen isotherms was determined from equation (53) using the BET method. The monolayer capacity of the argon isotherms was determined by the visual point B method. The surface area was determined at four temperatures, from the nitrogen isotherms using equation (54) repeated here for convenience

$$S = (N_m)(\sigma)(N^0) \quad (54)$$

Using the surface areas determined from the nitrogen isotherms, the value of σ (the cross sectional area) for argon at the four isotherm temperatures were determined. This was accomplished by using equation (54) in the form

$$\sigma = S / (N_m) (N^0) \quad (55)$$

The results are given in Table 5.

Table 5. Isotherm Data Based on $\sigma_{N_2} = 16.2A^{\sigma^2}$

Gas	T (°K)	N_m ($\frac{\mu\text{moles}}{\text{gm}}$)	σ (A^{σ^2})	$\frac{S}{m^2}$ ($\frac{\text{gm}}{\text{gm}}$)
Ar	72.14	60.4	15.7	5.7
Ar	77.12	60.3	15.4	5.6
Ar	82.88	60.0	15.5	5.6
Ar	89.96	60.8	15.6	5.7
N ₂	72.12	57.9	16.2	5.7
N ₂	77.11	57.6	16.2	5.6
N ₂	82.88	57.8	16.2	5.6
N ₂	90.07	58.8	16.2	5.7

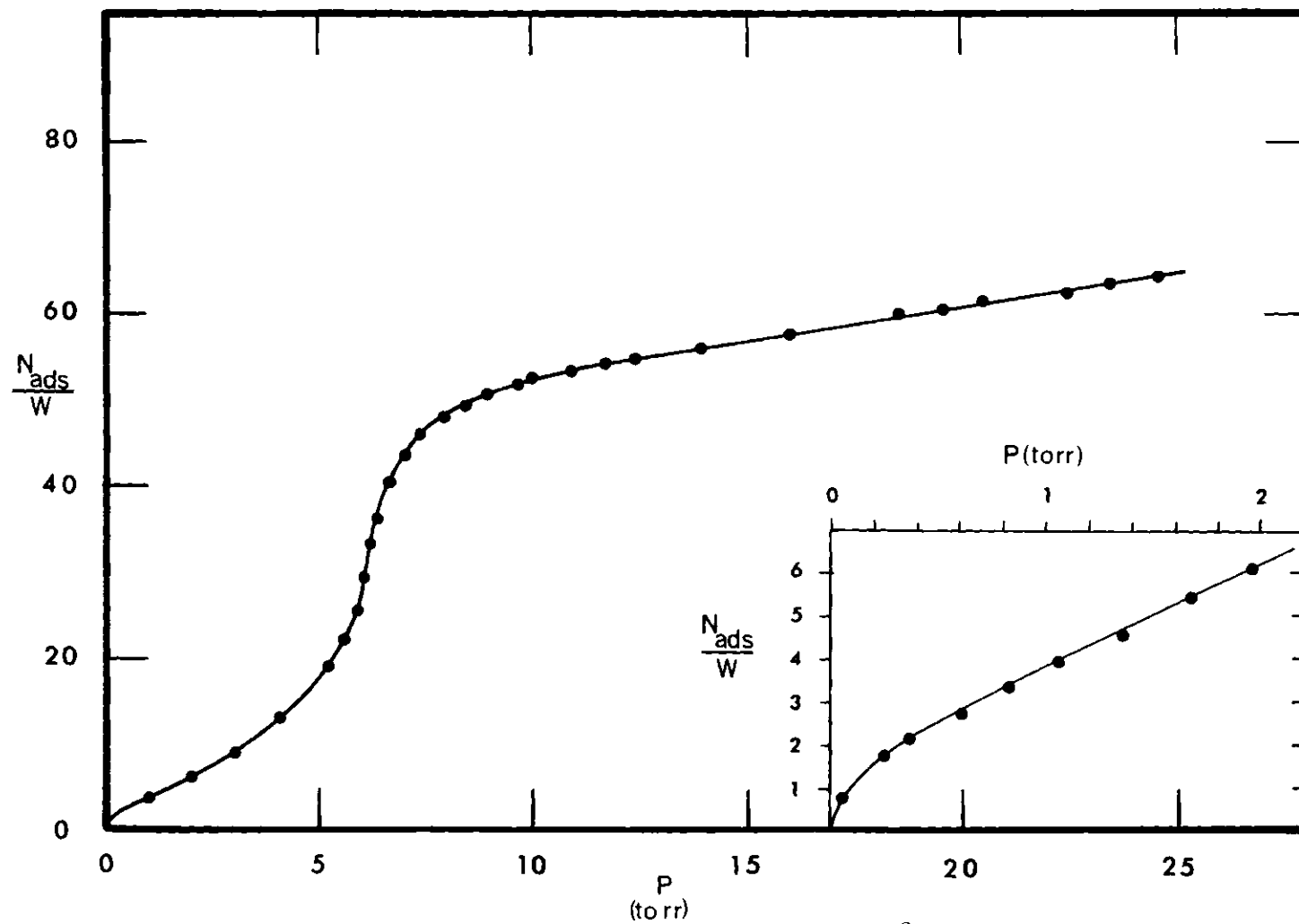


Figure 9. Argon Isotherm on NaCl at 72.14°K.

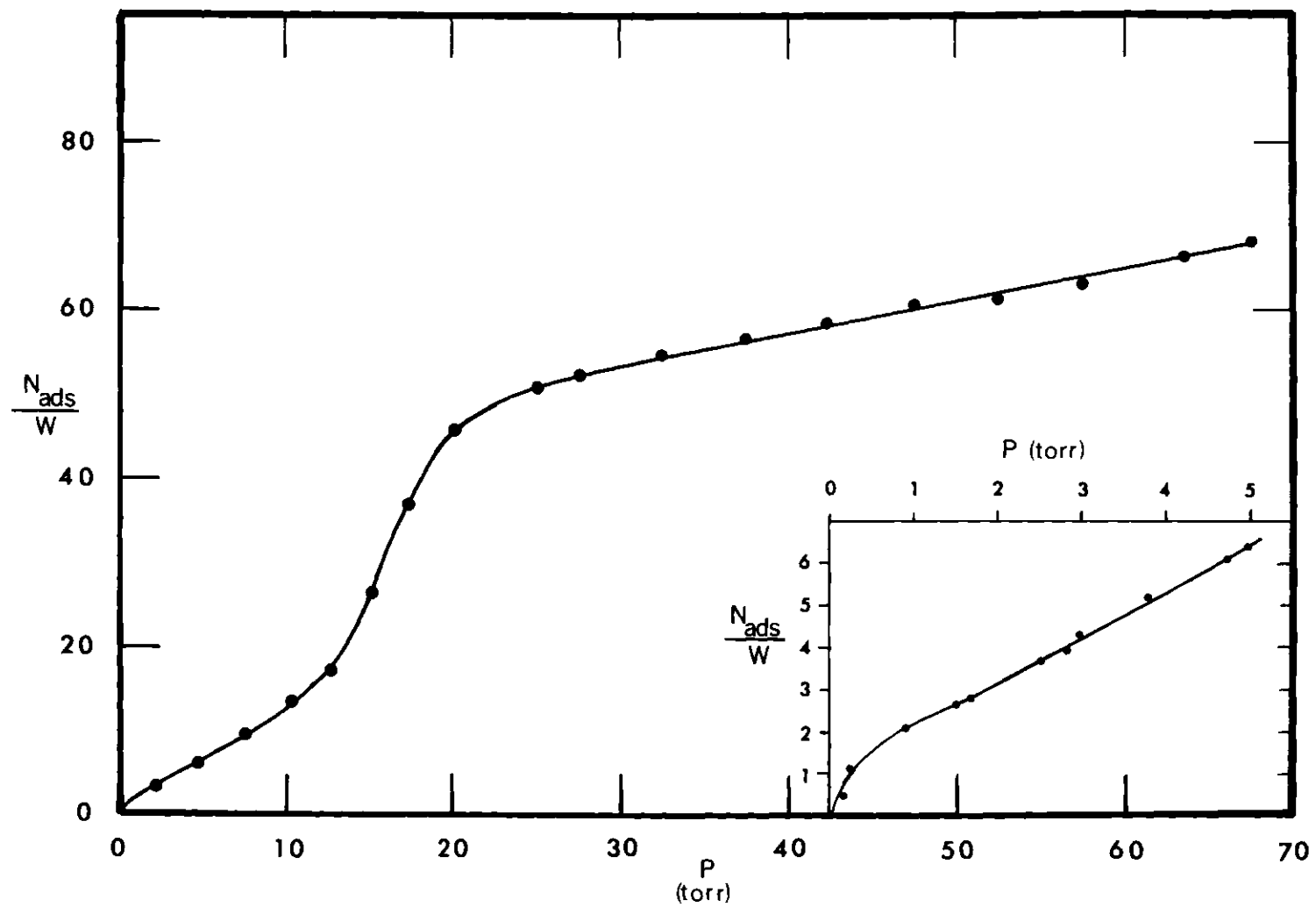


Figure 10. Argon Isotherm on NaCl at 77.12°K

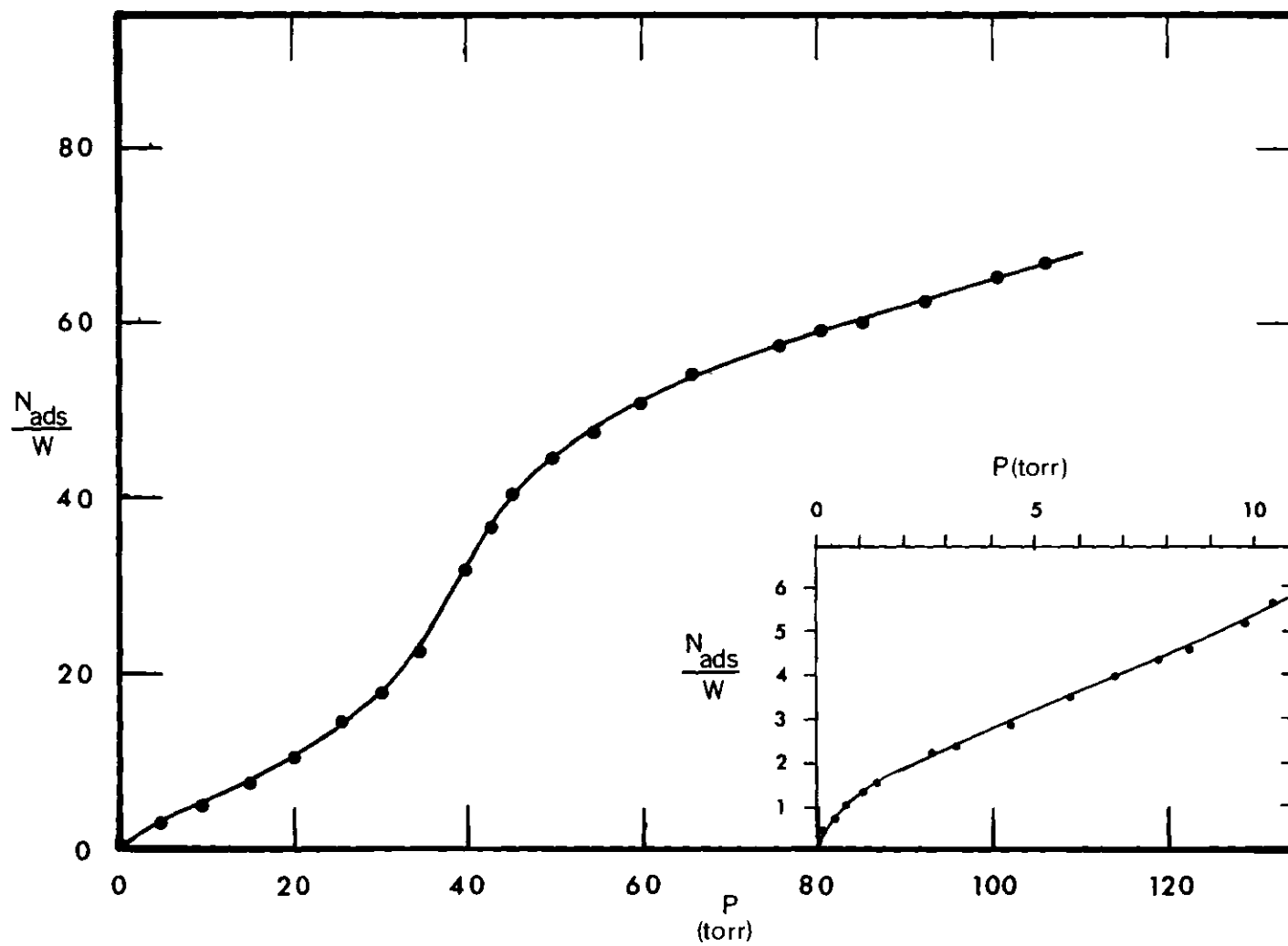


Figure 11. Argon Isotherm on NaCl at 82.88°K.

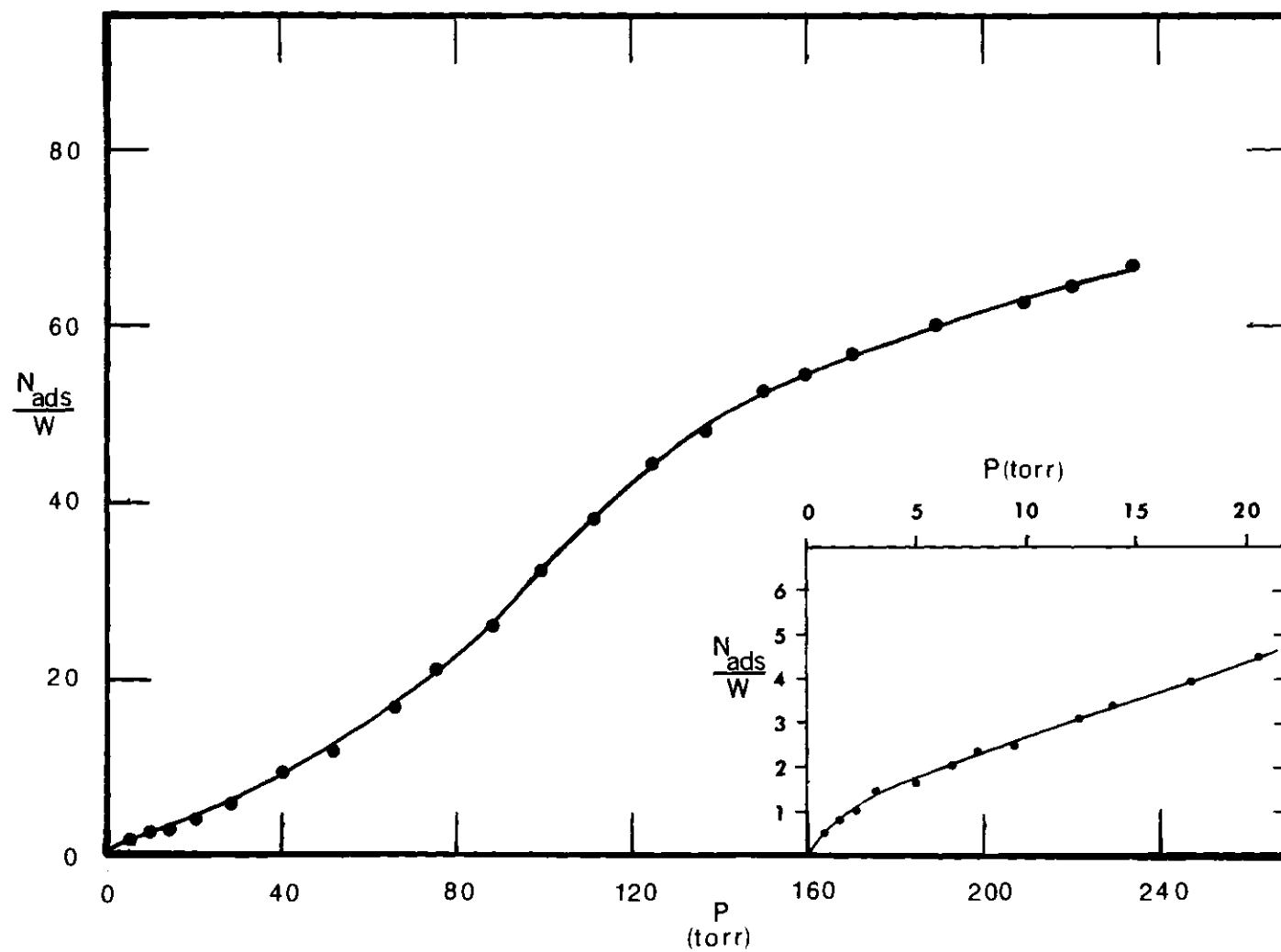


Figure 12. Argon Isotherm on NaCl at 89.96° K.

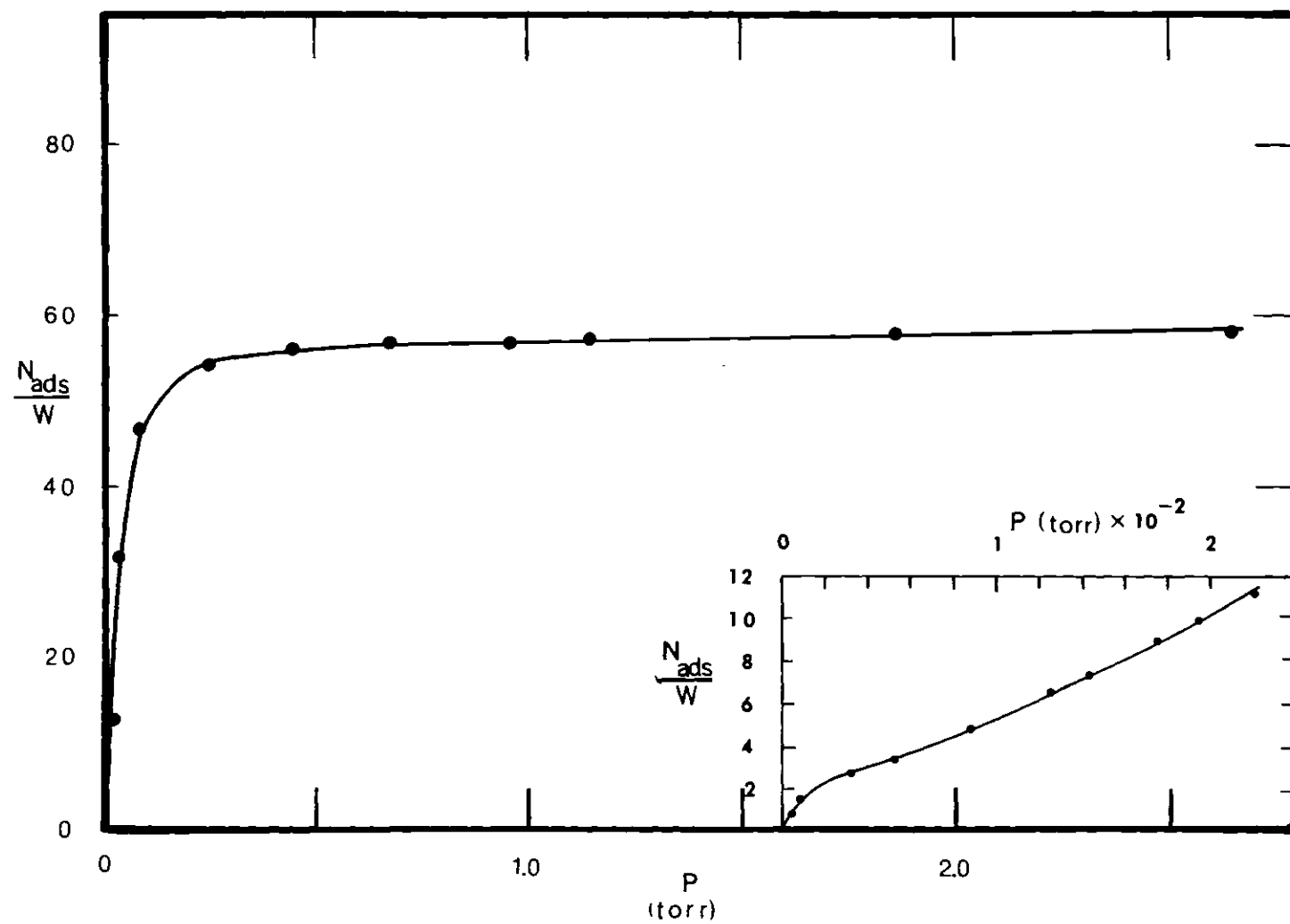


Figure 13. Nitrogen Isotherm on NaCl at 72.12°K.

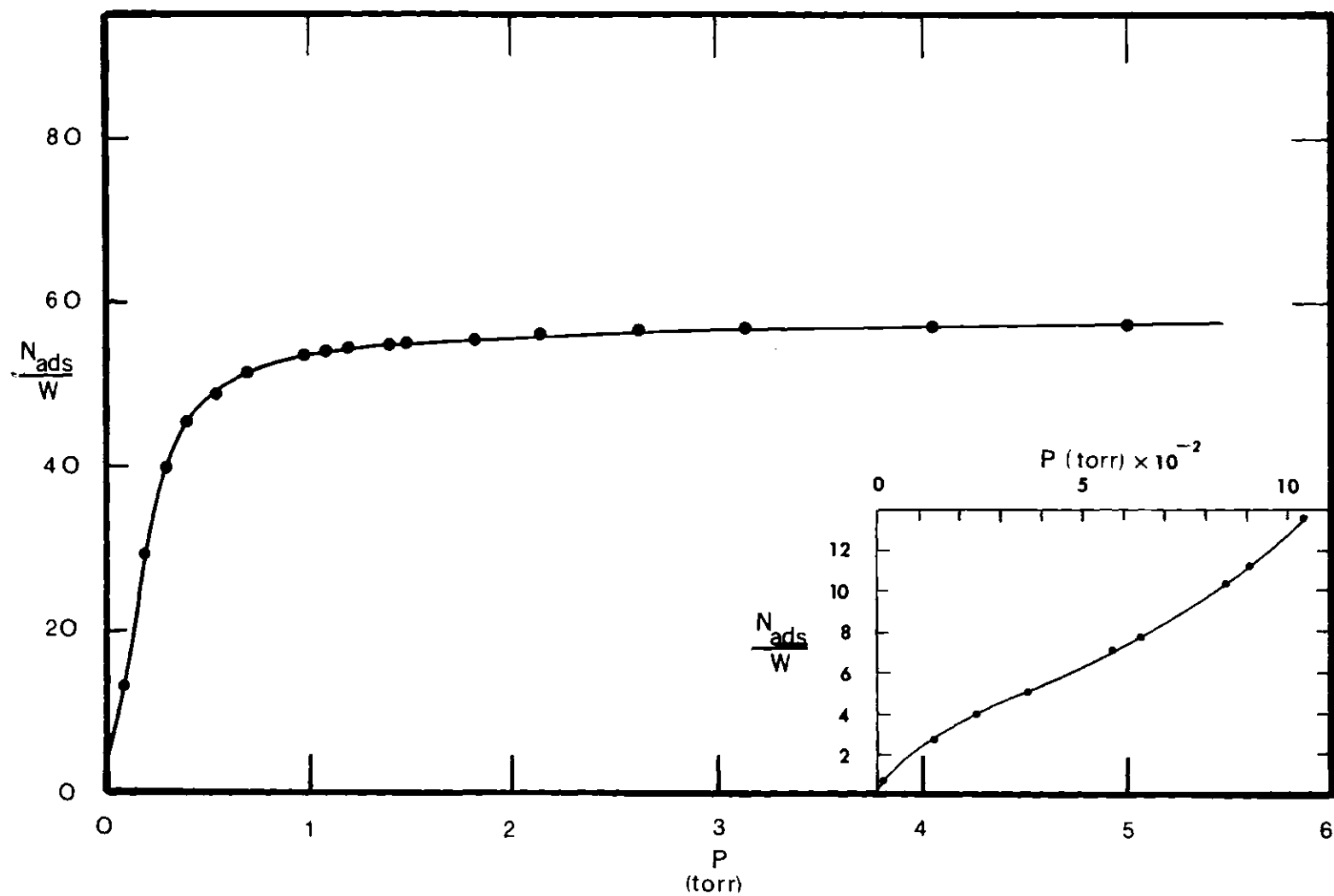


Figure 14. Nitrogen Isotherm on NaCl at 77.11°K.

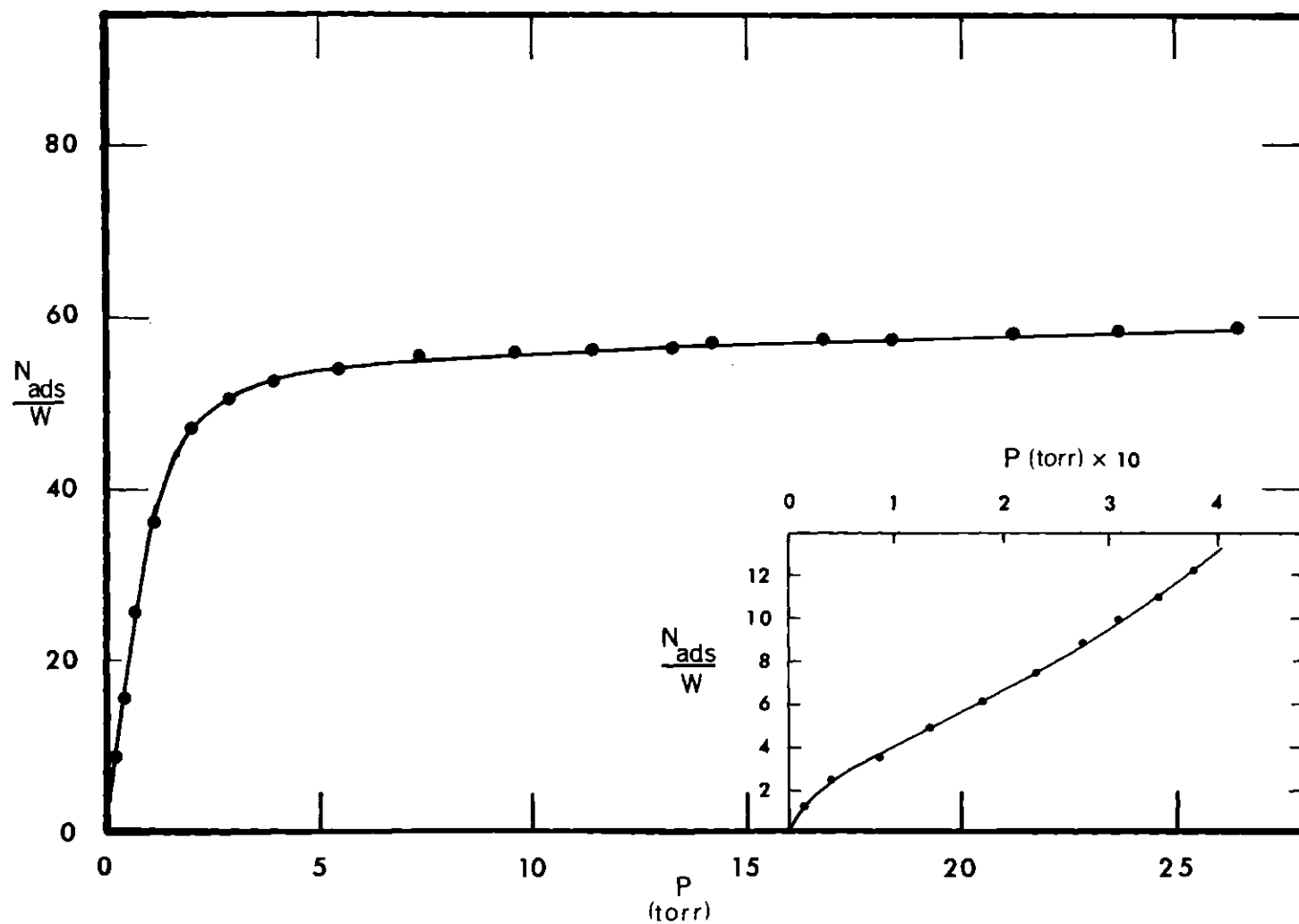


Figure 15. Nitrogen Isotherm on NaCl at 82.88°K.

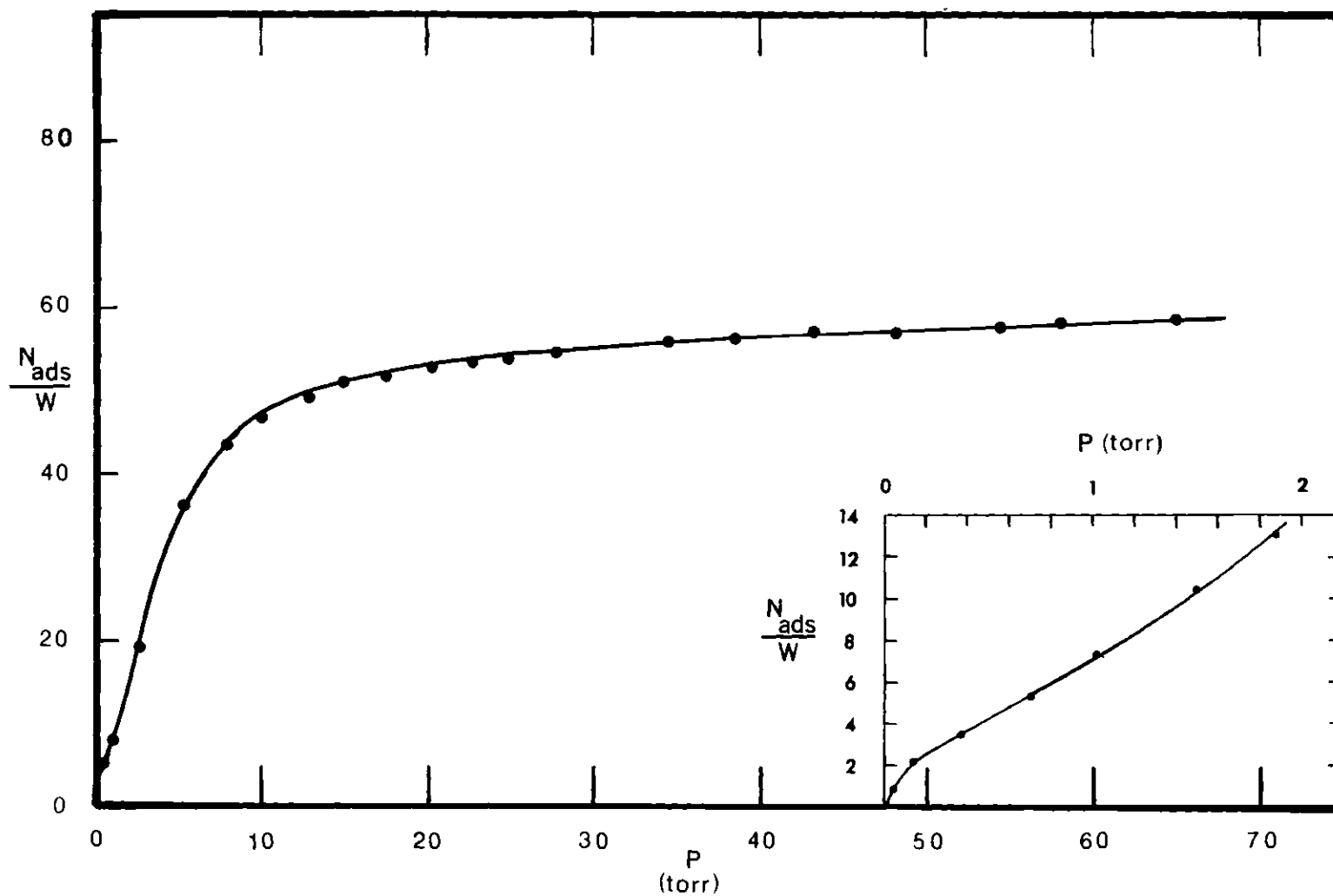


Figure 16. Nitrogen Isotherm on NaCl at 90.07°K.

CHAPTER V

SITE ENERGY DISTRIBUTION ANALYSIS

The concept of site energy distributions is normally associated with heterogeneous surfaces. A heterogeneous surface may be conveniently described by first defining a homogeneous and a uniform surface.² A uniform surface is defined as one having an adsorption potential, $u(\tilde{r})$, independent of the lateral position of the adsorbate molecule. A non-uniform but homogeneous surface is defined by the adsorption potential $u(\tilde{r})$ being dependent on the lateral position of the adsorbate molecules, but this dependence is periodic as in a perfect ionic crystal. A heterogeneous surface therefore is defined as one in which neither of the definitions of a uniform nor a homogeneous surface holds for the entire surface. It is possible, however, that the conditions for a uniform or a homogeneous surface may hold for regions of a heterogeneous surface.

There are basically two types of heterogeneous surfaces and a particular adsorbent may exhibit either or a combination of both. In the first case the heterogeneous surface is composed of large patches, each of which is homogeneous, for example, in a crystalline adsorbent exhibiting two or more crystalline planes on its surface. The second type of heterogeneity arises due to imperfections in the adsorbent surface, such as edges, cracks, dislocations, impurities, etc. All adsorbents display some degree of this second type of heterogeneity.

The first type of heterogeneity may be described by an energy

distribution of the adsorption sites. The second type of heterogeneity requires the spatial distribution of sites as well as the energy distribution of sites to describe the surface. In this work, the primary concern is with the possibility of the first type of heterogeneity. This type of heterogeneity would result if the surface of the sublimated sodium chloride particles exhibited more than one type of crystalline face. A site energy distribution analysis would permit determination of the number of crystalline faces exhibited by the particles.

Distribution Functions

Adsorption on a heterogeneous surface of the first type discussed above may be represented by

$$\Theta(P,T) = \sum_i \theta_i(Q,P,T) f(Q) \quad (56)$$

The term $\Theta(P,T)$ is the fraction of the total surface actually covered by the adsorbate at pressure P and temperature T . The fraction of each of the homogeneous patches covered is represented by the local isotherm function $\theta(Q,P,T)$, where Q is the adsorption energy of that patch. The frequency of occurrence of a patch with specific energy Q is $f(Q)$.

If the surface is very heterogeneous, such that the number of patches becomes very large, then equation (56) may be replaced by an integral of the form

$$\Theta(P,T) = \int_0^{\infty} \theta(Q,P,T) f(Q) dQ \quad (57)$$

where $\Theta(P,T)$ and $\theta(Q,P,T)$ have the same meaning as before, but $f(Q) dQ$

is now a continuous distribution function. The probability of there being a patch with an adsorption energy between Q and dQ is given by the distribution function $f(Q) dQ$. The integration is carried out over all positive values of Q , since only sites on which adsorption occurs are of interest. The lower limit of the integral is selected as zero because the local isotherm function θ is assumed to approach zero as the energy q approaches zero. Likewise as Q approaches infinity, the fraction of the surface with energy between Q and dQ will approach zero, thus $f(Q) dQ$ will approach zero.

An integral distribution function F is defined as

$$f(Q) = dF/dQ \quad (58)$$

where F is the fraction of the total surface for which the adsorption energy is equal to or greater than a given Q . Using this definition of F , equation (57) becomes

$$\Theta(P,T) = \int_0^1 \theta(Q,P,T) dF \quad (59)$$

Several attempts have been made to solve equation (57) analytically. Basically these attempts consist of assuming functions for two of the three quantities $\Theta(P,T)$, $\theta(Q,P,T)$ and $f(Q)$ and then integrating. Except for a few individual cases, the results are not really applicable to many adsorption studies, because in each case some particular analytical form must be assumed for the experimental isotherm. A discussion of these solutions is given by Adamson,⁴⁴ Ross and Olivier⁵ and Young

and Crowell.³

A semi-empirical graphical solution to equation (59) has been suggested by Adamson. This involves assuming a local isotherm $\theta(Q,P,T)$ and making a series of approximations to the integral distribution function F . The approximations are continued until a particular value of F is obtained, which, in conjunction with the assumed local isotherm $\theta(Q,P,T)$, predicts the experimentally observed isotherm θ_{obs} . This last approximation is taken as the integral site distribution function. Details of this solution are given in Appendix B.

Adamson has shown that for heterogeneous surfaces the distribution function obtained in this manner is independent of several choices for the local isotherm $\theta(Q,P,T)$, all of which reasonably reproduce the sub-monolayer region. The distributions were also found to be temperature independent. Hsieh⁴⁵ has confirmed this lack of dependence on the local isotherm function in a separate study.

For homogeneous surfaces, however, the site energy distribution function does become dependent on the choice of the local isotherm $\theta(Q,P,T)$. Different local isotherms result in shifting the distribution function along the energy scale by an amount equal to the difference in the average lateral interaction terms of the respective local isotherms. A change also occurs in the shape of the distribution functions. An example of this is shown in Figure 17, for Adamson's⁴⁶ results on the site distribution analysis for nitrogen on boron nitride (BN). Adamson used the isotherm data of Ross and Pultz⁴⁷ for this analysis. Three different local isotherm functions $\theta(Q,P,T)$ were employed.

Because of the simplicity of Adamson's method and the variety of

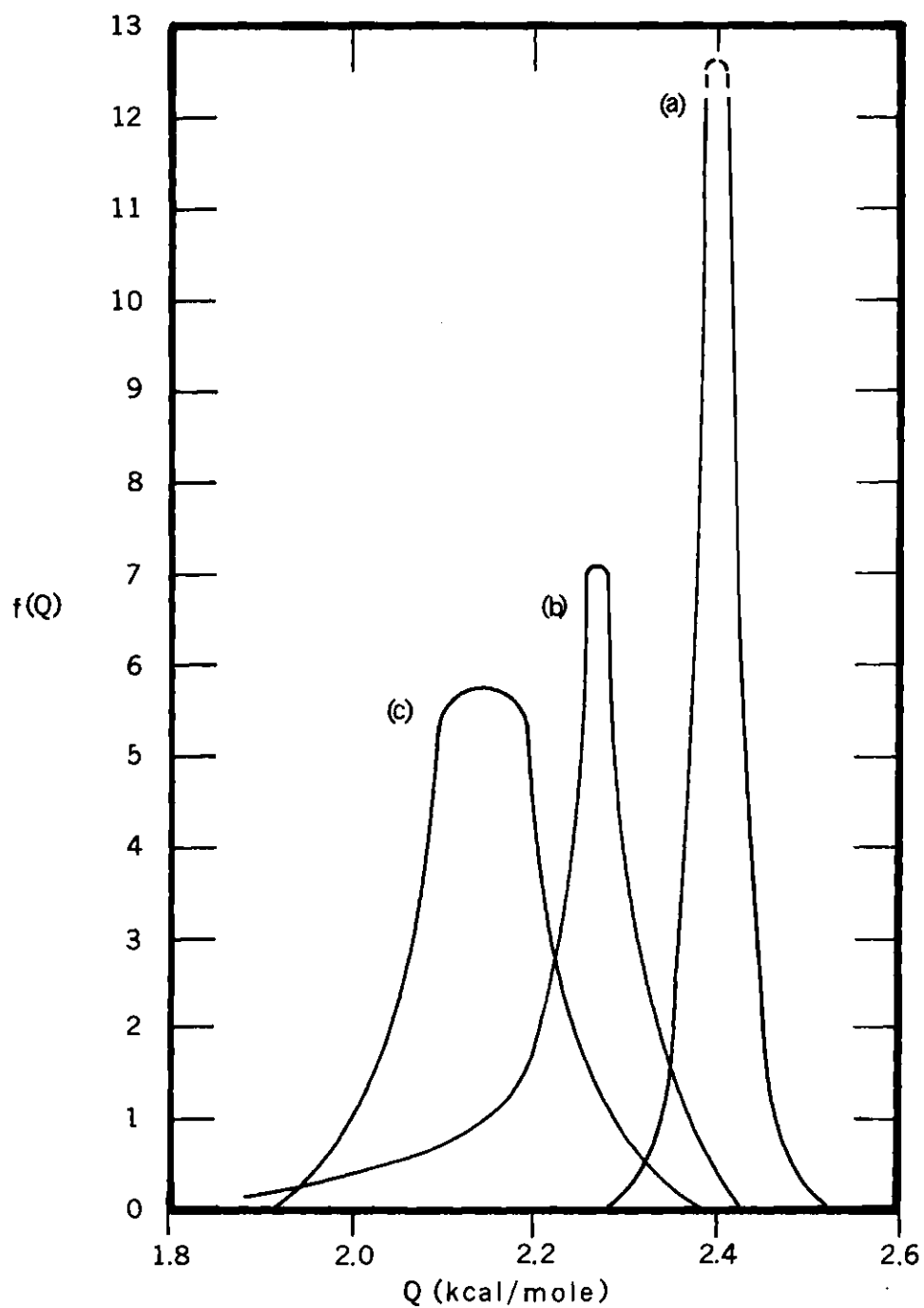


Figure 17. Interaction Energy Distributions for N_2 on BN Using Various Local Isotherms: (a) Langmuir; (b) Fowler and Guggenheim Equation; (c) Van der Waals.

reported data^{46,48} with which to compare the results, his method was selected for the present study.

Results

The local isotherm function $\theta(Q,P,T)$ employed was the Fowler and Guggenheim⁴⁹ equation

$$\theta = \frac{bP \exp(z\omega/RT)}{1 + bP \exp(z\omega/RT)} \quad (60)$$

$$b = (2\pi mkt)^{-1/2} (h/kT) q_{s,vib} \sigma \exp(Q/RT)$$

where m is the mass of the adsorbate molecule, σ the area occupied by a molecule of adsorbate, z the number of nearest neighbors and ω is the adsorbate-adsorbate interaction energy. The term $q_{s,vib}$ is the vibrational partition function

$$q_{s,vib} = \frac{\exp(-h\nu/2kT)}{1 - \exp(-h\nu/kT)} \quad (61)$$

where ν is the characteristic vibrational frequency perpendicular to the surface. Following Adamson the quantity $z\omega$ was set equal to one quarter the heat of vaporization. This allows comparison of the results of the present study to those of Adamson⁴⁶ and Hsieh,⁴⁸ who also used this approximation for $z\omega$. The effect of varying $z\omega$ will be discussed later in this chapter. The derivation and assumptions involved in equation (60) are given in Appendix C.

Site energy distribution analysis were made for three of the nitrogen isotherms. In the case of argon, insufficient data remained after multilayer corrections were made, for a complete distribution function. A partial distribution function was obtained, however, for the low temperature argon isotherm. The parameters used in equation (60) are presented in Table 6. The method of calculation is presented in Appendix B, while the results are tabulated in Appendix C and shown in Figures 18 and 19.

Table 6. Parameters for Equation (60).

Gas	T ($^{\circ}$ K)	$z\omega$ (cal/mole)	$v \times 10^{-12}$ (sec) $^{-1}$
N ₂	72.12	354.5	0.97
N ₂	77.11	350.4	1.03
N ₂	82.88	345.6	1.12
Ar	72.14	230.8	0.80
Ar	72.14	461.6	0.80

The results of the nitrogen-sodium chloride distribution functions are plotted in Figure 18. The solid line curve was obtained by drawing a smooth curve through the experimental data and fitting it to an analytical expression. Attempts to fit the curve to a gaussian, log normal and exponential distribution function were unsuccessful. An equation of the form

$$f(Q) = A \exp \left(-c |Q - Q_0|^n \right) \quad (62)$$

was then employed, where Q_0 is the mean value of Q . The parameters A , c and n were then varied until the best fit was obtained (Table 7). The smooth curve in Figure 18 was obtained from this best fit of equation (62).

A similar method was employed for the partial argon distribution function. Data were available for only half of the distribution. It was assumed that the distribution was symmetrical and a value of Q_0 was obtained by inspection.

In order to determine the effect of changing the value of $z\omega$, this quantity was varied for the argon distribution function. The values of $z\omega$ selected were one-quarter and one-eighth the heat of vaporization. The effect was to shift the distribution plot by one-sixteenth of the heat of vaporization. Plots of the data as well as the best fit to equation (62) are shown in Figure 19. The argon data obtained with $z\omega$ equal to one-eighth $\Delta\bar{H}_V$ was shifted along the energy scale by an amount equal to one-sixteenth $\Delta\bar{H}_V$, so it would superimpose the data obtained from using $z\omega$ equal to one-quarter $\Delta\bar{H}_V$. The values of A , c and n for the best fit to the argon data are given in Table 7.

A quantity similar to the 95% confidence limit of the gaussian distribution was determined from

$$P = \frac{\int_0^x \exp(-c|Y|^n) dY}{\int_0^\infty \exp(-c|Y|^n) dY} \quad (63)$$

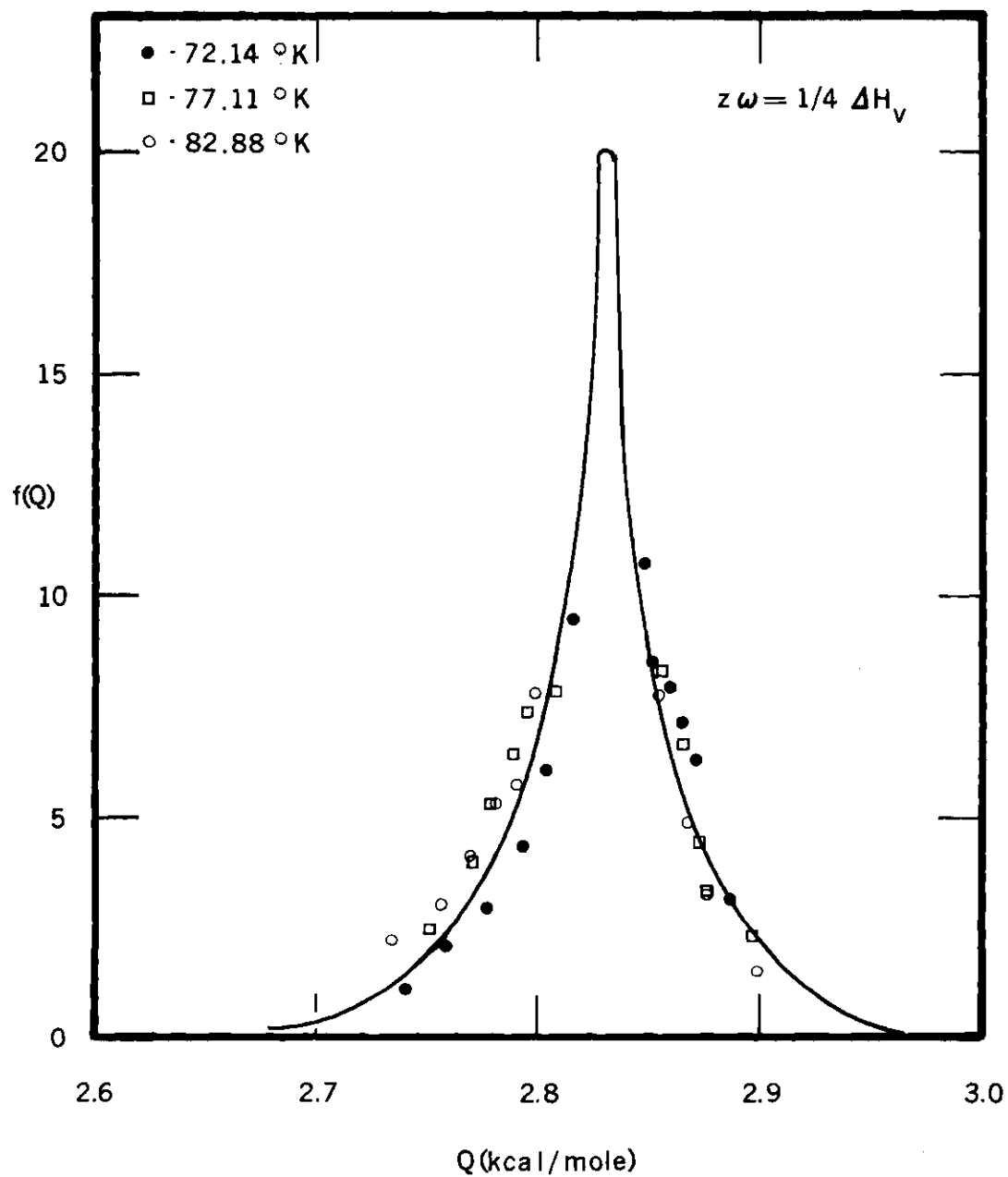


Figure 18. Interaction Energy Distribution for Nitrogen on Sodium Chloride.

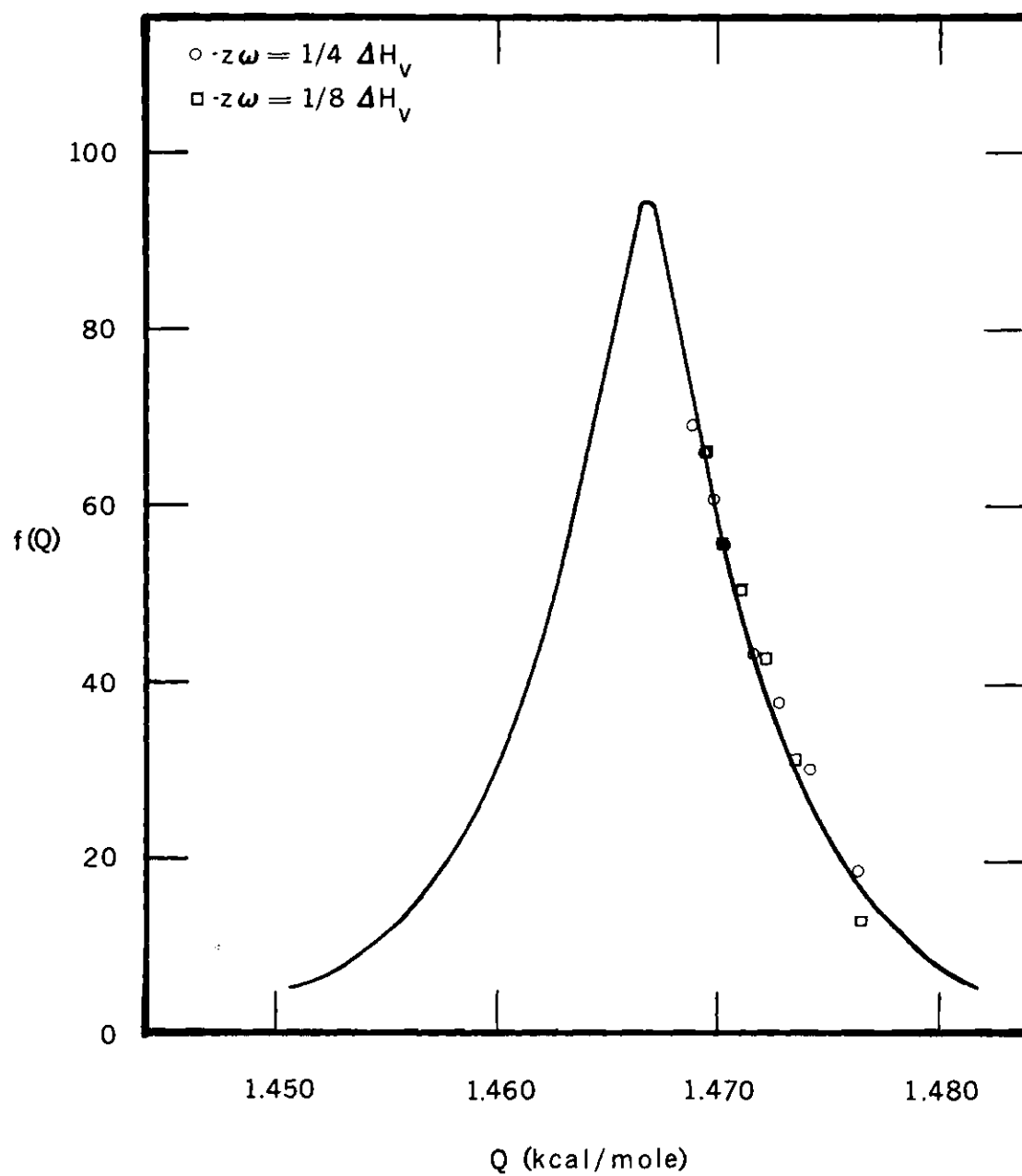


Figure 19. Interaction Energy Distribution for Argon on Sodium Chloride.

where P is the ratio of the areas under the curves given by the two integrals, Y is equal to $|Q-Q_0|$ and x is the value of Q at which $P = 0.95$. The integrals were solved by use of Simpson's rule. The values of x are listed in Table 7.

Table 7. Parameters for Equations (62) and (63)

Gas	A	c	n	x (kcal/mole)
N ₂	20.09	18.38	0.804	0.125
Ar	95.00	364.83	1.155	0.014

The results indicate a narrow energy distribution. For nitrogen the mean \pm the 95% confidence limit was found to be 2.834 ± 0.125 kcal/mole and for argon $1.467 \pm .014$ kcal/mole. Adamson's method for determining site energy distributions is admittedly not unique for homogeneous surfaces. As a result the energy of interaction Q_0 as well as the 95% confidence limits are approximate at best. However the shape of the distribution is very similar to that obtained by Adamson for nitrogen on boron nitride and by Hsieh⁴⁸ for argon on MT-3100 carbon black. Although these authors did not report a 95% confidence limit for their distributions, it may be estimated from their data. For argon on MT-3100 carbon black the 95% confidence limit is approximately ± 0.1 kcal/mole, and for nitrogen on boron nitride approximately ± 0.15 kcal/mole. Since

both of these adsorbents are considered as being homogeneous, it is concluded that the doubly heat treated sodium chloride sample is also nearly homogeneous.

It should be pointed out, however, that the isotherms presented in Chapter IV, show a slight step in the low pressure region. This step is attributed to adsorption on high energy sites. The point B method was used to estimate the area of the sample possessing these high energy sites. This area amounted to approximately 2% of the total surface. Adamson's semi-empirical solution to the site energy distribution function is evidently not sensitive enough for these sites to be observed in the distribution functions shown in Figures 18 and 19.

CHAPTER VI

ADSORPTION POTENTIAL

The total adsorption potential as given by equation (3) may be written as

$$\phi_T = \phi_A + \phi_R + \phi_E + \phi_Q \quad (64)$$

where ϕ_T is the total potential of adsorption. The contributions to the total potential due to the dispersion forces is ϕ_A , from the repulsive forces, ϕ_R , the electrostatic force, ϕ_E , and the quadrupole interaction, ϕ_Q . The division of ϕ_T into four parts is somewhat artificial as ϕ_A and ϕ_R may be inter-related by use of a pair potential.

In this work the modified Buckingham (6 - exp) pair potential is used to describe the attractive and repulsive interactions. This pair potential is given by

$$\phi(r) = -C/r^6 + B \exp(-\gamma \frac{r}{r_m}) \quad (65)$$

where

$$C = \frac{\epsilon}{1 - 6/\gamma} r_m^6 \quad (66)$$

$$B = \frac{6\epsilon}{\gamma - 6} \exp \gamma \quad (67)$$

and r_m is the equilibrium distance, γ a parameter determining the steepness of the repulsive potential wall and ϵ is the depth of the potential well. The (6 - exp) potential is used in this form because a similar form for the repulsive potential of the ions of the alkali halides is available.¹³ Mixed interactions which are the primary concern in this study, require a combining of the self interaction potentials, when the mixed interaction potential is not known independently. This combining can be accomplished by use of several rules for the various parameters just defined. These combining rules will be discussed in later sections.

The parameters of equation (65) for argon and nitrogen have been evaluated by several workers. The parameters, as determined by Sherwood and Prausnitz⁵⁰ for nitrogen and argon and those of Whalley and Schneider⁵¹ for argon, are shown in Table 8. The parameters of Sherwood and Prausnitz, determined from second virial coefficient data, were selected for this work. The effect of using other parameters will be discussed in Chapter VII.

Table 8. Modified Buckingham (6 - exp) Parameters

Pair	Ref.	ϵ/k ($^{\circ}\text{K}$)	r_m (\AA)	
Ar-Ar	50	152.0	3.644	18
$\text{N}_2\text{-N}_2$	50	160.2	3.695	30
Ar-Ar	51	131.5	3.784	15

Although the attractive and repulsive interactions are inter-related by equation (65), they can be conveniently discussed separately, just as the electrostatic interaction and the quadrupole interaction.

Attractive Potential

The value of C from equation (66) for the self interaction of the adsorbate molecules is denoted by C_{11} . For the interaction of the adsorbate molecule with the ions of the crystal, the values of C_{12} for the adsorbate-negative ion and C_{13} for the adsorbate-positive ion are required. These mixed interactions parameters are given by

$$C_{12} = \frac{\epsilon_{12}}{1 - 6/\gamma_{12}} r_{m12}^6 \quad (68)$$

for the (6 - exp) potential for the adsorbent-negative ion interaction. The remainder of this discussion will be in terms of this interaction, but an analogous argument is used for the adsorbate-positive ion interaction.

A convenient method⁵² has been outlined for determining the parameters C_{12} and C_{13} , based on a ratio of the values of C_{KM} obtained from the Kirkwood Muller¹² expression for self-interaction

$$C_{11_{KM}} = 6 mc^2 (\alpha_1 x_1 / 2) \quad (69)$$

and for mixed interactions

$$C_{12_{KM}} = 6 mc^2 \left(\frac{\alpha_1}{x_1} + \frac{\alpha_2}{x_2} \right)^{-1} \alpha_1 \alpha_2 \quad (70)$$

The term m is the mass of an electron, c is the velocity of light, and α and χ are the polarizability and diamagnetic susceptibilities of the respective species. The Kirkwood Müller values for C_{11} and C_{12} are too large when compared to results obtained from quantum mechanical calculations.⁵³ For this reason the following method was used to find the respective values of C .

The values of the self interaction and mixed interaction parameters for argon, xenon and krypton were calculated from equations (69) and (70) respectively. These results were then plotted against the same values as reported by Starkschall and Gordon⁵³ from quantum mechanical considerations. The data appear to form a straight line and a least squares fit to a linear equation gives

$$C_{SG} = 5.8 \times 10^{-12} + 0.2842 C_{KM} \quad (\text{units of ergs } \text{\AA}^6) \quad (71)$$

with a standard deviation of $\pm 3.015 \times 10^{-12}$ ergs \AA^6 . If the small intercept can be taken as insignificant, the constants are then proportional to one another.

This suggests that the mixed interaction parameters for the (6 - exp) pair potential may be given by

$$C_{12} = C_{11} (C_{12_{KM}} / C_{11_{KM}}) \quad (72)$$

The value of C_{11} for the adsorbate is determined from equation (66) using the data of Sherwood and Prausnitz. The quantities $C_{11_{KM}}$ and $C_{12_{KM}}$ were determined from equations (69) and (70), respectively, using

the polarizabilities and diamagnetic susceptibilities given in Table 9.

Table 9. Polarizabilities and Diamagnetic Susceptibilities

	α cm ³ /mole x 10 ²⁴	Ref.	χ cm ³ /mole x 10 ⁶	Ref.
Ar	1.63	4	-19.32	55
N ₂	1.76	10	-12.0	10
Na ⁺	0.303	54	- 5.9	56
Cl ⁻	3.058	54	-24.3	56

The attractive potential due to the interaction of the adsorbate with each ion is given by

$$\phi_{A_{12}} = C_{12}/r_{12}^6 \quad (73)$$

and

$$\phi_{A_{13}} = C_{13}/r_{13}^6 \quad (74)$$

The total potential due to the dispersion forces between the adsorbate molecule and all the ions of the crystal is given by ¹¹

$$\phi_A = \frac{C_{12}}{a^6} S_- (\rho) + \frac{C_{13}}{a^6} S_+ (\rho) \quad (75)$$

where $S_- (\rho)$ and $S_+ (\rho)$ are the inverse sixth power summations of the

molecule-ion distance to the negative and positive ions respectively. The term a is half the lattice parameter of the crystal and ρ is the reduced perpendicular distance of the adsorbate molecule above the crystal plane.

$$\rho = z/a \quad (76)$$

Details of the calculations of $S_{-}(\rho)$ and $S_{+}(\rho)$ are given in Appendix E.

Repulsive Potential

The repulsive portion of the (6 - exp) potential for self interaction of the adsorbate molecules is given by equation (67) as

$$B_{11} \exp \left(-\gamma \frac{r}{r_m} \right) \quad (77)$$

Huggins and Mayer¹³ have described the repulsive interaction between the ions of an alkali halide crystal as

$$B_{+} B_{-} \exp (-\beta r) \quad (78)$$

where B_{+} and B_{-} are parameters of the positive and negative ions respectively and β is an empirical constant, taken as 2.899 \AA^{-1} .

The pre-exponential parameter of equation (77) may be written as $B_{11} = (B_1)^2$. This suggests that the mixed pre-exponential parameter may be given by

$$B_{12} = B_{-}B_1 \quad (79)$$

$$B_{13} = B_{+}B_1 \quad (80)$$

which is the same as the geometric mean⁵⁷ combining rule.

$$B_{12} = (B_{11}B_{22})^{\frac{1}{2}} \quad (81)$$

Other combining rules have been proposed for the pre-exponential parameters and two of these have been considered. The arithmetic mean combining rule is given by

$$B_{12} = 1/2 (B_{11} + B_{22}) \quad (82)$$

and the harmonic mean combining rule is given by⁵⁸

$$B_{12} = \frac{2B_{11}B_{22}}{B_{11} + B_{22}} \quad (83)$$

To determine the effect of these various combining rules, calculations of the total potential were made using the combining rules of equations (81), (82) and (83) for the repulsive potential for the argon-sodium chloride system. For the nitrogen-sodium chloride system, only equation (76) was employed for the repulsive potential. A comparison of the results are presented in Chapter VII.

The combining law of Zener⁵⁹ is used for the exponential parameter

$$\beta_{12} = 1/2 (\beta_{11} + \beta_{22}) \quad (84)$$

where

$$\beta_{12} = \gamma/r_m \quad (85)$$

and β_{22} is the β parameter of Huggins and Mayer. This combining law proves to be consistent with the geometric mean rule for the pre-exponential parameter B , as will be discussed in Chapter VII.

The repulsive potential between an adsorbate molecule and each of the ions of the lattice is given by

$$\phi_{R12} = B_{12} \exp (-\beta_{12} r) \quad (86)$$

$$\phi_{R13} = B_{13} \exp (-\beta_{13} r) \quad (87)$$

The repulsive potential for interaction of the adsorbate molecule and all the ions of the crystal is given by¹¹

$$\phi_R = B_{12} S_- (\rho, \beta, a) + B_{13} S_+ (\rho, \beta, a) \quad (88)$$

where $S_- (\rho, \beta, a)$ and $S_+ (\rho, \beta, a)$ are the summations for the exponential of distance between the adsorbate molecule and all the ions. The details of these summations are given in Appendix F.

The mixed interaction parameters as defined by equations (72), (79), (82), (83) and (84), as well as the self-interaction parameters

for argon and nitrogen from the data of Sherwood and Prausnitz are presented in Table 10. In addition to the values of C , B and β , the usual parameters of the modified Buckingham (6 - exp) potential are presented.

Table 10. Potential Parameters

Pair	$C \times 10^{11}$ (ergs \AA^6)	$B \times 10^8$ (ergs)		
		Eq. (79)	Eq. (82)	Eq. (83)
Ar-Ar	7.37	68.88	-	-
Ar-Na ⁺	1.70	1.05	34.63	0.77
Ar-Cl ⁻	11.10	5.97	34.45	0.04
N ₂ -N ₂	7.03	5.91×10^{-10}	-	-
N ₂ -Na ⁺	1.79	306.95	-	-
N ₂ -Cl ⁻	13.15	1747.52	-	-
Pair	$\beta(\text{\AA}^6)^{-1}$	Geometric Mean Combining Rule		
		ϵ/k ($^{\circ}\text{K}$)	$r_m(\text{\AA})$	γ
Ar-Ar	4.9394	152.0	3.644	18
Ar-Na ⁺	3.9189	18.3	4.011	15.7
Ar-Cl ⁻	3.9189	130.4	3.947	15.5
N ₂ -N ₂	8.1191	160.2	3.695	30
N ₂ -Na ⁺	5.5088	9.1	4.715	26
N ₂ -Cl ⁻	5.5088	459.4	3.344	18.4

Electrostatic Potential

A non-polar molecule, with a polarizability of α , experiences an electrostatic force when placed in an electric field. Lennard-Jones and Dent¹⁵ have shown that this electrostatic interaction can be expressed as

$$\phi_E = -\frac{1}{2}\alpha F_z^2 \quad (89)$$

where F_z is the resultant field perpendicular to the surface at a particular point. F_z is defined as

$$F_z = (\partial F / \partial z)_{x,y} \quad (90)$$

where F is the total electrostatic potential above the surface and z is the perpendicular distance of the adsorbate molecule above the surface. The total electrostatic potential above the (100) plane of face centered cubic crystals has been derived by Lennard-Jones and Dent¹⁵ as

$$F = \frac{4ve}{a_o} \sum_{\ell=\pm 1,3,5,\dots} \sum_{m=\pm 1,3,5} (-1)^{\frac{\ell+m}{2}} (\ell^2+m^2)^{-\frac{1}{2}} \cos 2\pi \left(\frac{\ell x}{a_o} + \frac{my}{a_o} - \frac{\ell+m}{4} \right) \frac{\exp \left(-\frac{2\pi z}{a_o} (\ell^2+m^2)^{\frac{1}{2}} \right)}{1 + \exp(-\pi (\ell^2+m^2)^{\frac{1}{2}})} \quad (91)$$

where v is the valency of the ions, e the charge of an electron and a_o is the crystal lattice parameter. The coordinates x and y determine the lateral position of the adsorbate molecule over the lattice cell. At

the point $x = y = 0$, the molecule is directly above a positive ion. The term z is the distance of the adsorbate molecule above the point (x, y) in the crystal plane. Equation (91) considers only the first crystal plane. Successive planes are obtained by replacing z with $(n a_o + z)$ where $n = 1, 2, 3, \dots$. Equation (90) then becomes

$$F_z = \frac{8\pi ve}{a_o^2} \sum_{\ell=\pm 1, 3, 5 \dots} \sum_{m=\pm 1, 3, 5 \dots} \exp\left(-\frac{2\pi z}{a_o}(\ell^2 + m^2)^{\frac{1}{2}}\right) \cos 2\pi\left(\frac{\ell x}{a_o} + \frac{my}{a_o} - \frac{\ell+m}{4}\right) (-1)^{\frac{\ell+m}{2}} \left[1 + \exp(-\pi(\ell^2 + m^2)^{\frac{1}{2}})\right]^{-1} \quad (92)$$

From equation (92) it can be shown that the resultant field over the center of a cell and over the mid point of a lattice edge is zero. The variation of the perpendicular component of the electrostatic field F_z as a function of ρ , where $\rho = z/a$, is presented in Appendix G.

The use of equation (89) to express the electrostatic interaction, implies that the adsorbate molecule is adequately represented by a polarizable point. As discussed in Chapter I, Lenel⁷ calculated the electrostatic potential from equation (28), again presented here for convenience,

$$\phi_E = \int \frac{(P - P_o)^2 \rho_e}{J_E} d\tau \quad (28)$$

where P_o is the potential field at the center of the adsorbate molecule, P is the potential at a particular point, ρ_e is the electron density of the adsorbate molecule and $d\tau$ is a volume element experiencing the potential P . He found that this equation predicted an interaction energy

of 450 cal/mole compared with 250 cal/mole from equation (89) for argon on potassium chloride.² The implications of Lenel's calculations will be discussed in further detail in Chapter VII.

Quadrupole Potential

The interaction of a non-polar molecule, possessing a quadrupole moment Q , with an electric field F can be shown to be ²²

$$\phi_Q = \frac{1}{2} Q(d^2F/dt^2) \quad (93)$$

where the axis t is taken along the axis of symmetry of the quadrupole.

Using the expression for the electrostatic field given by Lennard-Jones and Dent, equation (91), Hayakawa¹⁷ evaluated the second derivative of equation (93). Four sites above the unit lattice cell were considered; site A above the center of the cell, site B above the mid point of a lattice edge, site C above a positive ion and site D above a negative ion. The maximum interaction of the quadrupole was found to occur for the following orientations of the quadrupole:

$$(i) \text{ Type A sites, } (\partial^2 F / \partial x \partial y)_z = e/a^3 \cdot \sigma_A; \quad (94)$$

$$(ii) \text{ Type B sites, } (\partial^2 F / \partial x \partial z)_y = e/a^3 \cdot \sigma_B; \quad (95)$$

$$(iii) \text{ Type C sites, } (\partial^2 F / \partial z^2)_{x,y} = e/a^3 \cdot \sigma_C; \quad (96)$$

$$\text{and } (iv) \text{ Type D sites, } (\partial^2 F / \partial x^2)_{z,y} = e/a^3 \cdot \sigma_D. \quad (97)$$

The axis x , y , and z are along the sides of a unit cell, e is the electron charge and a is one-half the lattice cell constant. The quantities σ are the summations of distance of the adsorbate molecule to all the ions of the crystal and is a function of ρ where ρ is defined

as z/a . Details of the calculations of the values of σ as a function of ρ are presented in Appendix H.

Equations (94) and (97) in their complete form, as shown in Appendix H, indicate that the maximum quadrupole interaction occurs when the axis of the quadrupole is parallel to the surface for sites A and D. For site C, equation (96) shows that the maximum interaction occurs when the axis of the quadrupole makes an angle of $\pi/2$ with the surface and for site B, equation (95), predicts the maximum interaction at an angle of $\pi/4$. These angles for maximum interaction were obtained from the equations given in Appendix H.

The calculation of the dispersion forces as discussed earlier is based on the assumption that the adsorbate molecules are freely rotating. If the molecules are hindered from rotating, such as is predicted for sites B and C, a correction needs to be applied to the total potential. An estimate of this correction has been made by Hill⁶⁰. For a rigid symmetrical diatomic molecule with an interatomic distance of $2d$, Hill represented the interaction of each atom of the molecule with the surface by a Lennard-Jones (6 - 12) potential

$$u = \epsilon_0 \left(\frac{r_m}{r} \right)^{12} - 2 \epsilon_0 \left(\frac{r_m}{r} \right)^6 \quad (98)$$

where r_m is the equilibrium distance of the atom from the surface of the adsorbent and ϵ_0 is the depth of the well. Using the attractive term of London (equation (27)), he derived an expression for the interaction of the entire molecule with the adsorbent by integration

$$U = \kappa \left\{ -\left(\frac{z}{r_m} + h_1\right)^{-3} - \left(\frac{z}{r_m} - h_1\right)^{-3} + \frac{1}{15} \left[\left(\frac{z}{r_m} + h_1\right)^{-9} + \left(\frac{z}{r_m} - h_1\right)^{-9} \right] \right\} \quad (99)$$

where κ is a constant, z is the distance of the center of the molecule above the surface of the adsorbent and h_1 is defined as

$$h_1 = h_o \cos \theta \quad (100)$$

$$h_o = d/r_m \quad (101)$$

The angle θ , is the angle between the axis of the molecule and the surface of the adsorbent. From this equation, it is seen that the maximum interaction due to dispersion forces occurs when θ is zero as in the case of sites A and D.

For θ equal to $\pi/2$, Hill has plotted the correction to the dispersion forces as a function of h_o . From this plot it is estimated that the correction for site B is about 100 cal/mole and for site C about 200 cal/mole. Admittedly, Hill's calculations are approximate and valid only as an estimate of the order of magnitude, since the interactions were integrated and the attractive term of London was used.

Additionally, when a molecule is adsorbed on a surface, the rotational degrees of freedom become torsional vibrations, if the molecule is restricted from rotating on the surface. The total interaction potential would be increased by an amount equal to the difference in the energy contributions from rotation and torsional vibrations. If the energy of the torsional vibrations is small compared to the energy of rotation and the molecule is considered to be a rigid rotor, then the

contribution to the total potential may be estimated from

$$E_{\text{rot}} = kT^2(\partial \ln q_r / \partial T) = kT \quad (102)$$

where q_r is the rotational partition function, assuming a rigid rotor. This amounts to about 150 cal/mole. Since Hill's calculations are approximate, the energy contributions due to the barrier of rotation and the loss of rotational degrees of freedom roughly cancel each other in this particular case and therefore are not considered.

The quadrupole interaction for nitrogen was calculated from equation (93), using the values of d^2F/dt^2 as given by equations (93) through (97). The value of Q was taken from Buckingham⁶¹ as -1.52×10^{-26} esu cm^2 .

Total Potential

The total potential was calculated from equation (64)

$$\phi_T = \phi_A + \phi_R + \phi_E + \phi_Q \quad (64)$$

Calculations of ϕ_T were made for four sites on a unit lattice cell. These sites are: type A over the center of a cell, CC, type B over a mid point of the cell edge, CE, type C over a sodium ion, Na^+ , and type D over a chloride ion, Cl^- . The total potential curves for these four sites are presented in Figures 20 through 22. The harmonic mean combining rule for the repulsive potential of the argon-sodium chloride interaction, predicted exceptionally large interaction energies (greater

than 150 kcal/mole) and small equilibrium distances (less than 0.9 \AA). For this reason, this data is not plotted, but will be discussed later in this Chapter. The data for all the potential energy curves is given in Appendix I.

In order to determine the force constant k_z for the mode of vibration normal to the surface of the adsorbent, the well region of the potential was fitted to a Taylor series about the minimum

$$\begin{aligned} \phi(z) = E_m + b_2(z - z_m)^2 - b_3(z - z_m)^3 + b_4(z - z_m)^4 - b_5(z - z_m)^5 \\ + b_6(z - z_m)^6 + \dots \end{aligned} \quad (103)$$

where E_m is the minimum of the potential curve and z_m is the equilibrium distance between the adsorbate molecule and the surface.

The values of E_m and the constants b are presented in Table 11 for the argon-sodium chloride system and in Table 12 for the nitrogen-sodium chloride system.

The force constant is given by

$$k_z = 2b_2 \quad (104)$$

and the characteristic frequency for harmonic vibration is given by

$$\nu = \frac{1}{2\pi} \sqrt{k_z/m} \quad (105)$$

where m is the mass of the molecule of adsorbate.

Table 11. Parameters for the Argon-Sodium Chloride Potential Curve

System	Geometric Mean Combining Rule			
	Ar-CC	Ar-CE	Ar-Na ⁺	Ar-Cl ⁻
E_m (kcal/mole)	-1.099	-0.9587	-1.093	-0.812
b_2 (kcal/mole A^{O^2})	13.842	12.3417	15.904	11.712
b_3 (kcal/mole A^{O^3})	66.524	69.1307	92.415	84.619
b_4 (kcal/mole A^{O^4})	155.742	209.8253	231.580	271.558

	Arithmetic Mean Combining Rule			
	Ar-CC	Ar-CE	Ar-Na ⁺	Ar-Cl ⁻
	-0.469	-0.438	-0.410	-0.456
	6.792	6.869	6.226	10.326
	27.803	30.282	25.377	46.068
	15.683	1.162	2.280	21.194

Table 12. Parameters for the Nitrogen-Sodium Chloride Potential Curve

System	N ₂ -CC	N ₃ -CE	N ₂ -Na ⁺	N ₂ -Cl ⁻
E_m (kcal/mole)	-2.496	-2.316	-2.712	-1.508
b_2 (kcal/mole A^{O^2})	58.311	73.571	65.883	44.789
b_3 (kcal/mole A^{O^3})	324.888	405.694	719.726	287.256
b_4 (kcal/mole A^{O^4})	560.779	602.918	3839.951	486.323
b_5 (kcal/mole A^{O^5})	759.242	509.469	3884.466	411.234
b_6 (kcal/mole A^{O^6})	226.499	97.148	1093.150	80.395

The energy levels of a one dimensional harmonic oscillator are non degenerate and given by

$$\epsilon_n = h\nu(n + \frac{1}{2}) ; n = 0, 1, 2, 3 \dots \quad (106)$$

The zero point energy is then given by

$$E_o = E_m + \frac{1}{2} h\nu \quad (107)$$

The average energy of each potential curve is obtained by first finding the average energy of vibration from the vibrational partition function

$$E_{av} = E_m + E_{vib} \quad (108)$$

where

$$E_{vib} = kT^2 (\partial \ln q_{vib} / \partial T) \quad (109)$$

and

$$q_{vib} = \frac{\exp(-h\nu/2kT)}{1 - \exp(-h\nu/kT)} \quad (110)$$

In Chapter I, it was pointed out that previous workers such as Hayakawa¹⁶⁻²⁰ and Orr¹¹ compared their experimental values to the zero point energy of the potential curve exhibiting the largest interaction energy. This method, however, seems valid only at the absolute of zero.

For temperatures greater than absolute zero there will be a thermal distribution of an adsorbed molecule over the various positions.

Assuming a Boltzman distribution for the adsorbed molecule among the various positions, the probability of finding the molecule over a particular position i is approximately given by

$$\frac{N_i}{N_T} \sim \frac{g_i \exp (-E_{av}^i/kT)}{\sum_i g_i \exp (-E_{av}^i/kT)} \quad (111)$$

where the g_i 's are weighting factors according to the relative contributions of each type of site on a lattice cell. For adsorption over the center of a cell, there is only one site, therefore $g = 1$, over the center of an edge, there are four sites, however each is shared by two cells, therefore $g = 2$. For adsorption over an ion, there are two of each type of ion, but each ion is shared by four cells, therefore $g = \frac{1}{2}$. These factors are shown in Table 13.

Table 13. Weighting Factors

Site	g
A - Center of Cell	1
B - Center of Edge	2
C - Over Na^+	$\frac{1}{2}$
D - Over Cl^-	$\frac{1}{2}$

The total average energy for the molecule, on the surface then is given

approximately by

$$E_{av}^T \approx \frac{N_A}{N_T} E_{av}^A + \frac{N_B}{N_T} E_{av}^B + \frac{N_C}{N_T} E_{av}^C + \frac{N_D}{N_T} E_{av}^D \quad (112)$$

To relate E_{av}^T to the experimentally determined isosteric heats of adsorption, the relationship of equation (25), derived in Chapter I, is employed

$$q_{st}^c = E_{av}^T + RT \quad (113)$$

where q_{st}^c is the calculated isosteric heat of adsorption at zero coverage.

The results of these calculations are presented in the following tables and plots: Tables 14, 15 and 16 contain the values of z_m , E_o , and E_{av} ; Table 17 contains the total average energy E_{av}^T and q_{st}^c . The data for the potential curves is presented in Appendix I, and the plots of this data are shown in Figures 20 through 22.

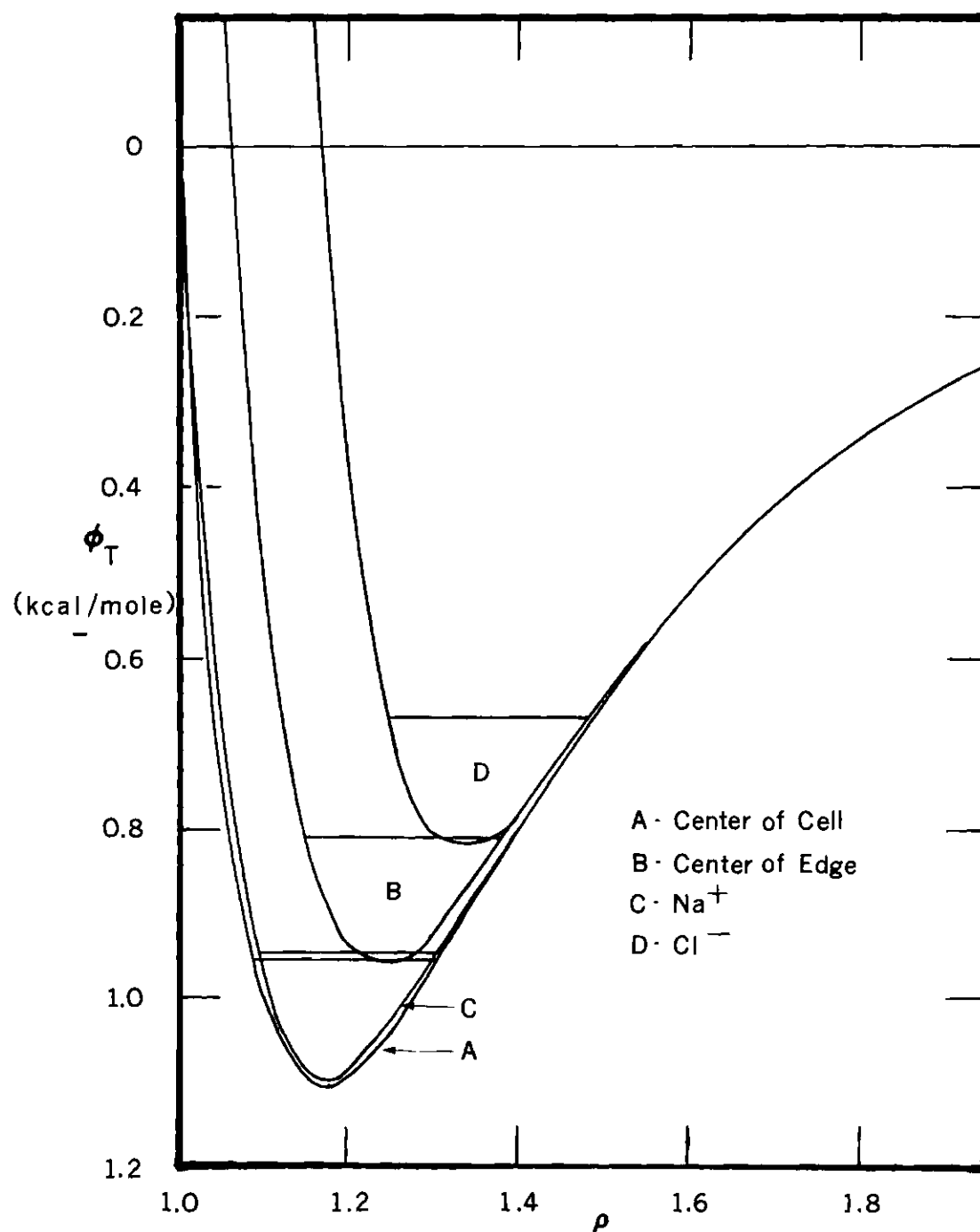


Figure 20. Potential Curves for Argon on the (100) Plane of NaCl Using the Geometric Mean Combining Rule for the Repulsive Potential Parameter B_{12} .

Table 14. Results Obtained from the Potential Energy Curve for Argon on the (100) Plane of Sodium Chloride, using the Geometric Mean Combining Rule for the Repulsive Potential Parameter B_{12} .

Site	T (°K)	z_m (Å)	$-E_o$ (kcal/mole)	$\nu \times 10^{-12}$ (sec) ⁻¹	$-E_{av}$ (kcal/mole)
A	72.14	3.32	1.095	0.103	0.956
	77.12				0.947
	82.88				0.935
	89.96				0.921
B	72.14	3.48	0.954	0.097	0.815
	77.12				0.805
	82.88				0.794
	89.96				0.780
C	72.14	3.30	1.088	0.110	0.949
	77.12				0.939
	82.88				0.928
	89.96				0.914
D	72.14	3.74	0.808	0.095	0.669
	77.12				0.659
	82.88				0.648
	89.96				0.633

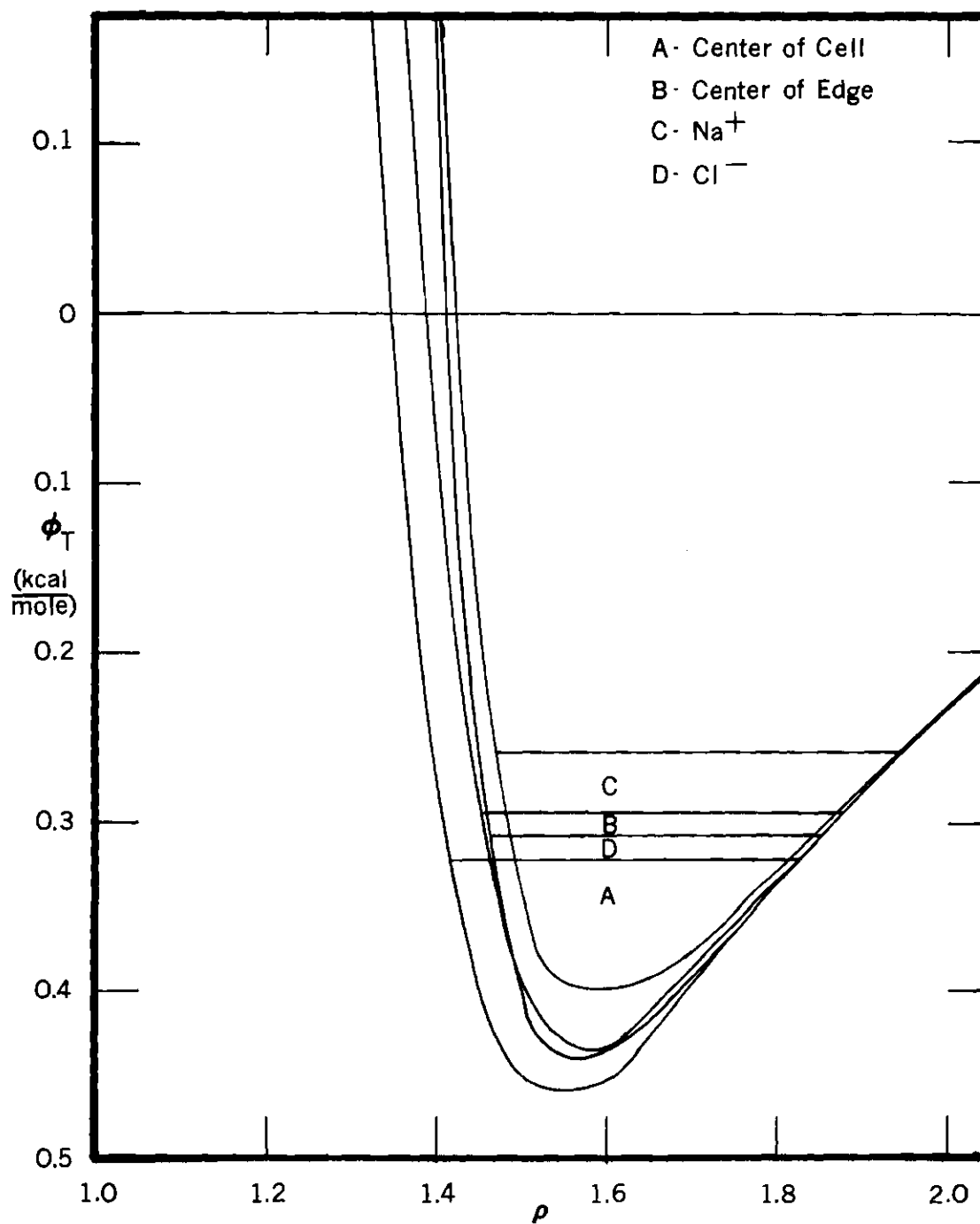


Figure 21. Potential Curves for Argon on the (100) Plane of NaCl Using the Arithmetic Mean Combining Rule for the Repulsive Potential Parameter B_{12} .

Table 15. Results Obtained from the Potential Energy Curve for Argon on the (100) Plane of Sodium Chloride, using the Arithmetic Mean Combining Rule for the Repulsive Potential Parameter B_{12} .

Site	T (°K)	z_m (Å)	$-E_o$ (kcal/mole)	$\nu \times 10^{-12}$ (sec) ⁻¹	$-E_{av}$ (kcal/mole)
A	72.14	4.34	0.466	0.072	0.322
	77.12				0.312
	82.88				0.301
	89.96				0.287
B	72.14	4.43	0.434	0.072	0.291
	77.12				0.281
	82.88				0.269
	89.96				0.256
C	72.14	4.50	0.407	0.069	0.263
	77.12				0.253
	82.88				0.242
	89.96				0.228
D	72.14	4.43	0.451	0.089	0.308
	77.12				0.298
	82.88				0.287
	89.96				0.273

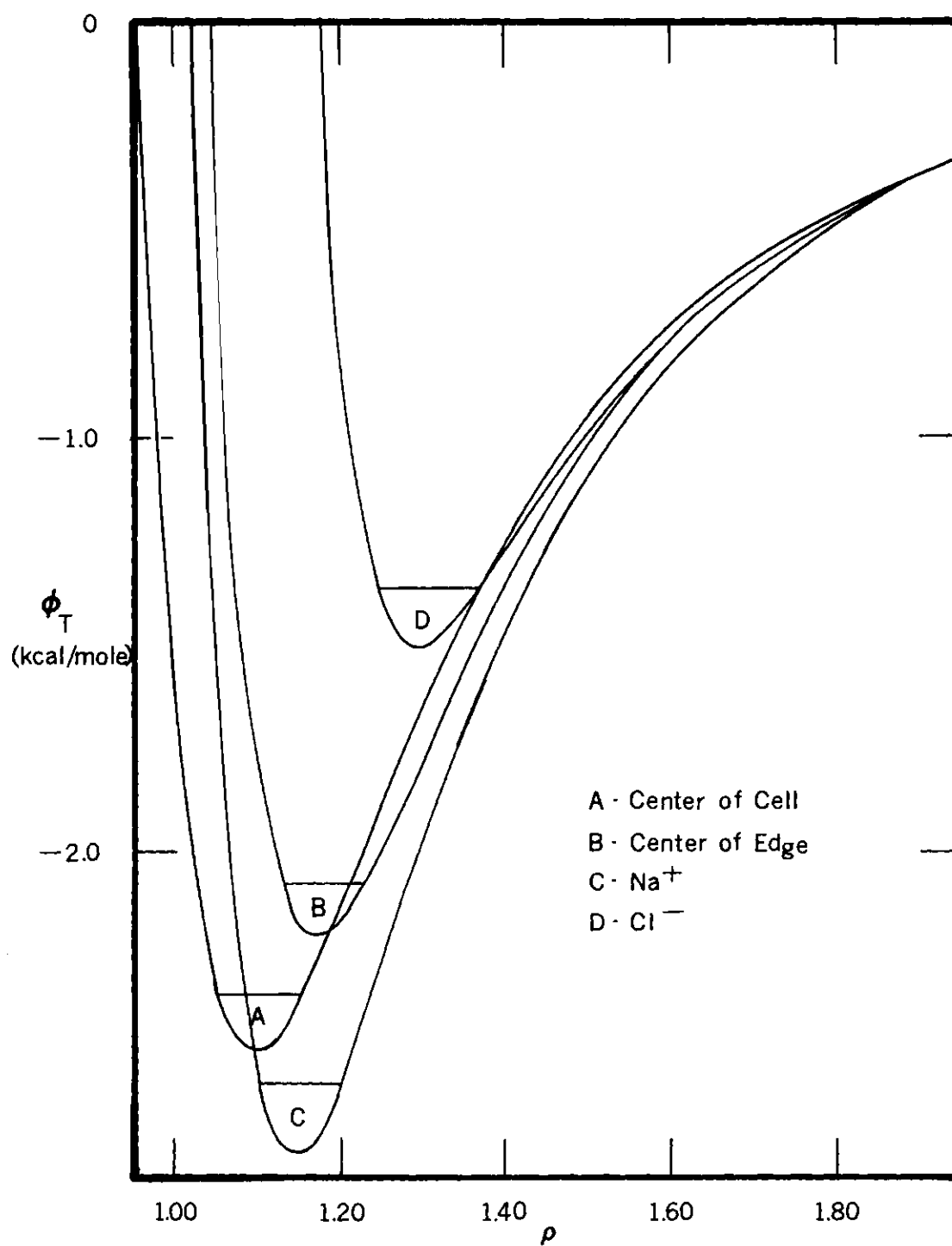


Figure 22. Potential Curves for Nitrogen on the (100) Plane of NaCl.

Table 16. Results Obtained from the Potential Energy Curve for Nitrogen on the (100) Plane of Sodium Chloride

Site	T (°K)	z_m (Å)	$-E_o$ (kcal/mole)	$\nu \times 10^{-12}$ (sec) ⁻¹	$-E_{av}$ (kcal/mole)
A	72.12	3.09	2.484	0.252	2.353
	77.11				2.343
	82.88				2.331
	90.07				2.317
B	72.12	3.31	2.303	0.283	2.172
	77.11				2.163
	82.88				2.151
	90.07				2.137
C	72.12	3.22	2.699	0.268	2.568
	77.11				2.558
	82.88				2.547
	90.07				2.533
D	72.12	3.66	1.497	0.221	1.364
	77.11				1.354
	82.88				1.343
	90.07				1.329

Table 17. Total Average Energy and q_{st}^c

System	T_0 (°K)	E_{av}^T (kcal/mole)	q_{st}^c (kcal/mole)
Ar-NaCl	72.14	0.091	1.044
(Geometric	77.12	0.888	1.041
Mean)	82.88	0.874	1.038
	89.96	0.857	1.035
Ar-NaCl	72.14	0.299	0.443
(Arithmetic	77.12	0.290	0.443
Mean)	82.88	0.278	0.443
	89.96	0.263	0.443
N ₂ -NaCl	72.12	2.453	2.596
	77.11	2.432	2.586
	82.88	2.410	2.575
	90.07	2.383	2.562

CHAPTER VII

ISOSTERIC HEATS

The isosteric heats of adsorption for both argon and nitrogen on the doubly heat treated sodium chloride were determined from the Clausius Clapeyron equation in the form

$$q_{st} = R(\partial \ln P / \partial (1/T)) \quad (114)$$

where R equals 1.9872 cal/(mole °K). The term $\partial \ln P / \partial (1/T)$ was determined by plotting the $\ln P$ versus $1/T$ at constant N_{ads} (micromoles/gm). The data were then fit to a least squares linear equation and the slope was taken as $\partial \ln P / \partial (1/T)$. The standard deviation for the nitrogen-sodium chloride isosteres ranged between 7×10^{-3} and 0.025. For the argon isosteres the standard deviation ranged between 10^{-2} and 0.05.

To determine the error in the isosteric heats consider the integrated form of equation (114)

$$q_{st} = R \left(\frac{T_1 T_2}{T_2 - T_1} \right) \ln (P_2/P_1) \quad (115)$$

The error in temperature measurements is negligible, therefore the main source of error is in the $\ln(P_2/P_1)$ term. A root mean square method is used to estimate the error in the isosteric heats.⁵ The per cent error in $\ln(P_2/P_1)$ is given by

$$\% \text{ Error} = \sqrt{(\% \text{ error } P_1)^2 + (\% \text{ error } P_2)^2} \quad (116)$$

The accuracy of the isosteric heats then is given by

$$q_{st} = R \left(\frac{T_1 T_2}{T_2 - T_1} \right) \ln (P_2/P_1) \left(1 \pm \frac{\% \text{Error}}{100} \right) \quad (117)$$

or

$$q_{st} = R \left(\frac{T_1 T_2}{T_2 - T_1} \right) \ln (P_2/P_1) \pm R \left(\frac{T_1 T_2}{T_2 - T_1} \right) \ln (P_2/P_1) \left(\frac{\% \text{Error}}{100} \right) \quad (118)$$

In the low pressure region (<5 torr), the error in pressure measurement is approximately $\pm 2\%$ and the error in reading the graph paper, plotting and the graph paper itself is estimated as $\pm 1\%$. Equation (118) then estimates the error in the heats of adsorption as ± 76 cal/mole for argon and ± 127 cal/mole for nitrogen.

In the high pressure region, the error in pressure measurement is approximately $\pm 1.8\%$ and the error in reading, plotting and the graph paper itself is again estimated as $\pm 1\%$. Equation (118) estimates the error in the heats of adsorption as ± 70 cal/mole for argon and ± 120 cal/mole for nitrogen.

The experimental error in the isotherms themselves was also determined by finding the standard deviation of the points about the best fitting smooth curve drawn between them. Extrapolating the standard deviation back to the pressure axis yielded an uncertainty of $\pm 3\%$ in the low pressure region. This is in close agreement with the errors

determined above for the low pressure region, and lends credibility to them.

The zero coverage isosteric heats were obtained by the method discussed in Chapter I. Plots of the isosteric heats as q_{st} (kcal/mole) versus N_{ads} (micromoles/gm) are shown in Figures 23 and 24. The calculated and experimental isosteric heats are compared in Table 18. The data of the isosteric heat plots is given in Appendix A.

Table 18. Theroetical and Experimental Isosteric Heats at Zero Coverage.

System	T (°K)	q_{st} (kcal/mole)		
		Experimental	Theoretical	
			Geometric Mean	Arithmetic Mean
Ar	72.14	1.640 ± .076	1.044	0.443
	77.12		1.041	0.443
	82.88		1.038	0.443
	89.96		1.035	0.443
N ₂	72.12	3.040 ± .127	2.596	
	77.11		2.586	
	82.88		2.575	
	90.07		2.562	

Discussion of Results

The results of the calculated versus the experimental zero coverage isosteric heats of adsorption are shown in Table 22. The calculations using the arithmetic mean combining rule for the repulsive potential of the argon-sodium chloride system predicts too small an interaction energy and too large an equilibrium distance (Table 15). For

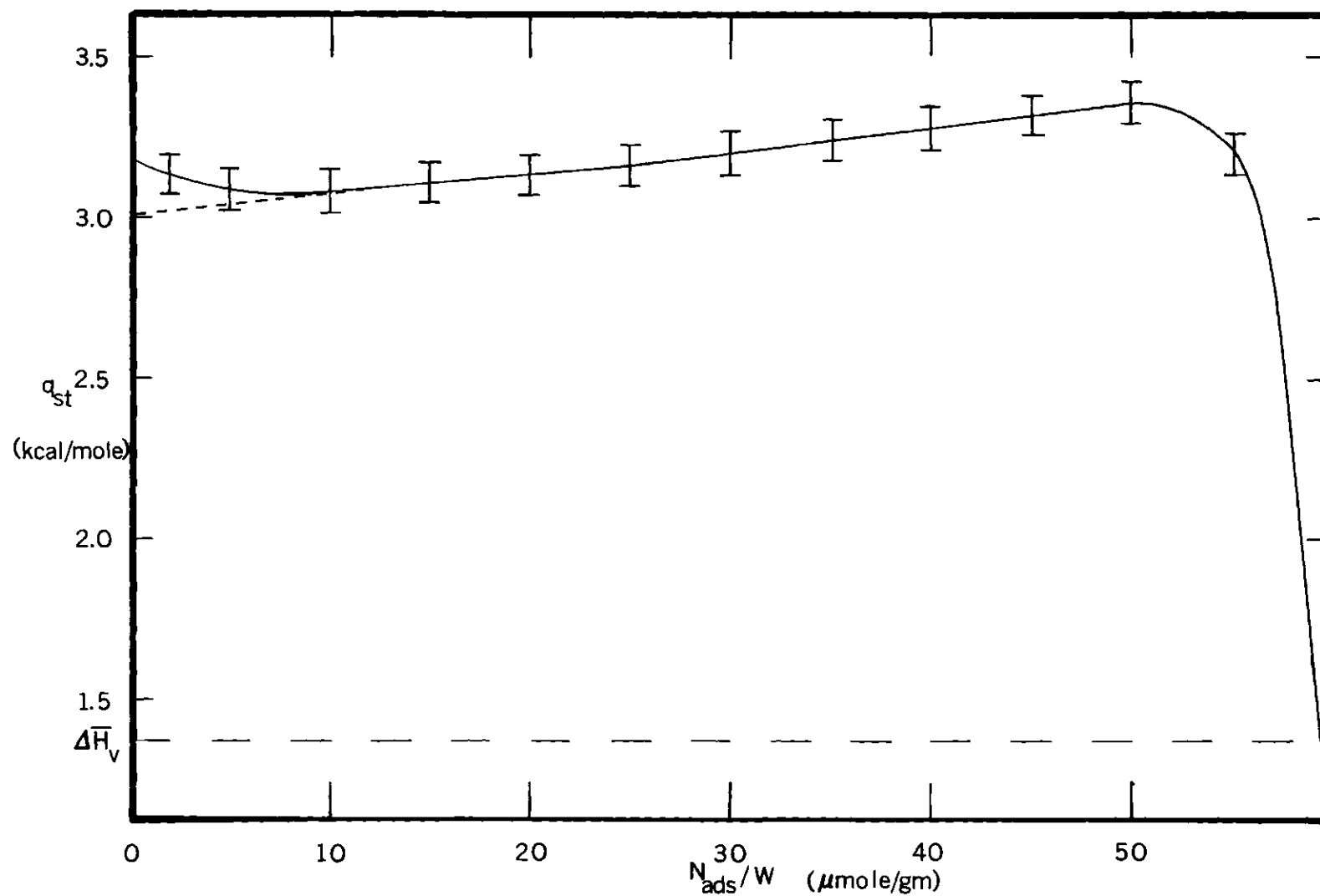


Figure 23. Isosteric Heat of Adsorption of Nitrogen on NaCl.

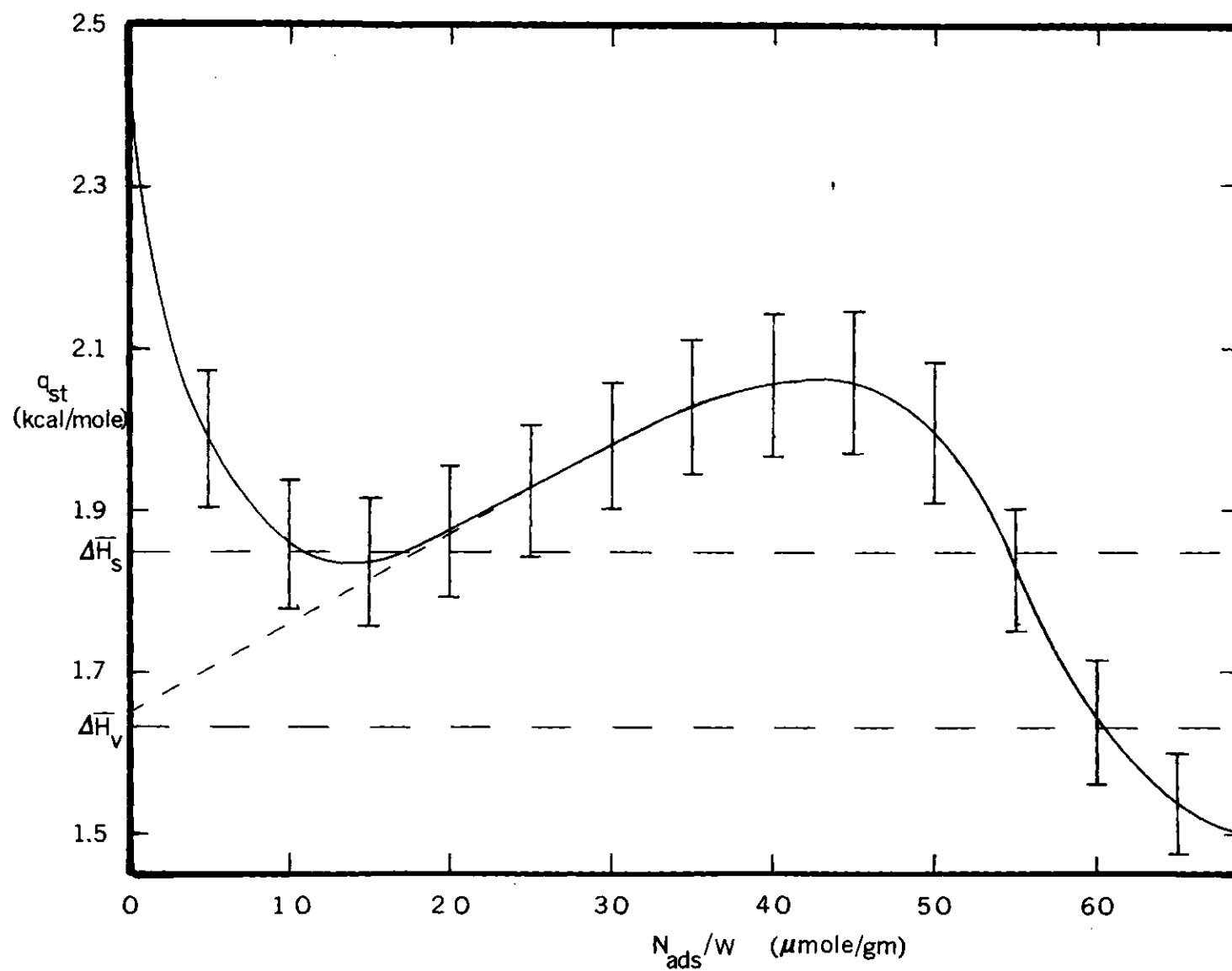


Figure 24. Isosteric Heat of Adsorption of Argon on NaCl.

this reason, this potential was dropped from further consideration and it was not considered for the nitrogen-sodium chloride system.

Although the calculated results for both the argon and nitrogen interactions using the geometric mean combining rule are not within the experimental error limits, the results are within 30% for the argon data and 15% for the nitrogen data. The difference between the calculated and experimental isosteric heats amounts to 600 cal/mole for the argon-sodium chloride system and to 450 cal/mole for the nitrogen-sodium chloride system. Since the difference in the calculated and experimental values are approximately the same for argon and nitrogen, it appears that some systematic correction is needed to bring the values into agreement. Several possible alternative methods of performing the calculations of Chapter VI will now be considered.

The results of using different combining rules for the repulsive potential, showed that the geometric mean combining rule results in the best agreement with experimental data. This is in agreement with Abrahamson's⁶² quantum mechanical results for the noble gases. He determined the repulsive potential for both self and mixed interactions and found that without assuming any form for the repulsive potential that the mixed interactions were correctly predicted by

$$\phi_{R_{12}}(r) = (\phi_{R_{11}}(r) \phi_{R_{22}}(r))^{\frac{1}{2}} \quad (119)$$

To further test this finding, the quantum mechanical data of Gordon and Kim⁶³ for the self and mixed interaction potential of argon

and krypton were examined since these are presumably more precise than the TFD values used by Abrahamson. Since the total potential was reported as a function of the internuclear distance between the atoms, the portion of the potentials attributed mainly to repulsive interactions (less than 3 \AA internuclear distance) was employed. Selecting the self interaction potential for argon and krypton at the same value of internuclear distance (r_i), the mixed interaction potential was calculated from equation (119). Values were calculated for internuclear distances of between 3 \AA and 0.05 \AA . The logarithm of the calculated data, $\ln \phi_R^C$, was plotted against the logarithm of the quantum mechanical results, $\ln \phi_R^{QM}$, in atomic units, and found to form a nearly straight line (Figure 25). A linear least squares fit to the data yields

$$\ln \phi_R^C = 0.0158 + 0.9962 \ln \phi_R^{QM} \quad (120)$$

(in atomic units)

with a standard deviation of ± 0.0126 atomic units.

This suggests that the combining rule of Zener⁵⁹ for the exponential parameter β is consistent with the geometric mean combining rule for the pre-exponential parameter B . Consider the self interaction repulsive potentials

$$\phi_{R_{11}}(r) = B_{11} \exp(-\beta_{11} r) \quad (121)$$

$$\phi_{R_{22}}(r) = B_{22} \exp(-\beta_{22} r) \quad (122)$$

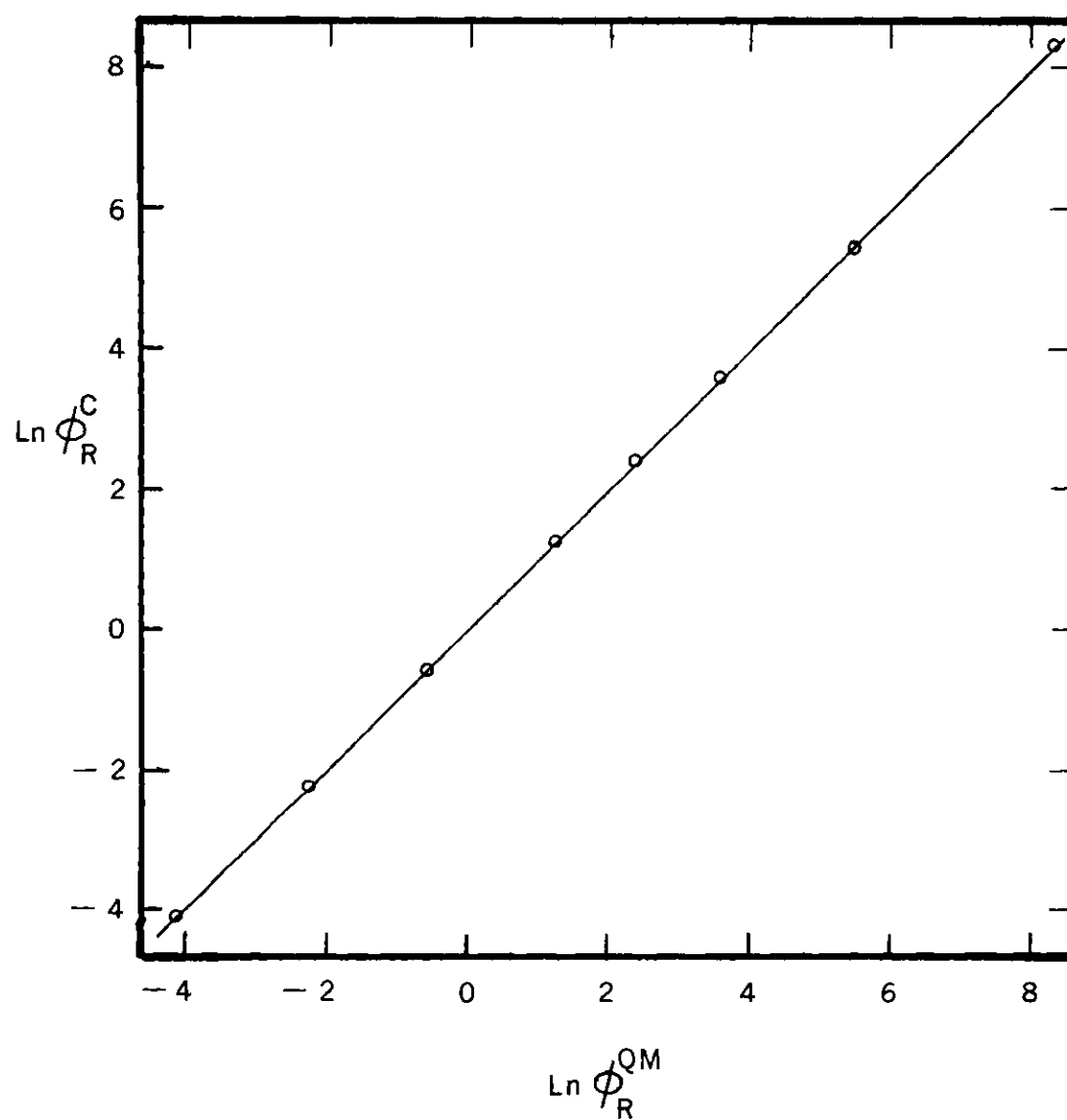


Figure 25. Calculated versus Theoretical Repulsive Potential for Ar-Kr System.

Substitution of equations (121) and (122) into equation (119) yields

$$\phi_{R_{12}} = (B_{11} B_{22})^{\frac{1}{2}} \exp (-\frac{1}{2}(\beta_{11} + \beta_{22}) r) \quad (123)$$

These results show that the combining rules used for the repulsive potential in the present study are valid, especially at the close inter-nuclear distances of 3 Å⁰ or less, where the repulsive potential becomes the predominant term in the total potential.

Although several combining rules were examined for the determination of the pre-exponential constant B, only one combining rule was used for the dispersion constant C, namely equation (72). The relationship between the values of C obtained from the Kirkwood-Muller¹² formula and the quantum mechanical values of Starkschall and Gordon⁵³ as shown in equation (71) was based on both the self and mixed interactions of argon, xenon and krypton. It is possible that this relationship does not exactly hold for the mixed interactions of gas molecules with ions. Assuming that the relationship of equation (71) does hold for the ion-ion self interactions, the following expressions are obtained

$$C_{22} = C_{11} (C_{22_{KM}} / C_{11_{KM}}) \quad (124)$$

$$C_{33} = C_{11} (C_{33_{KM}} / C_{11_{KM}}) \quad (125)$$

Equation (124) representing the mixed interaction with the chloride ion

will be discussed in the following presentation. An analogous argument applies for the mixed interaction with the sodium ion, which is represented in equation (125).

The geometric mean combining rule is given by⁵⁷

$$C_{12} = (C_{11} C_{22})^{\frac{1}{2}} \quad (126)$$

Substitution of equation (124) into equation (126), yields after algebraic rearrangement, the following expression

$$C_{12} = C_{11} (C_{12_{KM}} / C_{11_{KM}}) \left(\frac{\alpha_1 x_2 + \alpha_2 x_1}{2(\alpha_1 x_1 \alpha_2 x_2)^{\frac{1}{2}}} \right) \quad (127)$$

This expression differs from equation (72) by the factor ψ where

$$\psi = \frac{\alpha_1 x_2 + \alpha_2 x_1}{2(\alpha_1 x_1 \alpha_2 x_2)^{\frac{1}{2}}} \quad (128)$$

This factor then is a measure of the difference in calculating C_{12} by equation (72) and equation (127). The values of ψ are given in Table 19.

An alternative method of evaluating the constant C_{12} is by use of the harmonic mean combining rule⁵⁸

$$C_{12} = \frac{2C_{11}C_{22}}{C_{11} + C_{12}} \quad (129)$$

Again substituting equation (124) into equation (129) and rearranging

yields

$$C_{12} = C_{11} (C_{12_{KM}} / C_{11_{KM}}) \left(\frac{\alpha_1 \chi_2 + \alpha_2 \chi_1}{\alpha_1 \chi_1 + \alpha_2 \chi_2} \right) \quad (130)$$

This expression differs from equation (72) by the factor ψ' where

$$\psi' = \frac{\alpha_1 \chi_2 + \alpha_2 \chi_1}{\alpha_1 \chi_1 + \alpha_2 \chi_2} \quad (131)$$

The values of ψ' are given in Table 19.

Table 19. Values of ψ and ψ'

System	ψ	ψ'
Ar-Na ⁺	1.03	0.465
Ar-Cl ⁻	1.02	0.933
N ₂ -Na ⁺	1.14	0.611
N ₂ -Cl ⁻	1.00	0.841

It is evident from the factors for the harmonic mean combining rule (ψ'), that using this combining rule would predict an even smaller interaction potential. Since this is not the direction needed to improve agreement, this combining rule is rejected.

The factors for the geometric mean combining rule are nearly unity and thus the values of C_{12} determined by this mean are nearly identical to the values obtained from equation (72). It appears, therefore, that the use of equation (72) seems justified.

A second alternative to the calculation of Chapter VI is to employ a different potential for the self interaction of the adsorbate molecules. To determine the effect of changing this potential, the interaction of argon with sodium chloride was investigated. The (6 - exp) potentials of Whalley and Schneider⁵¹ and Sherwood and Prausnitz⁵⁰ as shown in Table 8 were compared.

Simplification of the calculations was obtained by summing only the interaction over the nearest ions of the crystal and integrating over the remainder. Using the (6 - exp) potential, the partial summation and integration over all the ions yields the following equation for the total potential over the center of a cell

$$\begin{aligned} \phi_T = & -(C_{12} + C_{13}) \left\{ \frac{2}{R_o} + \pi\rho \left[\frac{1}{3R_o^3} - \frac{z}{4R_o^4} \right] \right\} + (B_{12} + B_{13}) \\ & \left\{ 2e^{-\beta R_o} + \pi\rho \left[\frac{e^{-\beta R_o}}{\beta} \left((-R_o - \frac{1}{\beta}) \left(\frac{z}{\beta} - \frac{2}{\beta^2} \right) + R_o^2 \right) \right] \right\} \end{aligned} \quad (132)$$

where C_{12} , C_{13} , B_{12} , B_{13} and β are the mixed interaction parameters as determined by equations (72), (79) and (84). Details of the derivation of equation (132) are given in Appendix J. The values of these parameters using the Sherwood and Prausnitz potential are given in Table 10, while those from the potential of Whalley and Schneider are given in Table 20. The term R_o is the distance from the adsorbate molecule to a point in the crystal which forms the lower limit of the integration.

The use of equation (132) does not include the electrostatic forces. The issue of concern, however, is the effect of the adsorbate self-interaction potential on the total mixed interaction potential.

Although the partially integrated form is not as exact as the summations of Chapter VI, the magnitude of any difference due to the use of different adsorbate potentials should be evident. The results of this calculation are tabulated in Appendix J and plots of the data are shown in Figure 26.

Table 20. Mixed Interaction Parameters from the Potential of Whalley and Schneider

Parameter	Ar-Cl ⁻	Ar-Na ⁺	Ar-Ar
$C \times 10^{11}$ (ergs A ⁶)	13.3717	2.0520	8.8789
$B \times 10^8$ (ergs)	1.4299	0.2512	3.9549
β (A ⁰⁻¹)	3.4313	3.4313	3.9641

The potential minima of the two potential energy curves differ by less than 10 cal/mole and the predicted equilibrium distances differ by only 0.02 A⁰ (Table 21).

Table 21. Potential Minima and Equilibrium Distances

(6 - exp) Potential	E_m (kcal/mole)	r_m (A ⁰)
S & P	-0.791	3.38
W & S	-0.782	3.33

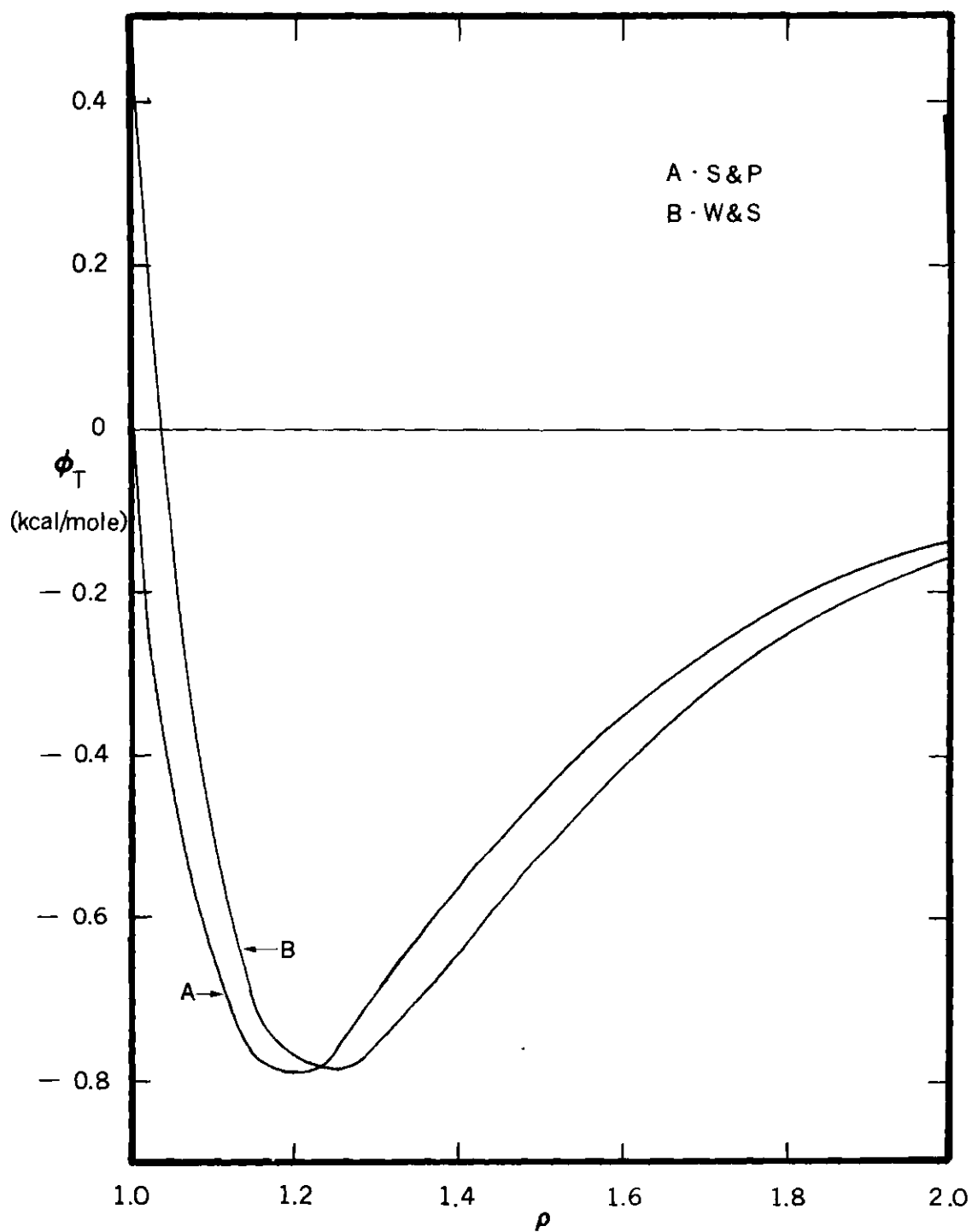


Figure 26. Partially Integrated Potential Curves for Argon over the Center of a Cell on the (100) Plane of NaCl.

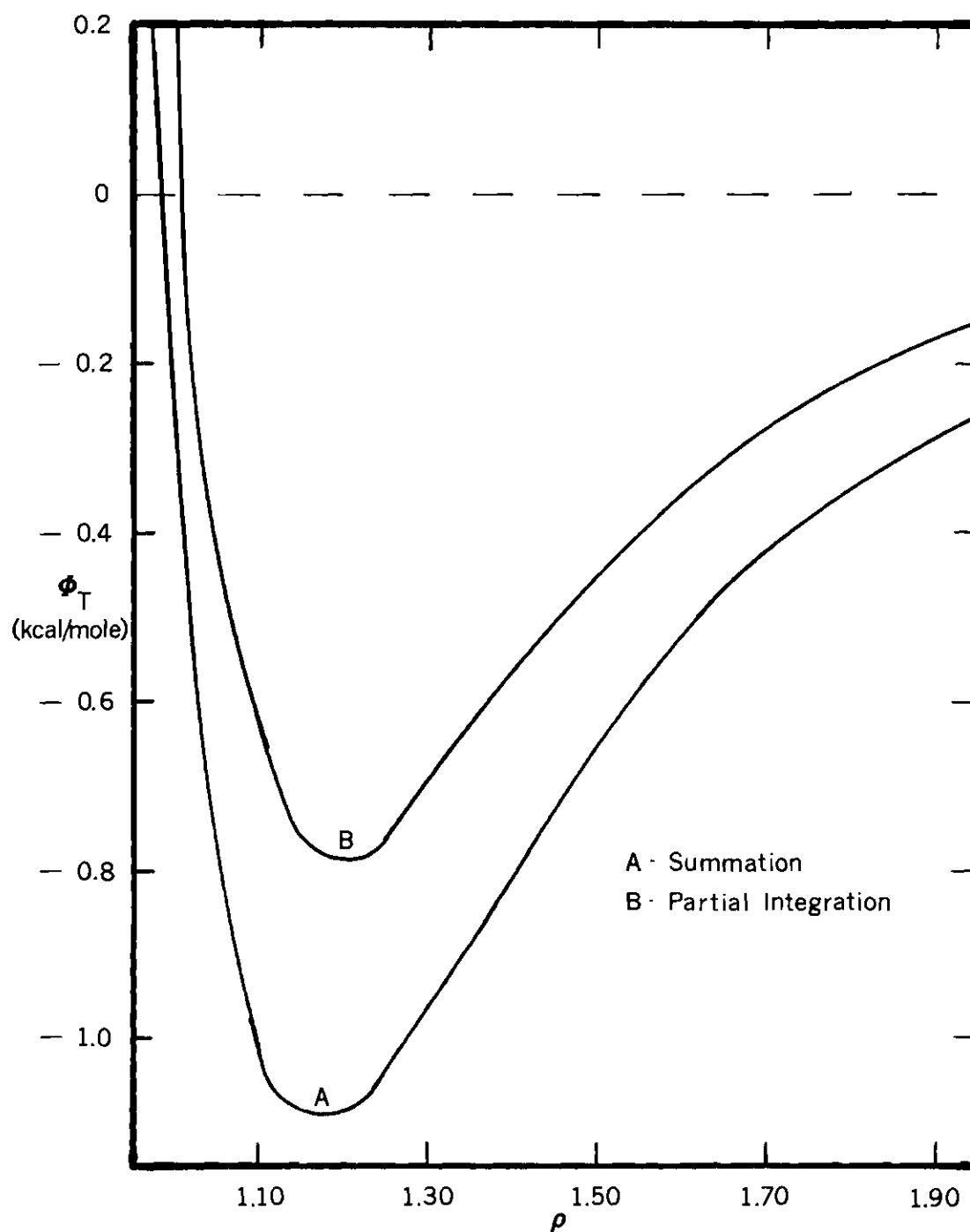


Figure 27. Partially Integrated and Summed Potential Curves for Argon over the Center of a Cell on the (100) Plane of NaCl.

From these results it appears that changing the self-interaction potential for the adsorbate has little effect in this instance on the total potential. This is due to a self compensation of the parameters of the two (6 - exp) potentials investigated. Thus the choices of a different potential for the self-interaction of the adsorbate for the calculations of Chapter VI would probably not result in an significant change in the total potential.

The integrated potential obtained from the data of Sherwood and Prausnitz was compared to the summation potential of Chapter VI for the position over the center of a lattice cell. The resulting plots are shown in Figure 27. The equilibrium distance of the integrated potential is 0.06 \AA^0 greater than the summed potential, while the potential minima is 0.304 kcal/mole less than the summed potential. These results clearly indicate the superiority of the summations of Chapter VI to the partially integrated method outlined above. Integration does not give proper weight to the nearest molecule-ion interactions.

A fourth consideration is the method of calculating the electrostatic potential. Equation (89) implies that the adsorbate molecule is adequately represented as a polarizable point. Since the cross sectional area of the argon atom is on the order of 5.7 \AA^0 and the unit cell area of the (100) plane of sodium chloride is 7.95 \AA^{02} , this assumption is not exactly valid. Lenel⁷ has considered this problem. He represented the electrostatic interaction by equation (28), repeated here for convenience

$$\phi_E = \int \frac{(P - P_o)^2 \rho_e}{J_E} d\tau \quad (28)$$

The systems Ar-KCl, Kr-KCl and Ar-KI were investigated by Lenel. The interaction over the ions was calculated and for adsorption over the center of a cell or over the mid point of a lattice edge, the interaction was estimated to be 80-90% of the maximum interaction found over an ion. The basis for this estimation is not explained by Lenel. His calculations are presumably more accurate than those obtained from equation (89); however the assumption of a reduction of 10-20% of the maximum interaction when the adsorbate is over the center of a cell or lattice edge is unclear. Lenel does not state how he obtained the reduction factors of 10-20%.

An estimate of the effect of equation (28) on the argon-sodium chloride system of this study was made in the following manner. The value of ϕ_E was calculated by equation (86) for the same systems studied by Lenel. Assuming proportionality, the logarithm of these data were then plotted against the logarithm of the values of ϕ_E^L obtained by Lenel's calculations. The data appeared to form a straight line and were fitted by a least squares fit to a linear equation in the form

$$\ln \phi_E^L = \ln k + a \ln \phi_E \quad (133)$$

and was found to be

$$\ln \phi_E^L = 0.534 + 1.084 \ln \phi_E \quad (134)$$

From equation (134) then the value of ϕ_E^L was estimated for the argon-sodium chloride system. The values of ϕ_E^L thus obtained were

substituted for ϕ_E in the potential curves for argon-sodium chloride systems found in Chapter VI. This increased the total average energy for the system to 1.115 kcal/mole and the calculated isosteric heat at 72.14°K to 1.258 kcal/mole. This value of the calculated isosteric heat is within 270 cal/mole of the error limits of the experimental isosteric heat. Although Pierotti² has stated that the problem of electrostatic forces cannot be solved exactly using classical methods, it appears that a more realistic, perhaps a quantum mechanical, representation of the electrostatic forces is required.

Besides the (100) plane of face centered cubic sodium chloride, a common equilibrium crystal face is the (111) plane found on octahedral sodium chloride. Two types of (111) planes are possible, one made up of all sodium ions and one made up of all chloride ions. Young²⁴ has calculated the energy of interaction for argon on the (111) planes of octahedral potassium chloride. He found the difference in the energy of interaction between the two (111) planes amounted to over 500 cal/mole. Since the polarizability⁵⁵ of the potassium ion (1.228 \AA^3) is much greater than that of the sodium ion (0.303 \AA^3), it is expected that the difference in the (111) planes of sodium chloride would be even greater. The site energy distributions calculated in Chapter V indicate a very narrow energy distribution, less than 200 cal/mole. For this reason the (111) planes are not considered as likely for the sodium chloride sample of this study as the (100) planes.

Several alternative approaches to the calculations of Chapter VI have been considered and it was found that a more realistic expression for the electrostatic force may bring closer agreement between the

calculated and experimental results. It is possible that other combining rules may be considered for the parameters of the dispersion and repulsive potentials. No claim is made here to have exhausted all possibilities.

Recommendations

More studies to determine exactly the crystal plane exhibited by the sublimated sodium chloride are needed. Low energy electron diffraction studies would be of great assistance in determining these planes. Additional isotherms on an adsorption apparatus with a greater precision in pressure measurements in the low pressure region would reduce the errors in the isosteric heats.

Further thermoetical work is also required, especially in the area of combining rules for the parameters of the dispersion and repulsive potentials. Since the parameters of the repulsive potential of Huggins and Mayer¹³ are empirically determined, an up-to-date re-examination of the potential in alkali halides is indicated.

The sample used in this study has been shown to possess a homogeneous surface. This then makes the isotherm data almost ideal for fitting to theoretical isotherm equations. From such work, various proposed models for adsorption, such as the Van der Waals theory,² significant structures theory⁶⁴, etc., can be tested.

Adsorption studies on RbF would be of interest to the present study since RbF and NaCl have the same crystal structure and nearly the same lattice constant (less than 0.01 Å difference). Differences in their adsorption behavior could then be related directly to the

differences in the ionic species. If both adsorbents exhibited localized adsorption processes, then the coverage per molecule, σ , will be the same for a particular adsorbate on each of the adsorbents.

If the two adsorbents were inert, such that the lateral interaction of the adsorbate molecules was independent of the presence of the surface, then comparable lateral interaction energies should be obtained from the two systems. However, if the solids are not inert, then the difference in the influence of these two adsorbents on the lateral interaction of the adsorbate can be estimated and tested against various models.^{65,70}

APPENDIX A

EXPERIMENTAL DATA AND ISOSTERIC HEATS

Table 22. Data for the Isotherm of Argon on Untreated Sodium Chloride
at 77.08 K.

P (torr)	P/P ₀	N _{ads} (μmoles per gram)
1.4924	.00756	5.10
3.4826	.0176	8.59
5.0755	.0257	10.97
6.4686	.0328	14.90
8.0606	.0409	18.45
9.8508	.0500	21.39
11.744	.0597	25.74
13.135	.0668	30.52
14.728	.0749	35.66
16.317	.0829	41.37
17.714	.0899	48.41
19.306	.0980	54.33
21.296	.1082	58.80
23.683	.1205	60.93
25.675	.1307	63.66
28.163	.1431	66.29
30.252	.1539	68.36
33.240	.1692	70.64
35.626	.1815	72.57
40.199	.2048	75.93
42.789	.2183	77.69
47.368	.2421	80.74
53.441	.2738	84.40
60.895	.3068	88.53
66.468	.3350	91.71
73.336	.3704	96.65
79.010	.3994	100.13
83.896	.4256	104.61
87.470	.4444	107.68
91.350	.4639	111.30
95.226	.4828	113.77
99.604	.5050	117.58
104.28	.5296	123.59
108.68	.5515	128.03
111.25	.5666	133.11
115.23	.5884	139.75
120.59	.6181	146.49
123.78	.6340	153.09
127.18	.6517	157.80
131.24	.6723	161.45
135.14	.6936	166.73
138.12	.7140	172.18

Table 22. Continued

P (torr)	P/P ₀	N _{ads} (μmoles per gram)
143.86	.7400	179.46
148.13	.7648	186.42
152.04	.7816	191.94
156.03	.7996	199.45
160.31	.8253	212.24
164.58	.8491	222.38
168.87	.872	235.15
172.76	.8916	248.83
177.81	.9117	262.56

Table 23. Data for the Isotherm of Nitrogen on Untreated Sodium Chloride at 77.25°K.

P (torr)	P/P ⁰	N _{ads} (μmoles per gram)
.7958	.0011	52.91
1.7908	.0024	65.25
2.1890	.0029	68.01
3.6813	.0049	69.99
8.7538	.0116	70.40
16.007	.0211	71.96
22.364	.0298	72.21
38.456	.0513	73.23
55.534	.0745	74.73
64.567	.0857	76.52
73.402	.0978	77.81
82.276	.1101	78.12
89.527	.1199	78.98
106.40	.1425	80.73
111.56	.1495	81.84
123.07	.1650	84.80
134.19	.1798	85.95
145.75	.1949	86.78
156.66	.2096	88.62
165.24	.2190	90.25
174.57	.2314	92.10
188.78	.2501	93.95
203.65	.2694	96.12
221.52	.2934	98.91
234.31	.3103	100.61
250.44	.3325	105.15
264.24	.3501	108.77
270.54	.3601	110.63
286.20	.3810	114.17
296.24	.3965	117.30
302.49	.4028	117.65
304.17	.4050	117.98
320.54	.4262	123.89
334.82	.4432	131.27
350.81	.4680	136.07
361.01	.4831	139.50
376.45	.4987	142.13
381.33	.5082	147.27
393.49	.5217	147.28
401.70	.5373	152.85
417.83	.5593	161.00

Table 24. Data for the Isotherm of Argon on Sodium Chloride at 77.22°K, after the Initial Heat Treatment.

P (torr)	P/P ₀	N _{ads} (μmoles per gram)
5.1716	.0255	8.89
9.3508	.0456	14.36
12.732	.0636	21.04
15.018	.0749	32.02
17.307	.0861	42.76
20.698	.1031	49.59
24.867	.1241	54.77
29.641	.1487	57.45
35.610	.1781	60.63
40.180	.2001	62.90
45.438	.2257	64.73
50.410	.2489	66.56
54.882	.2753	68.82
60.252	.2976	70.21
64.919	.3249	73.30
69.686	.3509	75.11
74.550	.3758	77.56
79.418	.3967	79.87
84.278	.4221	82.66
89.180	.4469	84.73
93.152	.4671	97.30
97.423	.4876	91.34
102.18	.512	94.81
105.72	.5304	99.39
110.00	.5541	103.65
115.76	.5791	107.53
118.15	.5890	110.76
121.42	.6061	115.22
125.48	.6261	121.01
129.25	.6434	125.77
133.31	.6660	131.14
141.32	.7031	144.66
145.88	.7270	151.89
152.13	.7563	160.53
157.97	.7886	171.38
162.92	.8110	183.23
169.96	.8560	201.59
174.22	.8673	217.06
179.87	.8968	234.78
187.79	.9347	274.69

Table 25. Data for the Isotherm of Argon on Doubly Heat Treated Sodium Chloride at 72.14°K.

P (torr)	P/P _o	N _{ads} (μmoles per gram)
.0468	.000547	.83
.2344	.00274	1.84
.3851	.00449	2.24
.6096	.00713	2.84
.8323	.00972	3.39
1.0863	.0127	4.02
1.3601	.0159	4.72
1.6651	.0194	5.47
1.9653	.0229	6.23
2.3248	.0270	7.15
2.6923	.C 14	8.14
3.0896	.0361	9.25
3.4969	.0408	10.49
3.8100	.0444	11.48
4.1794	.0488	12.86
4.3904	.0512	13.70
4.8964	.0571	16.08
5.2894	.0620	18.86
5.6422	.0660	22.07
5.8992	.0689	25.35
6.1007	.0713	29.36
6.2833	.0734	33.27
6.4317	.0751	36.45
6.7300	.0786	40.78
6.8616	.0801	41.84
7.0888	.0827	43.84
7.4550	.0827	45.99
7.9158	.0922	47.66
8.4018	.0979	49.18
8.9633	.1043	50.43
9.6006	.1117	51.67
10.087	.1182	52.64
10.889	.1271	53.67
11.722	.1365	54.53
12.397	.1446	55.22
13.173	.1535	55.87
13.918	.1622	56.54
14.549	.1694	56.96
15.471	.1802	57.77
16.014	.1862	58.17
16.841	.1959	58.83

Table 25. Continued

P (torr)	P/P ₀	N _{ads} (μ moles per gram)
17.651	.2061	59.73
18.598	.2169	60.44
19.569	.2285	61.10
20.510	.2396	61.84
21.444	.2505	62.64
22.435	.2621	63.30
23.552	.2739	64.19
24.630	.2874	65.05
26.046	.3041	66.21
27.025	.3150	66.91
27.509	.3209	67.38

Table 26. Data for the Isotherm of Argon on Doubly Heat Treated Sodium Chloride at 77.12°K.

P (torr)	P/P ₀	N _{ads} (μmoles per gram)
.0811	.0004	.55
.2380	.0012	1.10
.8868	.0046	2.06
1.4493	.0073	2.63
1.4974	.0074	2.72
2.5300	.0127	3.74
2.7937	.0143	3.99
2.9867	.0153	4.29
3.3067	.0166	4.45
3.8512	.0198	5.17
4.7430	.0243	6.03
4.9215	.0249	6.29
4.9888	.0256	6.28
5.7703	.0296	7.20
6.5180	.0336	8.08
7.2241	.0365	8.73
7.7093	.0393	9.65
8.0949	.0424	10.13
8.6006	.0448	10.94
9.5155	.0494	12.13
10.595	.0553	13.98
11.213	.0571	14.84
11.322	.0588	15.13
11.619	.0590	15.43
11.649	.0603	15.91
12.497	.0637	17.27
12.831	.0652	18.17
13.589	.0692	20.23
14.354	.0730	22.92
14.977	.0758	25.11
15.147	.0770	26.55
15.489	.0880	29.60
16.013	.0818	30.81
16.519	.0832	32.99
16.795	.0857	35.35
17.366	.0875	37.14
17.747	.0905	39.50
18.628	.0940	41.69
19.519	.0985	43.94
20.548	.1038	45.89
22.228	.1125	48.05
23.434	.1187	49.25

Table 26. Continued

P (torr)	P/P ⁰	N _{ads} (μmoles per gram)
25.147	.1272	50.86
26.631	.1348	59.92
27.776	.1406	52.49
32.598	.1634	55.06
37.570	.1882	57.14
42.369	.2109	58.71
47.431	.2359	60.31
52.412	.2610	61.82
57.476	.2864	63.92
67.511	.3368	68.04
72.486	.3616	70.43
77.555	.3867	72.61
86.839	.4361	78.30
92.101	.4635	80.97
96.871	.4870	84.57
101.64	.5113	88.14
106.21	.5343	92.94
110.28	.5542	96.52
114.07	.5724	102.57
118.09	.5923	107.70
122.06	.6111	112.15
125.44	.6277	118.27
129.30	.6490	123.65
133.17	.6695	129.22
137.63	.6865	133.92
142.12	.7095	140.34
147.07	.7358	146.81
151.42	.7577	154.24
156.08	.7808	161.86
155.29	.7846	164.79
159.94	.8045	171.60
164.80	.8298	183.99
169.94	.8580	202.64
175.99	.8904	223.26
186.99	.9462	278.53

Table 27. Data for the Isotherm of Argon on Doubly Heat Treated Sodium Chloride at 82.88°K.

P (torr)	P/P ⁰	N _{ads} (μmoles per gram)
.2421	.000529	.53
.4874	.00106	.83
.7728	.00169	1.10
1.0879	.00238	1.35
1.3979	.00307	1.54
1.7805	.00390	1.75
2.1647	.00475	1.96
2.6690	.00585	2.20
3.1638	.00693	2.43
3.6979	.00809	2.67
4.3855	.00959	2.96
5.0564	.0111	3.24
5.8708	.0129	3.59
6.8562	.0151	4.00
7.8345	.0172	4.40
8.5351	.0188	4.65
9.8550	.0210	5.21
10.391	.0228	5.39
11.742	.0257	6.14
13.181	.0289	6.89
14.677	.0371	7.57
16.078	.0352	8.27
17.509	.0383	9.02
18.942	.0414	9.67
19.833	.0434	10.12
21.450	.0470	11.18
23.765	.0522	12.84
26.946	.0591	15.21
30.128	.0661	18.22
32.320	.0708	20.83
33.311	.0733	22.28
34.304	.0750	23.71
37.291	.0819	28.11
39.178	.0858	31.11
41.166	.0899	34.64
43.257	.0946	37.66
45.242	.0989	40.38
47.330	.1033	43.26
49.616	.1083	45.30
51.995	.1137	46.98
54.190	.1183	48.40
56.583	.1238	50.03

Table 27. Continued.

P (torr)	P/P ⁰	N _{ads} (μmoles per gram)
59.942	.1306	51.61
62.942	.1380	53.35
66.422	.1455	54.19
69.702	.1528	55.83
73.382	.1604	59.09
76.864	.1679	58.29
80.745	.1765	59.30
84.813	.1856	60.58
88.199	.1927	61.97
92.862	.2029	62.66
97.145	.2124	64.09
101.12	.2212	65.19
105.90	.2317	67.19
110.17	.2405	68.13

Table 28. Data for the Isotherm of Argon on Doubly Heat Treated Sodium Chloride at 89.96°K.

P (torr)	P/P ⁰	N _{ads} (μmoles per gram)
.6443	.000635	.38
1.4641	.00144	.75
2.3992	.00236	1.08
3.2632	.00322	1.36
4.1732	.00411	1.58
5.0486	.00597	1.78
5.8075	.00572	1.96
6.6917	.00661	2.05
6.8478	.00676	2.16
7.8350	.00774	2.21
8.4725	.00835	2.38
8.4658	.00839	2.40
9.3119	.00917	2.50
9.8359	.00969	2.59
11.162	.0111	2.86
12.317	.0123	3.02
12.730	.0129	3.03
13.264	.0132	3.21
13.909	.0138	3.29
14.781	.0146	3.47
17.405	.0176	3.94
17.546	.0175	3.97
20.602	.0205	4.54
21.618	.0215	4.76
23.273	.0236	5.04
23.752	.0237	5.21
24.850	.0246	5.40
25.955	.0257	5.65
26.569	.0265	5.79
27.092	.0269	5.91
28.108	.0279	6.24
34.510	.0350	8.10
40.377	.0409	9.56
46.343	.0470	10.92
52.109	.0528	12.88
57.587	.0581	14.86
63.256	.0638	17.06
68.823	.0694	19.00
75.086	.0757	21.16
81.248	.0819	23.50
87.714	.0884	26.69
93.880	.0947	29.66

Table 28. Continued.

P (torr)	P/P ⁰	N _{ads} (μmoles per gram)
98.950	.0998	32.47
104.62	.1055	34.78
111.88	.1129	38.84
118.44	.1195	42.15
125.19	.1265	44.60
131.96	.1333	47.09
137.74	.1384	48.97
144.20	.1449	51.23
149.57	.1503	52.93
154.64	.1554	54.12
158.72	.1595	54.98
165.48	.1663	55.73
170.75	.1716	57.26
176.62	.1776	58.13
183.28	.1854	59.02
189.34	.1907	60.25
195.90	.1972	61.05
202.56	.2039	62.35
208.37	.2091	62.69
214.33	.2149	64.09
221.29	.2219	64.48
227.74	.2282	65.96
235.01	.2358	66.94

Table 29. Data for the Isotherm of Nitrogen on Doubly Heat Treated Sodium Chloride at 72.12°K.

P (torr)	P/P ⁰	N _{ads} (μmoles per gram)
.000332	.0000015	.85
.000899	.0000022	1.62
.00339	.0000087	2.80
.00535	.0000137	3.70
.00904	.0000231	4.04
.0126	.0000323	6.88
.0143	.0000367	7.53
.0175	.0000447	9.03
.0193	.0000494	9.80
.0220	.0000562	11.39
.0244	.0000625	12.58
.0251	.0000644	13.08
.0278	.0000711	14.94
.0282	.0000722	15.27
.0315	.0000804	17.46
.0325	.0000831	18.01
.0350	.0000895	20.00
.0364	.0000931	20.96
.0396	.000101	23.55
.0400	.000102	23.96
.0420	.000108	26.06
.0464	.000118	29.25
.0493	.000126	31.78
.0564	.000144	35.90
.0571	.000147	36.24
.0622	.000159	39.03
.0714	.000183	42.32
.0798	.000204	44.32
.0942	.000241	47.03
.1166	.000299	49.62
.1210	.000311	49.98
.1498	.000384	51.69
.2093	.000538	53.54
.2594	.000665	54.53
.4610	.00118	56.09
.5222	.00134	56.23
.6871	.00176	56.83
.9659	.00247	57.26
1.1360	.00291	57.33
1.8750	.00481	57.79
2.6430	.00678	58.04
2.7490	.00704	58.08

Table 29. Continued

P (torr)	P/P ⁰	N _{ads} (μmoles per gram)
3.5103	.00899	58.25
4.2803	.0109	58.35
5.2220	.0134	58.51
6.8690	.0176	58.68
8.4844	.0217	58.87
9.1913	.0236	59.05
11.502	.0294	59.18
12.581	.0322	59.29
14.266	.0365	59.42
16.008	.0409	59.55
17.776	.0454	59.65
19.455	.0497	59.71
22.281	.0569	59.89
21.429	.0547	60.01
23.721	.0606	60.18
25.791	.0658	60.28
27.55	.0703	60.35

Table 30. Data for the Isotherm of Nitrogen on Doubly Heat Treated Sodium Chloride at 77.11°K.

P (torr)	P/P ⁰	N _{ads} (μmoles per gram)
.00159	.00000214	.99
.0144	.0000194	2.90
.0252	.0000337	4.09
.0379	.0000511	5.24
.0574	.0000769	7.52
.0627	.0000846	7.93
.0859	.000115	10.47
.0903	.000121	11.31
.1056	.000141	13.97
.1152	.000156	14.70
.1214	.000160	15.13
.1335	.000179	16.94
.1358	.000183	18.19
.1492	.000201	19.71
.1564	.000211	21.64
.1756	.000336	24.13
.1765	.000238	25.19
.1858	.000250	26.08
.1951	.000263	28.21
.2050	.000276	29.18
.2186	.000295	31.77
.2234	.000301	31.80
.2395	.000322	34.04
.2474	.000334	35.44
.2583	.000348	35.94
.2701	.000365	37.55
.2807	.000379	39.94
.2908	.000404	39.95
.3219	.000436	41.76
.3303	.000446	42.55
.3553	.000482	43.51
.3851	.000524	45.09
.4098	.000554	45.98
.4560	.000621	47.48
.5222	.000706	49.11
.5420	.000737	49.36
.6426	.000873	50.80
.7052	.000953	51.59
.7398	.00101	51.91
.8354	.00115	52.75
.9278	.00128	53.31
1.0219	.00138	53.71

Table 30. Continued.

P (torr)	P/P ⁰	N _{ads} (μ moles per gram)
1.0069	.00139	53.76
1.0910	.00150	54.07
1.2048	.00166	54.52
1.4076	.00190	55.07
1.5068	.00204	55.14
1.8181	.00250	55.76
1.9307	.00260	55.88
2.1699	.00300	56.12
2.1697	.00353	56.52
2.6844	.00368	56.54
3.1626	.00434	56.82
3.3865	.00456	56.96
3.6407	.00500	57.06
4.0749	.00560	57.21
4.2059	.00567	57.26
4.3568	.00597	57.30
5.0615	.00682	57.53
5.6847	.00780	57.61
5.8992	.00796	57.72
6.5096	.00887	57.76
6.7983	.00918	57.90
9.2035	.0125	58.04
10.681	.0145	58.17
11.9309	.0162	58.20
13.1740	.0179	58.36
14.6067	.0199	58.44
15.9656	.0217	58.67
18.0653	.0245	58.86
18.3505	.0251	58.97
19.8528	.0269	59.01
21.8156	.0296	59.18
23.8480	.0324	59.35
25.7119	.0351	59.60
27.4411	.0375	59.52

Table 31. Data for the Isotherm of Nitrogen on Doubly Heat Treated Sodium Chloride at 82.88°K.

P (torr)	P/P ⁰	N _{ads} (μmoles per gram)
.0125	.00000902	1.14
.0408	.0000294	2.48
.0881	.0000633	3.71
.1354	.0000976	4.94
.1796	.000129	6.09
.2299	.000165	7.50
.2735	.000197	8.70
.3089	.000222	9.81
.3449	.000249	11.02
.3851	.000278	12.21
.4182	.000302	13.23
.4512	.000326	14.43
.4908	.000354	15.76
.5287	.000382	17.14
.5683	.000409	18.54
.6013	.000434	19.81
.6327	.000456	21.08
.6640	.000479	22.29
.7102	.000511	24.16
.7201	.000519	24.39
.7580	.000546	25.84
.8141	.000585	27.82
.8686	.000627	29.92
.9329	.000673	32.05
.9890	.000714	33.73
1.0730	.000774	36.04
1.1721	.000844	38.10
1.2907	.000930	40.28
1.4440	.00104	42.50
1.6007	.00115	44.23
1.7935	.00129	45.88
2.0178	.00145	47.45
2.2964	.00165	49.93
2.5372	.00182	49.78
2.8999	.00209	50.08
3.4081	.00246	52.19
4.0280	.00291	53.18
4.7749	.00345	54.04
5.4953	.00496	54.66
6.3544q	.00459	55.21
7.2784	.00524	55.58
8.3138	.00599	55.90

Table 31. Continued

P (torr)	P/P ⁰	N _{ads} (μmoles per gram)
9.6770	.00697	56.13
11.3877	.00823	56.50
13.2628	.00954	56.85
15.1903	.0102	57.08
16.8917	.0122	57.50
18.5395	.0134	57.58
21.1838	.0152	57.74
23.7019	.0171	57.98
26.4233	.0190	58.18
28.1523	.0203	58.14

Table 32. Data for the Isotherm of Nitrogen on Doubly Heat Treated Sodium Chloride at 90.07°K.

P (torr)	P/P ⁰	N _{ads} (μmoles per gram)
.0445	.0000165	1.10
.1539	.0000571	2.21
.3786	.000141	3.64
.6940	.000258	5.62
1.0502	.000391	7.71
1.4888	.000549	10.40
1.8732	.000691	13.14
2.2540	.000832	15.99
2.6129	.000866	18.80
3.0967	.00115	22.79
3.3522	.00124	24.65
3.8206	.00141	28.11
4.2100	.00155	30.37
4.7835	.00176	33.64
5.3247	.00196	36.37
5.8325	.00214	38.35
6.3997	.00236	40.28
7.1596	.00263	42.37
7.8669	.00289	43.91
8.6557	.00319	45.26
9.4514	.00348	46.39
9.9815	.00368	47.07
11.1496	.00411	48.30
11.6358	.00429	48.70
12.6458	.00467	49.48
13.9209	.00515	50.34
14.8993	.00550	51.06
16.9881	.00628	51.90
18.0928	.00669	52.32
19.3237	.00715	52.63
20.4700	.00753	52.77
21.5355	.00792	53.05
22.6718	.00833	53.25
23.7953	.00885	53.49
24.9637	.00927	53.78
25.5574	.00959	53.96
28.1428	.0106	54.74
33.4121	.0125	55.72
34.3051	.0129	55.90
38.5852	.0145	56.16
43.2578	.0162	56.34
48.4287	.0182	56.96

Table 32. Continued

P (torr)	P/P ⁰	N _{ads} (μ moles per gram)
54.2945	.0204	57.41
57.8736	.0218	57.87
65.0331	.0244	58.04
70.9999	.0267	58.56
83.5268	.0314	59.29

Table 33. Isostatic Heats of Adsorption for Argon on Sodium Chloride.

N_{ads} ($\mu\text{moles/gm.}$)	q_{st} (Kcal/mole)	N_{ads} ($\mu\text{moles/gm.}$)	q_{st} (Kcal/mole)
1	2.461	34	2.016
2.	2.213	35	2.024
3	2.081	36	2.031
4	2.031	37	2.038
5	1.980	38	2.045
6	1.941	39	2.051
7	1.904	40	2.056
8	1.881	41	2.060
9	1.869	42	2.063
10	1.859	43	2.066
11	1.848	44	2.065
12	1.841	45	2.062
13	1.838	46	2.055
14	1.834	47	2.046
15	1.834	48	2.034
16	1.856	49	2.018
17	1.866	50	1.995
18	1.877	51	1.971
19	1.886	52	1.946
20	1.896	53	1.919
21	1.908	54	1.883
22	1.919	55	1.838
23	1.928	56	1.791
24	1.939	57	1.748
25	1.949	58	1.712
26	1.959	59	1.680
27	1.969	60	1.640
28	1.979	61	1.625
29	1.988	62	1.601
30	1.998	63	1.578
31	2.007	64	1.562
32	2.016	65	1.546
33	2.024	66	1.534

Table 34. Isosteric Heats of Adsorption for Nitrogen on Sodium Chloride.

N_{ads} (μ moles/gm.)	q_{st} (Kcal./mole)	N_{ads} (μ moles/gm.)	q_{st} (Kcal./mole)
2	3.127	31	3.217
3	3.114	32	3.220
4	3.104	33	3.225
5	3.091	34	3.225
6	3.082	35	3.236
7	3.072	36	3.244
8	3.070	37	3.252
9	3.075	38	3.261
10	3.077	39	3.271
11	3.078	40	3.282
12	3.086	41	3.289
13	3.091	42	3.295
14	3.097	43	3.299
15	3.105	44	3.306
16	3.110	45	3.314
17	3.115	46	3.325
18	3.120	47	3.331
19	3.126	48	3.340
20	3.130	49	3.356
21	3.134	50	3.361
22	3.143	51	3.358
23	3.148	52	3.360
24	3.156	53	3.387
25	3.163	54	3.358
26	3.173	55	3.300
27	3.181	56	3.152
28	3.191	57	3.010
29	3.201	58	2.317
30	3.210	59	1.513

APPENDIX B

SITE ENERGY DISTRIBUTION ANALYSIS

In Chapter III, it was shown that adsorption on a heterogeneous surface composed of several different homogeneous patches could be described by

$$\Theta(P,T) = \int_0^{\infty} \theta(Q,P,T) f(Q) dQ \quad (57)$$

where $\Theta(P,T)$ is the fraction of the total surface occupied, $\theta(Q,P,T)$ is the fraction of each homogeneous patch of interaction energy Q that is occupied. The probability of there being a patch with an interaction energy between Q and dQ is given by the differential distribution function $f(Q) dQ$.

An integral distribution function was defined by

$$f(Q) = dF/dQ \quad (58)$$

where F is the fraction of the total surface for which the interaction energy is equal to or greater than a given Q . From the definition of equation (58), it follows that

$$\Theta(P,T) = \int_0^1 \theta(Q,P,T) dF \quad (59)$$

The first step in solving equation (59) by Adamson's graphical method⁴⁶

is to choose a local isotherm function $\theta(bP)$. For heterogeneous surfaces this graphical solution is independent of the choice of the local isotherm function as long as b is proportional to $\exp(Q/RT)$. One of the simplest isotherm functions fitting this requirement is the Langmuir equation with provisions for lateral interactions⁴⁹

$$\theta = \frac{bP \exp(z\theta\omega/RT)}{1 + bP \exp(z\theta\omega/RT)} \quad (60)$$

$$b = b_0 \exp(Q/RT) \quad (135)$$

The derivation of equations (60) and (135) and the definition of the terms contained therein are given in Appendix C.

The local isotherm function is then plotted as θ versus bP as shown in Figure 28. From this plot and equation (60), it is seen that 50% occupancy occurs at $bP = X$. The approximation is then made to replace (bP) by a step function which occurs at $bP = X$. Thus for $bP < X$, $\theta = 0$ and for $bP > X$, $\theta = 1$. Physically this means that sites of b values greater than X/P for a given value of P are completely filled and the rest are completely empty. The first approximation to F , then is given by $F = \theta_{\text{obs}}$. Consequently a plot of θ_{obs} versus X/P is constructed which is also a plot of F_1 versus b . The subscript (1) on F denotes the first approximation. A typical plot is shown in Figure 29a.

The second approximation is made by selecting a particular pressure P_i , and noting that for each value of b , a value of θ can be obtained from Figure 28 and a value of F from Figure 29a. This θ will

be the fraction of sites with energy proportional to b that are filled, and F will be the fraction of sites on the surface with energy equal to or greater than that which is proportional to b . By taking a series of b values, an auxiliary plot of θ versus F can then be constructed for the pressure P_i . A typical plot is shown in Figure 29a. The total surface occupancy at P_i is then the area under the curve, since

$$\Theta = \int_0^1 \theta dF \quad (136)$$

Generally the Θ calculated in this manner will be somewhat different than Θ_{obs} , because the distribution function F_1 used in determining it is not correct. The adjustment is then made, so that the second approximation to F is given by

$$F_2 = F_1 (\Theta_{\text{obs}} / \Theta_2) \quad (137)$$

where Θ_2 is the calculated Θ from equation (136), F_2 is then determined in this manner for the whole series of pressure values covering the experimental isotherm. The values of F_2 are then entered on the plot in Figure 29a, at their corresponding values of X/P . A curve is then drawn through the points (this is represented by the dashed curve in Figure 29a).

Additional approximations are made in the same manner. A pressure P_i is selected and for each value of b , the value of θ is obtained from Figure 28, while the value of F is obtained from the plot of the previously determined distribution function F_{N-1} . These values are plotted

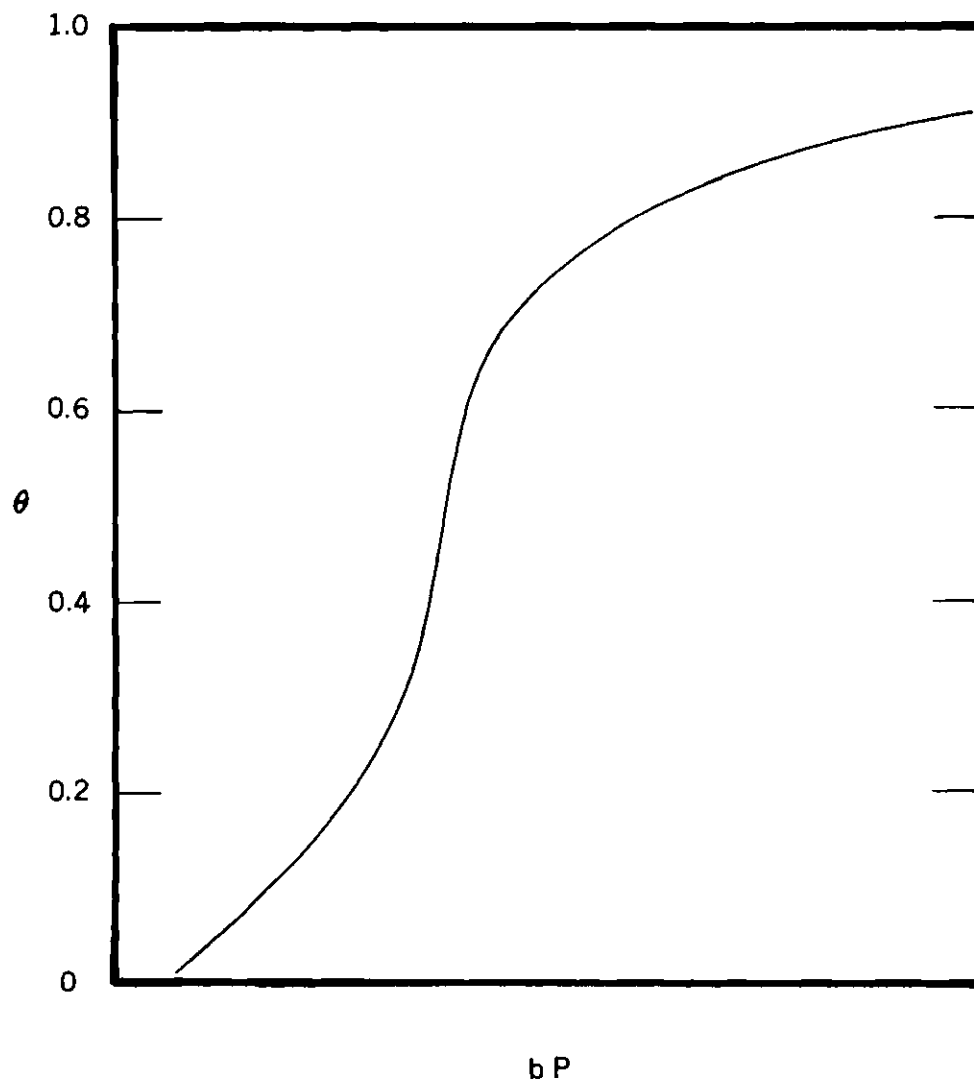


Figure 28. Typical Plot of the Fowler and Guggenheim Equation (60).

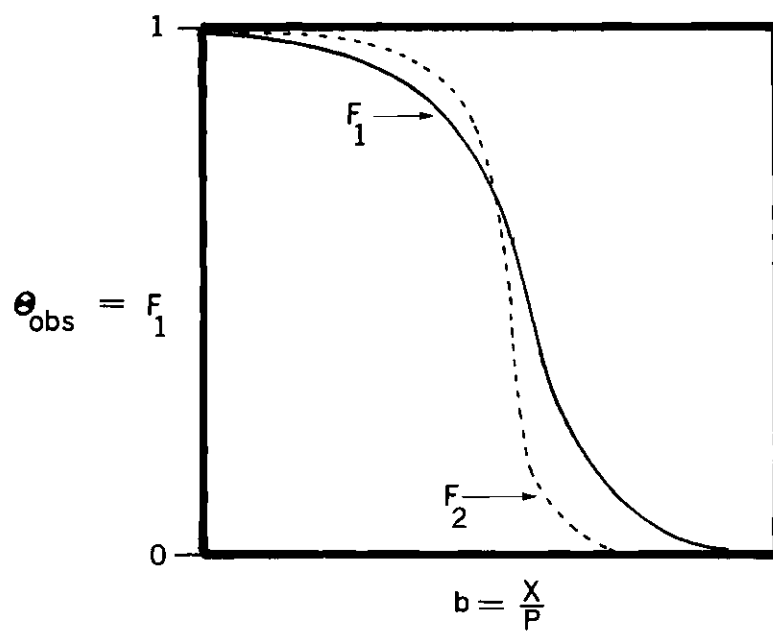


Figure 29a. Typical Plot of θ_{obs} versus X/P .

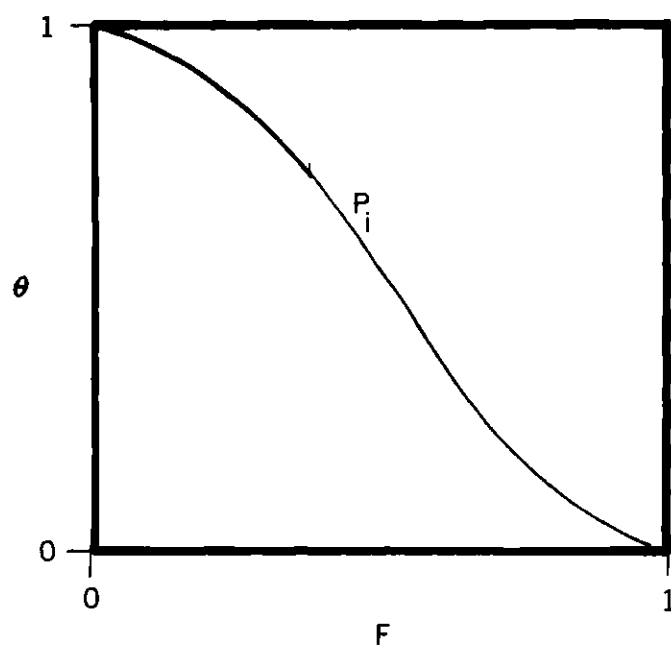


Figure 29b. Typical Plot of θ versus F at Pressure P_i .

and again a value of Θ_N is obtained. The new approximation to F is given by,

$$F_N = F_{N-1} (\Theta_{\text{obs}} / \Theta_N) \quad (138)$$

where Θ_N is the total occupancy using the distribution function F_{N-1} and F_N is the n th approximation to F. From equation (138), it is seen that when $\Theta_N = \Theta_{\text{obs}}$, then $F_N = F_{N-1}$, and thus F_N is the sought distribution function.

It turns out that there will be no exact solution to equation (59), because the experimental data have some error and the assumed local isotherm will not be exactly correct for the system. Adamson⁴⁶ points out, however, that "a point is reached, often fairly quickly, where successive approximations do not differ by much and moreover, nonsystematically so that no continuing trends are apparent." Thus for heterogeneous surfaces, it has been found that three approximations are usually sufficient. For the sodium chloride surface of this work, twelve approximations were required.

The final F versus b plot may then be converted to one of F versus Q from the relationship of equation (135). Finally the differential site energy distribution function is obtained from

$$f(Q) = \Delta F / \Delta Q \quad (139)$$

This may then be plotted as F(Q) versus Q as shown in Figures 18 and 19.

The computations were carried out on a Burroughs 5500 Computer.

APPENDIX C

FOWLER AND GUGGENHEIM EQUATION

The Fowler and Guggenheim equation is based upon the following assumptions:⁴⁹

1. Adsorption occurs on a site, that is the adsorption is localized.
2. Adsorption on a particular site is independent of whether or not adjacent sites are filled.

The partition function for the adsorbate molecules in the gas phase is given by

$$P.F._g = q_g^N / N! \quad (140)$$

where the molecular partition function q is defined as

$$q_g = q_{g,trans} q_{g,int} \quad (141)$$

The partition function for the adsorbate molecules in the adsorbed phase is

$$q_s = q_{s,site} q_{s,int} e^{(Q/RT)} e^{(Q_1/RT)} \quad (142)$$

where the factor $e^{(Q/RT)}$ gives the partition function the same zero of

energy as the gas phase molecules and thus allows their comparison. Q is defined as the energy required to take a molecule in its lowest energy state in the adsorbed phase and form a molecule in the gas state in its lowest energy level. The term q_s is a function of temperature only and not of the degree of occupancy of sites. Q_1 is the lateral interaction energy between the adsorbed molecules.

The probability of a site being occupied is N/S , where N is the number of adsorbed molecules and S is the number of sites. If each site has z nearest neighbors, then the probability of the nearest neighbor sites being filled is zN/S . This involves $zN/2S$ molecules, with the factor of one half correcting for double counting. If the lateral interaction energy, that is the interaction energy between two adsorbed molecules, is ω , then the total added energy upon adsorption is $\frac{1}{2}(z N\omega)/S$. Therefore

$$Q_1 = \frac{1}{2}(z N\omega)/S \quad (143)$$

and equation (142) becomes

$$q_s = q_{s,\text{site}} q_{s,\text{int}} e^{(Q/RT)} e^{(z N\omega)/(2SRT)} \quad (144)$$

The complete partition function is then obtained by multiplying q_s by the number of distinguishable ways of placing N molecules on S sites. The first molecule has S ways of placing it, the second has $(S - 1)$, etc., therefore for N molecules there are $S!/(S - N)!$ ways of placing the molecules.

Since the molecules are indistinguishable, $N!$ of these ways of

placing the molecules on sites are also indistinguishable. The total partition function for N molecules in the adsorbed phase is

$$(P.F.)_s = \frac{S!}{(S - N)! N!} (q_s)^N \quad (145)$$

where q_s is given by equation (144).

The helmholtz free energy is given by

$$A = -kT \ln (P.F.) \quad (146)$$

and the chemical potential is given by

$$u = (\delta A / \delta N)_T \quad (147)$$

Applying equations (146) and (147) to equation (139) results in the following expression for the chemical potential of the adsorbed molecules

$$u_s = kT \left(\ln \frac{\theta}{1 - \theta} - \ln q_s - \frac{z\theta\omega}{RT} \right) \quad (148)$$

where θ is equal to N/S .

The chemical potential of the molecules in the gas state is obtained by applying equations (146) and (147) to equation (140)

$$u_g = -kT \ln (q_g/N) \quad (149)$$

At equilibrium, $u_s = u_g$, therefore setting equations (148) and (149)

equal to each other and simplifying yields

$$\frac{\theta}{1-\theta} = \frac{q'_s}{q_g/N} \exp(z\theta\omega/RT) \quad (150)$$

Evaluation of q_g/N yields

$$q_g/N = \left(\frac{2\pi m kT}{h^2}\right)^{3/2} \frac{kT}{P} q_{g,int} \quad (151)$$

From equation (144) the term q'_s can be evaluated

$$q'_s = q_{s,site} q_{s,int} \exp(Q/RT) \quad (152)$$

Upon adsorption, the three degrees of translational freedom are supposed to appear as two degrees of translational freedom within a two dimensional box of confines a^2 , where a^2 equals σ , the area of the adsorption site. The other degree of freedom appears as a degree of vibration in the adsorption bond normal to the surface. Thus $q_{s,site}$ is defined as

$$q_{s,site} = q_{s,trans} q_{s,vib} \quad (153)$$

The term $q_{s,trans}$ is evaluated as

$$q_{s,trans} = \left(\frac{2\pi m kT}{h^2}\right) \sigma \quad (153)$$

The term $q_{s,vib}$ is given as

$$q_{s,vib} = \frac{\exp(-h\nu/2kT)}{1 - \exp(-h\nu/kT)} \quad (154)$$

where ν is the characteristic vibrational frequency perpendicular to the surface.

Substituting equations (151), (153) and (154) into equation (150) and assuming that $q_{g,int}$ is equal to $q_{s,int}$, the following equation is obtained after rearrangement

$$\theta = \frac{bP e^{(z\theta\omega)/RT}}{1 + bP e^{(z\theta\omega)/RT}} \quad (60)$$

where

$$b = b_o e^{(Q/RT)}$$

$$b_o = (2\pi mkt)^{-1/2} (h/kt) q_{s,vib} \sigma$$

APPENDIX D

RESULTS OF THE SITE ENERGY DISTRIBUTION FUNCTION

Table 35. Results of the Site Energy Distribution Function

F	Q (kcal/mole)				
	N ₂			Ar	
	72.12°K	77.11°K	82.88°K	z = 1/8 H _v 72.14°K	z = 1/4 H _v 72.14°K
0	3.264	3.782	3.756	2.356	2.284
.05	2.894	2.899	2.914	1.598	1.478
.10	2.879	2.878	2.884	1.594	1.475
.15	2.871	2.867	2.869	1.592	1.473
.20	2.864	2.859	2.858	1.591	1.472
.25	2.857	2.853	2.852	1.590	1.471
.30	2.851	2.847	2.845	1.589	1.470
.35	2.847	2.841	2.839	1.588	1.469
.40	2.842	2.835	2.843	1.587	1.468
.45	2.838	2.830	2.826	1.587	1.467
.50	2.833	2.824	2.819	1.587	1.466
.55	2.828	2.818	2.813	-	-
.60	2.824	2.812	2.807	-	-
.65	2.819	2.805	2.800	-	-
.70	2.814	2.799	2.794	-	-
.75	2.808	2.792	2.785	-	-
.80	2.799	2.784	2.776	-	-
.85	2.788	2.774	2.764	-	-
.90	2.772	2.762	2.747	-	-
.95	2.747	2.742	2.725	-	-
1.00	2.215	2.086	2.453	-	-

APPENDIX E

THE INVERSE SIXTH POWER SUMMATIONS OF THE MOLECULE-ION DISTANCES

The method of determining the inverse sixth power summations of distance to the positive ions, $S_+(\rho)$ and to the negative ions, $S_-(\rho)$ was presented by Orr.¹¹ These summations are obtained by first finding the inverse sixth power summations to all the ions of the lattice. Three such summations to all of the ions are considered:

Σ_1 , the inverse sixth power summation of distance from a point at a distance normal to the surface plane, and situated above the center of a lattice cell;

Σ_2 , where the point is situated over the mid point of a lattice cell edge;

Σ_3 , where the point is situated above an ion.

In these summations the unit distances ℓ , m and n are used, where

$$\ell = z/a$$

$$m = y/a$$

$$n = x/a$$

and a is one half the crystal lattice constant.

The quantity Σ_1 is evaluated by dividing the solid into four equivalent sections by the planes $n=0$ and $m=0$. There are two types of lattice

points (ions) in each of these sections; those on the plane $m = n$ and those not on the plane. The distance R_1 to each of the lattice points on the plane $m = n$ is given by

$$R_1 = \left[(\rho + \ell)^2 + \frac{n^2}{2} \right]^{\frac{1}{2}}$$

therefore

$$\sum_{\ell=0,1,2}^{\infty} \sum_{n=1,3,5}^{\infty} R_1^{-6} = \sum_{\ell=0,1,2}^{\infty} \sum_{n=1,3,5}^{\infty} \left[(\rho + \ell)^2 + \frac{n^2}{2} \right]^{-3} \quad (155)$$

The distance R_2 to each lattice point not on the plane in each section is given by

$$R_2 = \left[(\rho + \ell)^2 + m(m + n) + \frac{n^2}{2} \right]^{\frac{1}{2}}$$

therefore,

$$\sum_{\ell=0,1,2}^{\infty} \sum_{m=1,2,3}^{\infty} \sum_{n=1,3,5}^{\infty} R_2^{-6} = \sum_{\ell=0,1,2}^{\infty} \sum_{m=1,2,3}^{\infty} \sum_{n=1,3,5}^{\infty} \left[(\rho + \ell)^2 + m(m + n) + \frac{n^2}{2} \right]^{-3} \quad (156)$$

Therefore Σ is given by the sum of equations (155) and (156) multiplied by four to account for all the sections

$$\Sigma = 4 \left(\sum_{\ell=0,1,2}^{\infty} \sum_{n=1,3,5}^{\infty} \left[(\rho + \ell)^2 + \frac{n^2}{2} \right]^{-3} + 2 \sum_{\ell=0,1,2}^{\infty} \sum_{m=1,2,3}^{\infty} \sum_{n=1,3,5}^{\infty} \left[(\rho + \ell)^2 + m(m + n) + \frac{n^2}{2} \right]^{-3} \right) \quad (157)$$

For the quantity Σ , the solid is divided into two equivalent sections by the plane $n = 0$. The distance, R_3 , to each lattice point in each of these sections is

$$R_3 = \left[(\rho + \ell)^2 + m^2 + \left(\frac{n}{2}\right)^2 \right]^{\frac{1}{2}}$$

therefore,

$$\Sigma R_3^{-6} = \sum_{\ell=0,1,2}^{\infty} \sum_{m=0,\pm 1,\pm 2}^{\infty} \sum_{n=1,3,5}^{\infty} \left[(\rho + \ell)^2 + m^2 + \left(\frac{n}{2}\right)^2 \right]^{-3} \quad (158)$$

Therefore Σ is given by twice equation (158)

$$\Sigma = 2 \sum_{\ell=0,1,2}^{\infty} \sum_{m=0,\pm 1,\pm 2}^{\infty} \sum_{n=1,3,5}^{\infty} \left[(\rho + \ell)^2 + m^2 + \left(\frac{n}{2}\right)^2 \right]^{-3} \quad (159)$$

For the quantity Σ there are two types of lattice points, those on the axis directly below the point and those not on this axis. The distance R_4 , to each point on the axis is given by

$$R_4 = \rho + \ell$$

Therefore

$$\Sigma R_4^{-6} = \sum_{\ell=0,1,2}^{\infty} (\rho + \ell)^{-6} \quad (160)$$

The remainder of the solid is divided into four equivalent sections by the planes $m = 0$ and $n = 0$. The distance R_5 to each lattice point in one of these sections is given by

$$R_5 = \left[(\rho + \ell)^2 + m^2 + n^2 \right]^{1/2}$$

therefore for the four sections

$$\sum_5^{-6} = 4 \sum_{\ell=0,1,2} \sum_{m=0,1,2} \sum_{n=1,2,3} \left[(\rho + \ell)^2 + m^2 + n^2 \right]^{-3} \quad (161)$$

Therefore \sum_3 is given by the sum of equations (160) and (161)

$$\sum_3 = \sum_{\ell=0,1,2} (\rho + \ell)^{-6} + 4 \sum_{\ell=0,1,2} \sum_{m=0,1,2} \sum_{n=1,2,3} \left[(\rho + \ell)^2 + m^2 + n^2 \right]^{-3} \quad (162)$$

These equations are valid for the (100) plane of both the simple cubic and the face centered cubic structures.

The quantities $S_+(\rho)$ and $S_-(\rho)$ may be expressed as functions of \sum_1 , \sum_2 , and \sum_3 . Orr has given the expressions relating these quantities for the four types of sites discussed in chapter VI.

1. Site A, above the center of a lattice cell

$$S_+(\rho) = \frac{1}{2} \sum_1(\rho) \quad (163)$$

$$S_-(\rho) = \frac{1}{2} \sum_1(\rho) \quad (164)$$

2. Site B, above the mid point of a lattice edge

$$S_+(\rho) = \frac{1}{2} \sum_2(\rho) \quad (165)$$

$$S_-(\rho) = \frac{1}{2} \sum_2(\rho) \quad (166)$$

3. Site C, above the positive ion

$$S_+(\rho) = \left(\frac{1}{2}\right)^6 \left[\sum_1(\rho/2) + 2 \sum_2\left(\frac{\rho+1}{2}\right) + \sum_3\left(\frac{\rho}{2}\right) \right] \quad (167)$$

$$S_-(\rho) = \left(\frac{1}{2}\right)^6 \left[\sum_1\left(\frac{\rho+1}{2}\right) + 2 \sum_2(\rho/2) + \sum_3\left(\frac{\rho+1}{2}\right) \right] \quad (168)$$

4. Site D, above the negative ion

$$S_+(\rho) = \left(\frac{1}{2}\right)^6 \left[\sum_1\left(\frac{\rho+1}{2}\right) + 2 \sum_2\left(\frac{\rho}{2}\right) + \sum_3\left(\frac{\rho+1}{2}\right) \right] \quad (169)$$

$$S_-(\rho) = \left(\frac{1}{2}\right)^6 \left[\sum_1(\rho/2) + 2 \sum_2\left(\frac{\rho+1}{2}\right) + \sum_3(\rho/2) \right] \quad (170)$$

The values of \sum_1 , \sum_2 and \sum_3 for ρ , $\rho/2$ and $(\rho + 1)/2$ are presented in Tables 36, 37 and 38. These summations are general and may be used for any simple cubic or face centered cubic structure. The summations $\sum_1(\rho/2)$, $\sum_2\left(\frac{\rho+1}{2}\right)$ etc., are found by substituting $(\rho/2)$, $\left(\frac{\rho+1}{2}\right)$ etc., for ρ in equations (157), (159) and (162). The calculations were made on a Burroughs 5500 Computer by summing over 20,000 lattice points.

Table 36. Summations ($\Sigma(\rho)$) of the Inverse Sixth Power of Distance from Equations (157), (159), and (162) for the (100) Plane of the Face Centered Cubic Structure.

ρ	Σ 1	Σ 2	Σ 3
.35	17.6588	41.1409	547.9388
.40	14.9028	31.2635	247.7265
.45	12.4490	23.6379	123.6649
.50	10.3218	17.8686	66.9078
.55	8.5153	13.5547	38.7261
.60	7.0050	10.3464	23.7492
.65	5.7568	7.9618	15.3158
.70	4.7338	6.1843	10.3222
.75	3.8997	4.8522	7.2311
.80	3.2218	3.8467	5.2400
.85	2.6715	3.0813	3.9110
.90	2.2247	2.4934	2.9948
.95	1.8614	2.0375	2.3448
1.00	1.5652	1.6806	1.7713
1.05	1.2331	1.3985	1.5184
1.10	1.1243	1.1735	1.2498
1.15	.9605	.9224	1.0416
1.20	.8249	.8453	.8776
1.25	.7120	.7249	.7465
1.30	.6177	.6356	.6404
1.35	.5385	.5431	.5534
1.40	.4717	.4740	.4815
1.45	.4150	.4159	.4215
1.50	.3667	.3666	.3710
1.55	.3253	.3246	.3282
1.60	.2897	.2886	.2916
1.65	.2589	.2576	.2602
1.70	.2323	.2308	.2332
1.75	.2091	.2074	.2097
1.80	.1888	.1871	.1892
1.85	.1710	.1692	.1712
1.90	.1553	.1554	.1554
1.95	.1414	.1397	.1415
2.00	.1292	.1292	.1292

Table 37. Summations ($\Sigma(\rho/2)$) of the Inverse Sixth Power of Distance from Equations (157), (159), and (162) for the (100) Plane of the Face Centered Cubic Structure.

ρ	Σ 1	Σ 2	Σ 3
.35	28.2550	93.7090	34820.6681
.40	26.8141	85.0982	15630.0599
.45	25.3062	76.5946	7712.2224
.50	23.7594	68.4071	4100.6904
.55	22.1998	60.6887	2316.5895
.60	20.6504	53.5406	1376.0600
.65	19.1313	47.0184	852.7259
.70	17.6588	41.1409	547.9388
.75	16.2461	35.8989	363.3594
.80	14.9028	32.2635	247.7265
.85	13.6358	27.1928	173.1037
.90	12.4490	23.6379	123.6649
.95	11.3444	20.5471	90.1341
1.00	10.3218	17.8686	66.9078
1.05	9.3796	15.5532	50.5087
1.10	8.5153	13.5547	38.7261
1.15	7.7251	11.8316	30.1236
1.20	7.0050	10.3464	23.7492
1.25	6.3504	9.0661	18.9602
1.30	5.7568	7.9618	15.3158
1.35	5.2195	7.0084	12.5089
1.40	4.7338	6.1443	10.3222
1.45	4.2952	5.4709	8.6005
1.50	3.8997	4.8522	7.2311
1.55	3.5431	4.3147	6.1313
1.60	3.2218	3.8467	5.2400
1.65	2.9323	3.4384	4.5115
1.70	2.6715	3.0813	3.9110
1.75	2.4365	2.7683	3.4122
1.80	2.2247	2.4934	2.9948
1.85	3.0337	2.2513	2.6431
1.90	1.8614	2.0375	2.3448
1.95	1.7058	1.8484	2.0900
2.00	1.5652	1.6806	1.8713

Table 38. Summations ($\Sigma(\frac{\rho+1}{2})$) of the Inverse Sixth Power of Distance from Equations (157), (159), and (162) for the (100) Plane of the Face Centered Cubic Structure.

ρ	Σ 1	Σ 2	Σ 3
.35	5.2195	7.0084	12.5089
.40	4.7338	6.1843	10.3222
.45	4.2952	5.4709	8.6005
.50	3.8997	4.8522	7.2311
.55	3.5431	4.3147	6.1313
.60	3.2218	3.8467	5.2400
.65	2.9393	3.4384	4.5115
.70	2.6715	3.0813	4.9110
.75	2.4365	2.7683	3.4122
.80	2.2247	2.4934	2.9946
.85	2.0337	2.2413	2.6431
.90	1.8614	2.0375	2.3448
.95	1.7058	1.8484	2.0900
1.00	1.5652	1.6806	1.8713
1.05	1.4381	1.5315	1.6824
1.10	1.3231	1.3985	1.5184
1.15	1.2189	1.2798	1.3753
1.20	1.1243	1.1735	1.2498
1.25	1.0385	1.0385	1.1393
1.30	.9605	.9924	1.0416
1.35	.8895	.9151	.9549
1.40	.8249	.8453	.8776
1.45	.7659	.7822	.8085
1.50	.7120	.7249	.7465
1.55	.6628	.6729	.6404
1.60	.6177	.6256	.6404
1.65	.5764	.5825	.5948
1.70	.5385	.5431	.5534
1.75	.5037	.5070	.5158
1.80	.4717	.4740	.4815
1.85	.4422	.4437	.4502
1.90	.4150	.4159	.4215
1.95	.3899	.3902	.3852
2.00	.3667	.3666	.3710

APPENDIX F

EXPONENTIAL SUMMATIONS OF DISTANCE

The exponential summations of distance to the positive ions $S_+(\rho, \beta, a)$ and to the negative ions $S_-(\rho, \beta, a)$ are determined in a similar manner as $S_+(\rho)$ and $S_-(\rho)$ in Appendix E. The summations are derived in terms of the summation to all the ions for the same three cases considered earlier; Σ'_1 is similar to Σ_1 ; Σ'_2 is similar to Σ_2 ; and Σ'_3 is similar to Σ_3 . β is the exponential constant, a is one half the crystal lattice constant, and ℓ , m , and n are the same as defined in Appendix E. Since the summations to the individual ions are derived in a similar manner as those in Appendix E, they will not be repeated. The summations are given by

$$\begin{aligned} \Sigma'_1 = & 4 \sum_{\ell=0,1,2}^{\infty} \sum_{n=1,3,5}^{\infty} \left(\exp \left[- \left((\rho + \ell)^2 + \frac{n^2}{2} \right)^{\frac{1}{2}} \beta a \right] \right) \\ & + 8 \sum_{\ell=0,1,2}^{\infty} \sum_{m=1,2,3}^{\infty} \sum_{n=1,3,5}^{\infty} \left(\exp \left[- \left((\rho + \ell)^2 + m(m+n) + \frac{n^2}{2} \right)^{\frac{1}{2}} \beta a \right] \right) \end{aligned} \quad (171)$$

$$\Sigma'_2 = 2 \sum_{\ell=0,1,2}^{\infty} \sum_{m=0,\pm 1,\pm 2}^{\infty} \sum_{n=1,3,5}^{\infty} \left(\exp \left[- \left((\rho + \ell)^2 + m^2 + \left(\frac{n}{2} \right)^2 \right)^{\frac{1}{2}} \beta a \right] \right) \quad (172)$$

$$\begin{aligned} \Sigma' = \sum_{\ell=0,1,2}^{\infty} \left(\exp - \left[(\rho + \ell) \beta a \right] \right) \\ + 4 \sum_{\ell=0,1,2}^{\infty} \sum_{m=0,1,2}^{\infty} \sum_{n=1,2,3}^{\infty} \left(\exp \left[-((\rho + \ell)^2 + m^2 + n^2)^{1/2} \beta a \right] \right) \quad (173) \end{aligned}$$

The summations of distance, $S_+(\rho, \beta, a)$ and $S_-(\rho, \beta, a)$ are found by the following combinations:

1. Site A, above the center of a lattice cell

$$S_+(\rho, \beta, a) = \frac{1}{2} \Sigma'(\rho, \beta, a) \quad (174)$$

$$S_-(\rho, \beta, a) = \frac{1}{2} \Sigma'(\rho, \beta, a) \quad (175)$$

2. Site B, above the mid point of a lattice edge

$$S_+(\rho, \beta, a) = \frac{1}{2} \Sigma'(\rho, \beta, a) \quad (176)$$

$$S_-(\rho, \beta, a) = \frac{1}{2} \Sigma'(\rho, \beta, a) \quad (177)$$

3. Site C, above a positive ion

$$S_+(\rho, \beta, a) = \frac{1}{2} \Sigma'(\rho/2, \beta, 2a) + \frac{2}{2} \Sigma'(\frac{\rho+1}{2}, \beta, 2a) + \frac{1}{3} \Sigma'(\rho/2, \beta, 2a) \quad (178)$$

$$S_-(\rho, \beta, a) = \frac{1}{2} \Sigma'(\frac{\rho+1}{2}, \beta, 2a) + \frac{2}{2} \Sigma'(\rho/2, \beta, 2a) + \frac{1}{3} \Sigma'(\frac{\rho+1}{2}, \beta, 2a) \quad (179)$$

4. Site D, above a negative ion

$$S_+(\rho, \beta, a) = \sum_1' \left(\frac{\rho+1}{2}, \beta, 2a\right) + 2\sum_2' (\rho/2, \beta, 2a) + \sum_3' \left(\frac{\rho+1}{2}, \beta, 2a\right) \quad (180)$$

$$S_-(\rho, \beta, a) = \sum_1' (\rho/2, \beta, 2a) + 2\sum_2' \left(\frac{\rho+1}{2}, \beta, 2a\right) + \sum_3' (\rho/2, \beta, 2a) \quad (181)$$

In Tables 39 through 44 are presented the calculated values of \sum_1' , \sum_2' and \sum_3' for ρ , $\rho/2$, and $(\rho + 1)/2$. These values are for the argon-sodium chloride and the nitrogen-sodium chloride systems only and are not of general use. The calculations were carried out on a Burroughs 5500 Computer by summing over 54 lattice points.

Table 39. Summations of the Exponential of Distance ($\Sigma'(\rho, \beta, a)$) from Equations (171), (172), and (173) for Argon on the (100) Plane of Sodium Chloride.

$$\beta = 3.91895 \text{ \AA}^{-1}$$

$$a = 2.8201 \text{ \AA}^0$$

ρ	$\Sigma' \times 10^{+8}$ 1	$\Sigma' \times 10^{+8}$ 2	$\Sigma' \times 10^{+8}$ 3
.70	6711.73	15058.52	44246.40
.75	4519.65	9575.61	25546.28
.80	3005.39	6033.43	14757.68
.85	1975.94	3771.42	8530.29
.90	1285.92	2341.20	4933.76
.95	829.206	1444.60	2855.40
1.00	530.283	8886.667	1653.63
1.05	336.589	541.696	958.285
1.10	212.201	329.590	555.693
1.15	132.962	199.811	322.445
1.20	82.8486	120.746	187.220
1.25	51.3620	72.7588	108.772
1.30	31.6953	43.7312	63.2325
1.35	19.4768	26.2244	36.7798
1.40	11.9225	15.6938	21.4049
1.45	7.2726	9.3745	12.4634
1.50	4.4219	5.5903	7.2605
1.55	2.6807	3.3287	4.2315
1.60	1.2607	1.9793	2.4671
1.65	.9774	1.1754	1.4389
1.70	.5880	.6972	.8396
1.75	.3530	.4131	.4899
1.80	.2115	.2446	.2860
1.85	.1265	.1446	.1670
1.90	.0755	.0854	.0976
1.95	.0550	.0505	.0569
2.00	.0268	.0298	.0333

Table 40. Summations of the Exponential of Distance ($\Sigma'(\rho/2, \beta, 2a)$ from Equations (171), (172), and (173) for Argon on the (100) Plane of Sodium Chloride.

$$\beta = 3.91895 \text{ \AA}^{-1}$$

$$a = 2.8201 \text{ \AA}^0$$

ρ	$\Sigma' \times 10^{+8}$ 1	$\Sigma' \times 10^{+8}$ 2	$\Sigma' \times 10^{+8}$ 3
.70	10.6769	276.9469	43680.998
.75	8.2981	200.2424	25137.010
.80	6.3629	142.7481	14465.500
.85	4.8167	100.4314	8324.453
.90	3.6016	69.8006	4790.456
.95	2.6616	47.9644	2756.755
1.00	1.9451	32.6141	1586.430
1.05	1.4064	21.9607	912.9378
1.10	1.0067	14.6538	525.3670
1.15	.7137	9.6962	302.3326
1.20	.5014	6.2659	173.9833
1.25	.3492	4.1493	100.1222
1.30	.2412	2.6863	57.6174
1.35	.1653	1.7282	33.1572
1.40	.1125	1.1055	19.0810
1.45	.0759	.7033	10.9806
1.50	.0509	.4451	6.3191
1.55	.0340	.2404	3.6365
1.60	.0225	.1759	2.0927
1.65	.0149	.1099	1.2043
1.70	.0097	.0684	.6939
1.75	.0065	.0424	.3988
1.80	.0041	.0262	.2295
1.85	.0027	.0161	.1321
1.90	.0017	.0099	.0760
1.95	.0011	.0061	.0437
2.00	.0007	.0037	.0252

Table 41. Summations of the Exponential of Distance ($\Sigma'(\frac{\rho+1}{2}, \beta, 2a)$) from Equations (171), (172), and (173) for Argon on the (100) Plane of Sodium Chloride

$$\beta = 3.91895 \text{ \AA}^{-1}$$

$$a = 2.8201 \text{ \AA}$$

ρ	$\Sigma' \times 10^{+12}$ 1	$\Sigma' \times 10^{+12}$ 2	$\Sigma' \times 10^{+12}$ 3
.70	97.4043	683.6874	6930.636
.75	63.5331	423.8955	2988.479
.80	41.2395	271.9363	2295.323
.85	26.6457	161.3464	1320.939
.90	17.1411	99.0910	760.1448
.95	10.9811	60.6874	437.4919
1.00	7.0070	37.0702	251.7786
1.05	4.4543	22.5881	144.9010
1.10	2.8216	13.7322	83.3928
1.15	1.7812	8.3295	47.9943
1.20	1.1208	5.0421	27.6221
1.25	.7031	3.0463	15.8975
1.30	.4397	1.8370	9.1497
1.35	.2743	1.1059	5.2661
1.40	.1705	.6646	3.3009
1.45	.1058	.3988	1.7445
1.50	.0755	.2389	1.0041
1.55	.0405	.1429	.5779
1.60	.0249	.0854	.3327
1.65	.0153	.0509	.1915
1.70	.0094	.0304	.1102
1.75	.0094	.0881	.0635
1.80	.0035	.0107	.0365
1.85	.0021	.0064	.0210
1.90	.0013	.0038	.0121
1.95	.0008	.0023	.0069
2.00	.0005	.0013	.0040

Table 42. Summations of the Exponential of Distance ($\Sigma'(\rho, \beta, a)$) from Equations (171), (172), and (173) for Nitrogen on the (100) Plane of Sodium Chloride.

$$\beta = 5.50881 \text{ \AA}^{-1}$$

$$a = 2.8201 \text{ \AA}^0$$

ρ	$\Sigma' \times 10^{+12}$ 1	$\Sigma' \times 10^{+12}$ 2	$\Sigma' \times 10^{+12}$ 3
.70	774792.9897	3147711.3665	18960210.3904
.75	444355.4738	1661503.8833	8723899.1343
.80	250361.9368	865512.1974	4014530.7189
.85	138826.2043	445709.4471	1847673.9118
.90	75880.4957	227231.4340	850535.1856
.95	40941.1278	114831.6096	391602.7863
1.00	21832.7464	57582.6817	180341.5457
1.05	11520.2949	28678.4349	83071.4906
1.10	6020.8748	14196.9938	38275.7397
1.15	3119.4853	6990.3557	17640.8321
1.20	1603.5339	3425.5451	8132.9133
1.25	818.3756	1671.5007	3750.6940
1.30	404.9360	812.5009	1720.7999
1.35	209.1266	393.5967	798.5097
1.40	104.8231	190.0808	368.6310
1.45	52.2785	91.5410	170.2390
1.50	25.9528	43.9743	78.6472
1.55	12.8292	21.0762	36.3468
1.60	6.3171	10.0805	16.8037
1.65	3.0993	4.8123	7.7715
1.70	1.5155	2.2934	3.5954
1.75	.7388	1.0912	1.6640
1.80	.3591	.5185	.7704
1.85	.1741	.2460	.3568
1.90	.0842	.1166	.1653
1.95	.0406	.0552	.0766
2.00	.0196	.0261	.0355

Table 43. Summations of the Exponential of Distance ($\Sigma'(\rho/2, \beta, 2a)$) from Equations (171), (172), and (173) for Nitrogen on the (100) Plane of Sodium Chloride.

$$\beta = 5.50881 \text{ \AA}^{-1}$$

$$a = 2.8201 \text{ \AA}^0$$

	$\Sigma' \times 10^{+12}$ 1	$\Sigma' \times 10^{+12}$ 2	$\Sigma' \times 10^{+12}$ 3
.70	90.3529	11631.3293	18936853.7835
.75	63.3965	7373.1173	8709087.8390
.80	43.6481	4581.7817	4005322.7369
.85	29.5121	2795.0129	1842054.0170
.90	19.6121	1675.9820	847163.4442
.95	12.8199	989.0663	389611.7571
1.00	8.2495	575.1102	179183.0404
1.05	5.2297	329.8455	82406.5534
1.10	3.2685	186.7819	37898.8997
1.15	2.0154	104.5256	17429.7619
1.20	1.2268	57.8553	8015.9742
1.25	.7378	31.6983	3686.5589
1.30	.4386	17.2034	1695.4541
1.35	.2579	9.2548	779.7419
1.40	.1501	4.9381	358.6046
1.45	.0865	2.6448	164.9228
1.50	.0494	1.3748	75.8483
1.55	.0279	.7180	34.8827
1.60	.0157	.3727	16.0426
1.65	.0087	.1923	7.3780
1.70	.0048	.0987	3.3932
1.75	.0026	.0504	1.5605
1.80	.0014	.0256	.7127
1.85	.0008	.0130	.3301
1.90	.0004	.0065	.1518
1.95	.0002	.0033	.0698
2.00	.0001	.0016	.0321

Table 44. Summations of the Exponential of Distance ($\Sigma'(\frac{\rho+1}{2}, \beta, 2a)$) from Equations (171), (172), and (173) for Nitrogen on the (100) Plane of Sodium Chloride.

$$\beta = 5.50881 \text{ \AA}^{-1}$$

$$a = 2.8201 \text{ \AA}$$

ρ	$\Sigma' \times 10^{+12}$ 1	$\Sigma' \times 10^{+12}$ 2	$\Sigma' \times 10^{+12}$ 3
.70	.0048	.0987	3.3932
.75	.0026	.0504	1.5605
.80	.0014	.0256	.7177
.85	.0008	.0129	.3301
.90	.0004	.0065	.1518
.95	.0002	.0033	.0698
1.00	.0001	.0016	.0321
1.05	.0001	.0008	.0148
1.10	-	.0004	.0068
1.15	-	.0002	.0031
1.20	-	.0001	.0014
1.25	-	-	.0007
1.30	-	-	.0003
1.35	-	-	.0001
1.40	-	-	.0001
1.45	-	-	-
1.50	-	-	-
1.55	-	-	-
1.60	-	-	-
1.65	-	-	-
1.70	-	-	-
1.75	-	-	-
1.80	-	-	-
1.85	-	-	-
1.90	-	-	-
1.95	-	-	-
2.00	-	-	-

APPENDIX G

THE ELECTROSTATIC FIELD

The equation for the electrostatic field component F_z , perpendicular to the surface crystal plane was derived by Lennard-Jones and Dent¹⁵ and presented in equation (92)

$$F_z = \frac{8\pi ve}{a_o^2} \sum_{\ell=\pm 1, 3, 5} \sum_{m=\pm 1, 3, 5} (1 + \exp -\pi(\ell^2 + m^2)^{\frac{1}{2}})^{-1} \exp \left[-\frac{2\pi z}{a_o} (\ell^2 + m^2)^{\frac{1}{2}} \right] \cos 2\pi \left(\frac{\ell x}{a_o} + \frac{my}{a_o} - \frac{\ell+m}{4} \right) (-1)^{\frac{\ell+m}{2}} \quad (92)$$

In this equation a_o is the crystal lattice constant, 5.6402 \AA^0 for sodium chloride, which is different from a , which has been used throughout this paper ($a = 2.8201 \text{ \AA}^0$ for sodium chloride). The term a is one half the crystal lattice constant. This equation is perfectly general for any face centered cubic structure and may be employed using the appropriate value of a_o .

Summations of equation (92) have been carried out for various values of ρ where

$$\rho = z/a = 2z/a_o \quad (182)$$

To use these summations which are presented in Table 45, the values of

F_z must be multiplied by $(5.6402)^2/a_0^2$ where a_0 is the appropriate crystal lattice parameter.

Table 45. The F_z Component of the Electrostatic Field over the Ions of the (100) Plane of Sodium Chloride, from Equation (92).

ρ	$F_z \times 10^{-6}$ (gm. ^{$\frac{1}{2}$} /cm. ^{$\frac{1}{2}$} sec.)	ρ	$F_z \times 10^{-6}$ (gm. ^{$\frac{1}{2}$} /cm. ^{$\frac{1}{2}$} sec.)
.35	4.3605	1.20	.0728
.40	3.2312	1.25	.0582
.45	2.4391	1.30	.0466
.50	1.8677	1.35	.0373
.55	1.4459	1.40	.0299
.60	1.1287	1.45	.0239
.65	.8866	1.50	.0191
.70	.6998	1.55	.0153
.75	.5543	1.60	.0123
.80	.4402	1.65	.0098
.85	.3503	1.70	.0079
.90	.2792	1.75	.0063
.95	.2228	1.80	.0050
1.00	.1179	1.85	.0040
1.05	.1422	1.90	.0032
1.10	.1137	1.95	.0026
1.15	.0909	2.00	.0021

APPENDIX H

QUADRUPOLE POTENTIAL SUMMATIONS

The interaction energy of a quadrupole Q in an electric field F is given by equation (93)

$$\phi_Q = \frac{1}{2} Q(d^2F/dt^2) \quad (93)$$

In Chapter VI, it was shown that the quadrupole interaction was a maximum for the four cases of interest under the following conditions:

$$1. \text{ Type A sites, } d^2F/dt^2 = (\partial^2F/\partial x \partial y)_z = \frac{e}{a^3} \sigma_A; \quad (94)$$

$$2. \text{ Type B sites, } d^2F/dt^2 = (\partial^2F/\partial x \partial y)_y = \frac{e}{a^3} \sigma_B; \quad (95)$$

$$3. \text{ Type C sites, } d^2F/dt^2 = (\partial^2F/\partial z^2)_{x,y} = \frac{e}{a^3} \sigma_C; \quad (96)$$

$$4. \text{ Type D sites, } d^2F/dt^2 = (\partial^2F/\partial x^2)_{z,y} = \frac{e}{a^3} \sigma_D. \quad (97)$$

Using the form of Lennard-Jones and Dent for the electrostatic field, equation (91), the values of the σ 's can be evaluated

$$\sigma_A = -2\pi^2 \sum_{\ell=\pm 1,3,5} \sum_{m=\pm 1,3,5} \frac{(-1)^{\frac{\ell+m}{2}}}{(\ell^2+m^2)^{\frac{1}{2}}} \frac{\exp\left[-\frac{2\pi z(\ell^2+m^2)^{\frac{1}{2}}}{a_0}\right]}{1 + \left[\exp -\pi(\ell^2+m^2)^{\frac{1}{2}}\right]} \quad (183)$$

$$\sigma_B = 2\pi^2 \sum_{\ell=\pm 1,3,5} \sum_{m=\pm 1,3,5} \frac{(-1)^{\frac{\ell+m}{2}}}{\ell} \sin 2\pi \left[-\frac{\ell+m}{8}\right] \frac{\exp\left[-2\pi z(\ell^2+m^2)^{\frac{1}{2}}\right]}{1 + \exp\left[-\pi(\ell^2+m^2)^{\frac{1}{2}}\right]} \quad (184)$$

$$\sigma_C = 2\pi^2 \sum_{\ell=\pm 1, 3, 5} \sum_{m=\pm 1, 3, 5} (-1)^{\frac{\ell+m}{2}} (\ell^2+m^2)^{\frac{1}{2}} \cos 2\pi \left[-\frac{\ell+m}{4} \right] \frac{\exp \left[-2\pi z (\ell^2+m^2)^{\frac{1}{2}} \right]}{1 + \exp \left[-\pi (\ell^2+m^2)^{\frac{1}{2}} \right]} \quad (185)$$

$$\sigma_D = -2\pi^2 \sum_{\ell=\pm 1, 3, 5} \sum_{m=\pm 1, 3, 5} (-1)^{\frac{\ell+m}{2}} \frac{\ell^2}{(\ell^2+m^2)^{\frac{1}{2}}} \cos 2\pi \left[\frac{\ell+m}{4} \right] \frac{\exp \left[-\frac{2\pi z}{a_0} (\ell^2+m^2)^{\frac{1}{2}} \right]}{1 + \exp \left[-\pi (\ell^2+m^2)^{\frac{1}{2}} \right]} \quad (186)$$

The summations of the σ 's are presented in Table 46 as a function of ρ . These summations are general for any face centered cubic structure, by using the appropriate value of a in equations (94) through (97).

Table 46. Values of σ from Equations (183), (184), (185), and (196) for the (100) Plane of Face Centered Cubic Sodium Chloride.

ρ	σ_A	σ_B	σ_C	σ_D
.80	1.5309	2.1738	3.3458	1.6730
.85	1.2349	1.7526	2.6456	1.3229
.90	.9944	1.4105	2.0950	1.0476
.95	.7996	1.1337	1.6624	.8312
1.00	.6424	.9104	1.3222	.6611
1.05	.5157	.7306	1.0541	.5270
1.10	.4139	.5861	.8420	.5210
1.15	.3321	.4701	.6734	.3367
1.20	.2664	.3770	.5388	.2694
1.25	.2136	.3023	.4310	.2155
1.30	.1712	.2422	.3445	.1722
1.35	.1371	.1950	.2751	.1375
1.40	.1098	.1552	.2197	.1098
1.45	.0878	.1242	.1756	.0877
1.50	.0702	.0994	.1407	.0703
1.55	.0563	.0796	.1130	.0665
1.60	.0453	.0640	.0908	.0454
1.65	.0367	.0518	.0725	.0362
1.70	.0300	.0422	.0566	.0283
1.75	.0248	.0347	.0422	.0210
1.80	.0207	.0287	.0287	.0143
1.85	.0172	.0237	.0167	.0083
1.90	.0141	.0192	.0078	.0039
1.95	.0109	.0149	.0055	.0027
2.00	.0076	.0108	.0015	.0080

APPENDIX I

POTENTIAL ENERGY CURVE DATA

Table 47. Total Potential of Argon above the (100) Plane of Sodium Chloride using the Harmonic Mean Combining Rule, for the Repulsive Potential Parameter B_{12} .

ϕ_T				
Kcal./Mole				
ρ	Site A	Site B	Site C	Site D
.35	17.4474	-	-154.5797	-
.40	11.1394	-	-90.5561	-
.45	6.1134	-	-57.5945	-
.50	2.3429	-	-39.0018	-
.55	-.3111	16.7246	-27.6366	-
.60	-2.0435	8.4726	-20.2308	-
.65	-3.0631	3.2583	-15.1711	-
.70	-3.5624	.1379	-11.6886	29.7 69
.75	-3.5624	-1.5976	-8.6476	13.8561
.80	-3.6149	-2.4535	-6.5898	5.3206
.85	-3.3906	-2.7739	-5.1502	.9312
.90	-3.0975	-2.7861	-4.1125	-1.1771
.95	-2.7796	-2.6330	-2.7613	-2.0647
1.00	-2.4645	-2.4044	-2.3094	-2.3214
1.05	-2.1683	-2.1503	-1.9525	-2.2706
1.10	-1.8988	-1.8995	-1.6660	-2.0853
1.15	-1.6590	-1.6666	-1.4329	-1.8546
1.20	-1.4488	-1.4571	-1.2400	-1.6230
1.25	-1.2656	-1.2731	-1.0805	-1.4055
1.30	-.1078	-1.1133	-.9462	-1.2212
1.35	-.9721	-.9753	-.9462	-1.0589
1.40	-.8555	-.8568	-.8325	-.9206
1.45	-.7551	-.7549	-.7376	-.8036
1.50	-.6687	-.6676	-.6540	-.7046
1.55	-.5942	-.5923	-.5821	-.6205
1.60	-.5297	-.5275	-.5196	-.5205
1.65	-.4738	-.4712	-.4659	-.4881
1.70	-.4253	-.5224	-.4191	-.4358
1.75	-.3829	-.3798	-.3781	-.3906
1.80	-.3449	-.4328	-.3422	-.3514
1.85	-.3128	-.3101	-.3104	-.3173
1.90	-.2842	-.2848	-.2822	-.2875
1.95	-.2587	-.2559	-.2574	-.2613
2.00	-.2367	-.2368	-.2352	-.2383

Table 48. Total Potential of Argon above the (100) Plane of Sodium Chloride using the Arithmetic Mean Combining Rule, for the Repulsive Potential Parameter B_{12} .

ρ	ϕ_T Kcal./mole			
	Site A	Site B	Site C	Site D
1.10	8.5014	14.2540	25.5488	24.8836
1.15	4.8575	8.1264	14.2891	13.7968
1.20	2.6118	4.4608	7.8297	7.4662
1.25	1.2517	2.2929	4.1404	3.8781
1.30	.4456	1.0301	2.0467	1.8497
1.35	-.0176	.3099	.8724	.7277
1.40	-.2711	-.0875	.2256	.1193
1.45	-.3987	-.2956	-.1829	-.2607
1.50	-.4519	-.3936	-.3340	-.3913
1.55	-.4519	-.4292	-.3975	-.4398
1.60	-.4627	-.4292	-.3976	-.4290
1.65	-.4503	-.4305	-.3976	-.4290
1.70	-.3965	-.3883	-.3776	-.3949
1.75	-.3657	-.3595	-.3539	-.3667
1.80	-.3355	-.3307	-.3279	-.3375
1.85	-.3071	-.3029	-.3020	-.3091
1.90	-.3070	-.2805	-.2774	-.2827
1.95	-.2567	-.2535	-.2545	-.2584
2.00	-.2355	-.2354	-.2337	-.2365

Table 49. Total Potential of Argon above the (100) Plane of Sodium Chloride using the Geometric Mean Combining Rule for the Repulsive Potential Parameter B_{12} .

ρ	ϕ Kcal./mole			
	Site A	Site B	Site C	Site D
.70	25.2211	64.7169	56.1849	341.4063
.75	15.6791	39.4678	30.9962	193.3249
.80	9.2738	23.4212	16.6176	108.6907
.85	5.0831	13.4000	8.4669	60.4801
.90	2.4168	7.2542	3.8948	33.1319
.95	.7764	3.5617	1.3759	17.7062
1.00	-.1903	1.3981	.0269	9.0737
1.05	-.7249	.1728	-.6591	4.2984
1.10	-.9888	-.4860	-.9738	1.7023
1.15	-1.0888	-.8097	-1.0847	.3295
1.20	-1.0935	-.9393	-1.0869	-.3632
1.25	-1.0454	-.9611	-1.0340	-.6786
1.30	-.9719	-.9257	-.9577	-.8018
1.35	-.8886	-.8630	-.8728	-.8168
1.40	-.8044	-.7894	-.7888	-.7809
1.45	-.7339	-.7148	-.7205	-.7248
1.50	-.6497	-.6437	-.6441	-.6591
1.55	-.5826	-.5780	-.5763	-.5943
1.60	-.5228	-.5190	-.5140	-.5336
1.65	-.4696	-.4662	-.4627	-.4791
1.70	-.4227	-.4195	-.4171	-.4306
1.75	-.3815	-.3781	-.3769	-.3876
1.80	-.3449	-.3416	-.3413	-.3497
1.85	-.3128	-.3094	-.3099	-.3163
1.90	-.2842	-.2843	-.2819	-.2868
1.95	-.2587	-.2557	-.2573	-.2609
2.00	-.2367	-.2367	-.2351	-.2380

Table 50. Total Potential of Nitrogen above the (100) Plane of Sodium Chloride using the Geometric Mean Combining Rule, for the Repulsive Potential Parameter B_{12} .

ρ	ϕ Kcal./Mole			
	Site A	Site B	Site C	Site D
.90	4.1321	24.9655	28.2304	201.1824
.95	.1977	9.9668	9.7063	88.9883
1.00	-1.6351	2.7870	1.7572	38.1274
1.05	-2.3355	-.4629	-1.4374	15.2936
1.10	-2.4848	-1.7845	-2.5316	5.2175
1.15	-2.3719	-2.1909	-2.7290	.9132
1.20	-2.1519	-2.1852	-2.5690	-.8088
1.25	-1.9029	-2.0121	-2.2885	-1.3118
1.30	-1.6614	-1.7858	-1.9907	-1.5033
1.35	-1.4424	-1.5585	-1.7132	-1.4207
1.40	-1.2508	-1.3497	-1.4699	-1.2760
1.45	-1.0858	-1.1673	-1.2625	-1.1222
1.50	-.9452	-1.0108	-1.0879	-.9799
1.55	-.8260	-.8779	-.9417	-.8552
1.60	-.7250	-.7661	-.8183	-.7456
1.65	-.6394	-.6718	-.7134	-.6554
1.70	-.5669	-.5924	-.6215	-.5756
1.75	-.5053	-.5349	-.5400	-.5056
1.80	-.4525	-.4673	-.4665	-.4441
1.85	-.4061	-.4175	-.4014	-.3902
1.90	-.3654	-.3775	-.3477	-.3450
1.95	-.3280	-.3339	-.3134	-.3116
2.00	-.2943	-.3018	-.2780	-.2782

APPENDIX J

INTEGRATED POTENTIAL

Integrating over the distances between the adsorbate molecule and all the ions does not give proper weight to the closest ions. For this reason the closest ions are summed and the remainder are integrated. Consider a unit lattice square of side length ℓ with alternating positive and negative ions at the corners. The interaction energy of an adsorbate molecule, over the center of the cell at a perpendicular distance of z , with each of the ions of this cell represented by

$$\phi_1 = 2u_{12}(r) + 2u_{13}(r) \quad (187)$$

where

$$u_{12}(r) = -\frac{C_{12}}{r^6} + B_{12} \exp(-\beta r) \quad (188)$$

$$u_{13}(r) = -\frac{C_{13}}{r^6} + B_{13} \exp(-\beta r) \quad (189)$$

The distance from the molecule to one of these ions is designated as R_o , where

$$R_o = \left[z^2 + (\ell/\sqrt{2})^2 \right]^{1/2} = \left[z^2 + \frac{\ell^2}{2} \right]^{1/2} \quad (190)$$

The interaction with the remaining ions is given by

$$\begin{aligned}\phi_2 = & \frac{\rho}{2} \int_{R_o}^{\infty} \int_0^{\cos^{-1}(z/r)} \mu_{12}(r) 2\pi r_{12}^2 \sin \theta \, d\theta \, dr \\ & + \frac{\rho}{2} \int_{R_o}^{\infty} \int_0^{\cos^{-1}(z/r)} \mu_{13}(r) 2\pi r_{13}^2 \sin \theta \, d\theta \, dr\end{aligned}\quad (191)$$

where ρ is the density of the solid.

The total potential is given by

$$\phi_T = \phi_1 + \phi_2$$

The total potential may be solved by considering the attractive and repulsive forces separately. The attractive force is given by

$$\begin{aligned}\phi_A = & -\frac{2}{R_o^6} (C_{12} + C_{13}) + \frac{\rho}{2} \int_{R_o}^{\infty} \int_0^{\cos^{-1}(z/r)} \left(-\frac{C_{12}}{r_{12}^6}\right) 2\pi r_{12}^2 \sin \theta \, d\theta \, dr \\ & + \frac{\rho}{2} \int_{R_o}^{\infty} \int_0^{\cos^{-1}(z/r)} \left(-\frac{C_{13}}{r_{13}^6}\right) 2\pi r_{13}^2 \sin \theta \, d\theta \, dr\end{aligned}\quad (192)$$

Factoring out the constants, integrating and simplifying

$$\phi_A = -(C_{12} + C_{13}) \left[\frac{2}{R_o^6} + \pi\rho \left(\frac{1}{3R_o^3} - \frac{z}{4R_o^4} \right) \right] \quad (193)$$

The repulsive force is given by

$$\begin{aligned} \phi_R = & (B_{12} + B_{13}) (2 \exp[-\beta R_0]) + \pi \rho B_{12} \int_{R_0}^{\infty} \int_0^{\cos^{-1}(z/r)} \exp[-\beta r_{12}] r_{12}^2 \sin \theta \, d\theta \, dr \\ & + \pi \rho B_{13} \int_{R_0}^{\infty} \int_0^{\cos^{-1}(z/r)} \exp[-\beta r_{13}] r_{13}^2 \sin \theta \, d\theta \, dr \end{aligned} \quad (194)$$

Factoring out the constants, integrating and simplifying

$$\phi_R = (B_{12} + B_{13}) \left\{ 2 \exp[-\beta R_0] + \pi \rho \left[\frac{e^{-\beta R_0}}{\beta} \left\{ \left(-R_0 - \frac{1}{\beta}\right) \left(\frac{z}{\beta} - \frac{2}{\beta^2}\right) + R_0^2 \right\} \right] \right\} \quad (195)$$

The total potential then is given by the sum of equations (193) and (195)

$$\begin{aligned} \phi_T = & -(C_{12} + C_{13}) \left[\frac{2}{R_0^6} + \pi \rho \left(\frac{1}{3R_0^3} - \frac{1}{4R_0^4} \right) \right] \\ & + (B_{12} + B_{13}) \left\{ 2e^{-\beta R_0} + \pi \rho \left[\frac{e^{-\beta R_0}}{\beta} \left\{ \left(-R_0 - \frac{1}{\beta}\right) \left(\frac{z}{\beta} - \frac{2}{\beta^2}\right) + R_0^2 \right\} \right] \right\} \end{aligned} \quad (196)$$

Table 51. Total Potential for Argon over the Center of a Cell, on the (100) Plane of Sodium Chloride from Equation (196).

ρ	ϕ_T Kcal./Mole	
	Sherwood and Prausnitz Potential for Argon	Whalley and Schneider Potential for Argon
.90	2.9105	3.2318
.95	1.2267	1.5796
1.00	.2225	.5158
1.05	-.4170	-.1195
1.10	-.6373	-.4918
1.15	-.7630	-.6858
1.20	-.7646	-.7668
1.25	-.7911	-.7785
1.30	-.6869	-.7501
1.35	-.6451	-.7001
1.40	-.5774	-.6406
1.45	-.5123	-.7786
1.50	-.4525	-.5183
1.55	-.3988	-.4620
1.60	-.3515	-.4106
1.65	-.3109	-.3646
1.70	-.2742	-.3237
1.75	-.2420	-.2877
1.80	-.2148	-.2561
1.85	-.1911	-.2284
1.90	-.1704	-.2041
1.95	-.1525	-.1829
2.00	-.1368	-.1643

BIBLIOGRAPHY

1. Y. Larher, J. Chim. Phys., 65, 974 (1968).
2. R. A. Pierotti and H. E. Thomas, "Surface and Colloid Science Volume IV," John Wiley and Sons, New York, 1971, pp. 93-259.
3. D. M. Young and A. D. Crowell, "Physical Adsorption of Gases," Butterworths, London, 1962.
4. H. Margenau, Rev. Mod. Phys., 11, 1 (1939).
5. S. Ross and J. Oliver, "On Physical Adsorption," Interscience Publishers, New York, 1964.
6. J. Aston, Advances in Chemistry Series, 33, 325 (1961).
7. F. Lenel, Z. Phys. Chem., B23, 379 (1933).
8. F. London, Z. Phys. Chem., II, 222 (1930).
9. J. Mayer, J. Chem. Phys., I, 270 (1931).
10. Landolt-Bornstein, "Zahlenwert und Funktionen," Springer-Verlag, Berlin, 1950.
11. W. Orr, Trans. Faraday Soc., 35, 1247 (1939).
12. A. Muller, Proc. Roy. Soc., A154, 624 (1936).
13. M. Huggins and J. Mayer, J. Chem. Phys., I, 643 (1933).
14. K. F. Herzfeld, Phys. Rev., 52, 374 (1937).
15. J. Lennard-Jones and Dent, Trans. Faraday Soc., 24, 92 (1928).
16. T. Hayakawa, Bull. Chem. Soc. Japan, 30, 124 (1957).
17. T. Hayakawa, Bull. Chem. Soc. Japan, 30, 236 (1957).
18. T. Hayakawa, Bull. Chem. Soc. Japan, 30, 243 (1957).
19. T. Hayakawa, Bull. Chem. Soc. Japan, 30, 332 (1957).
20. T. Hayakawa, Bull. Chem. Soc. Japan, 30, 337 (1957).
21. E. A. Mason and W. E. Rice, J. Chem. Phys., 22, 522 (1954).

22. L. Drain, Trans. Faraday Soc., 49, 650 (1953).
23. D. M. Young, Trans. Faraday Soc., 47, 1228 (1951).
24. D. M. Young, Trans. Faraday Soc., 48, 548 (1952).
25. B. B. Fisher and W. G. McMillan, J. Chem. Phys., 28, 549 (1958).
26. B. B. Fisher and W. G. McMillan, J. Chem. Phys., 28, 555 (1958).
27. B. B. Fisher and W. G. McMillan, J. Chem. Phys., 28, 562 (1958).
28. F. Thompkins and D. Young, Trans. Faraday Soc., 47, 77 (1951).
29. A. Craig and R. McIntosh, Can. J. of Chem., 30, 448 (1952).
30. J. B. Moffat and R. McIntosh, Can J. of Chem., 35, 1511 (1957).
31. D. M. Young and J. A. Morrison, J. of Sci. Instr., 31, 90 (1954).
32. W. F. Espenscheid, E. Matijevic and M. Kerker, J. Phys. Chem., 68, 2831 (1964).
33. S. Ross and H. Clark, J. Am. Chem. Soc., 76, 4291 (1954).
34. S. Ross and W. Winkler, J. Am. Chem. Soc., 76, 2637 (1954).
35. S. Ross and H. Clark, J. Am. Chem. Soc., 76, 4297 (1954).
36. B. W. Davis, J. Colloid Interface Sci., 31, 353 (1969).
37. F. W. Lytle and J. T. Stoner, Science, 141, 1721 (1965).
38. "TRC Tables," Thermodynamic Research Center, Texas A & M, College Station, Texas.
39. S. Weber, Commun. Phys. Lab. Univ. Leiden, No. 246b, (1937).
40. G. Miller, J. Phys. Chem., 67, 1359 (1963).
41. J. Hirschfelder, C. Curtiss and R. Bird, "Molecular Theory of Gases and Liquids," John Wiley and Sons, New York, 1967.
42. A. Grinberg, Surface Science, 2, 314 (1964).
43. "Handbook of Chemistry and Physics," The Chemical Rubber Company, Cleveland, Ohio, 1970.
44. A. Adamson, "Physical Chemistry of Surfaces," Interscience, New York, 1967.

45. P. Y. Hsieh, J. Catalysis, 2, 211 (1963).
46. A. Adamson, I. Ling, L. Dormant and M. Orem, J. Colloid Interface Sci., 21, 445 (1966).
47. S. Ross and W. W. Pultz, J. Colloid Sci., 13, 397 (1958).
48. P. Y. Hsieh, J. Phys. Chem., 68, 1068 (1964).
49. R. H. Fowler and E. A. Guggenheim, "Statistical Thermodynamics," Cambridge, 1965.
50. A. Sherwood and J. Prausnitz, J. Chem. Phys., 41, 42 (1964).
51. E. Whalley and W. G. Schneider, J. Chem. Phys., 23, 1944 (1955).
52. R. A. Magee, M.S. Thesis, Georgia Institute of Technology, Atlanta, Georgia, 1972.
53. G. Starkschall and R. Gordon, J. Chem. Phys., 54, 663 (1971).
54. A. Michael, J. Chem. Phys., 51, 5730 (1969).
55. C. Barter, R. Meisenheimer and D. Stevenson, J. Phys. Chem., 64, 1312 (1960).
56. V. Trew and S. Hussin, Trans. Faraday Soc., 57, 223 (1961).
57. E. Moelwyn-Hughes, "Physical Chemistry," Pergamon, London, 1961.
58. B. Fender and G. Halsey, J. Chem. Phys., 36, 1881 (1962).
59. C. Zener, Phys. Rev., 37, 556 (1931).
60. T. Hill, J. Chem. Phys., 16, 181 (1948).
61. R. Buckingham, J. Am. Chem. Soc., 90, 3104 (1968).
62. A. A. Abrahamson, Phys. Rev., 133, A990 (1964).
63. R. Gordon and Y. Kim, J. Chem. Phys., 56, 3122 (1972).
64. H. Eyring, T. Ree and N. Hirai, Proc. Natl. Acad. Sci. U. S., 44, 683 (1958).
65. O. Sinanoglu and K. S. Pitzer, J. Chem. Phys., 32, 1279 (1960).
66. A. D. McLachlan, Mol. Phys., 7, 381 (1964).

VITA

Daniel Joseph Jackson Jr. was born on 17 May 1942 in Buffalo, New York. As a graduate of Bishop Timon High School, located in Buffalo,, New York, he entered Canisius College, also located in Buffalo, and received the degree Bachelor of Science in June 1963. Upon graduation, he was commissioned as an Officer in the Chemical Corps of the United States Army. He served as an instructor at the U. S. Army Chemical Corps School at Fort McClellan, Alabama from June 1965 to January 1967. He then served a tour of duty in Vietnam where he was awarded The Bronze Star with Two Oak Leaf Clusters and The Distinguished Flying Cross. The U. S. Army provided the opportunity for advanced schooling, whereupon he entered the graduate division of the Georgia Institute of Technology in September 1968, to study for the degree of Doctor of Philosophy in the School of Chemistry.